SAE Aerospace
An SAE International Group

AEROSPACE INFORMATION REPORT

SAE AIR5666

Issued 2012-10

Icing Wind Tunnel Interfacility Comparison Tests

RATIONALE

With all the complexities of icing tunnels there are variation in results at specified environmental conditions. To be able to compare results between different tunnels, the icing community desires that the results be as standard as possible. As a first step towards a standard, a comparison of ice shapes produced at a number of icing tunnels is needed to determine the magnitude of the differences that exist between icing test facilities.

TABLE OF CONTENTS

TO PLACE A DOCUMENT ORDER: **Tel: 877-606-7323 (inside USA and Canada)**
Tel: +1 724-776-4970 (outside USA)
Fax: 724-776-0790
Email: CustomerService@sae.org
SAE WEB ADDRESS: **http://www.sae.org**

SAE values your input. To provide feedback on this Technical Report, please visit
http://www.sae.org/technical/standards/AIR5666

1. SCOPE

This SAE Aerospace Information Report (AIR) presents and discusses the results of tests of three models in six icing wind tunnels in North America and Europe. This testing activity was initiated by the Facility Standardization Panel of the SAE AC-9C Aircraft Icing Technology Subcommittee. The objective of the testing activity was to establish a benchmark that compared ice shapes produced by icing wind tunnels available for use by the aviation industry and to use that benchmark as a basis for dialogue between facility owners to improve the state-of-the-art of icing wind tunnel technology.

1.1 Purpose

The purpose of this AIR is to discuss the results of these tests. It documents that for any particular test-condition specifications the ice accretions produced in all of the participating facilities bore a broad resemblance to one another, but there were substantial facility-to-facility differences in ice shape and volume of accreted ice. Possible causes of the differences are discussed.

2. REFERENCES

2.1 Applicable Documents

The following publications form a part of this document to the extent specified herein. The latest issue of SAE publications shall apply. The applicable issue of other publications shall be the issue in effect on the date of the purchase order. In the event of conflict between the text of this document and references cited herein, the text of this document takes precedence. Nothing in this document, however, supersedes applicable laws and regulations unless a specific exemption has been obtained.

2.1.1 SAE Publications

Available from SAE International, 400 Commonwealth Drive, Warrendale, PA 15096-0001, Tel: 877-606-7323 (inside USA and Canada) or 724-776-4970 (outside USA), www.sae.org.

AIR4906 Droplet Sizing Instrumentation Used in Icing Facilities

AIR5320 Summary of Icing Simulation Test Facilities

ARP5624 Aircraft Inflight Icing Terminology

ARP5905 Calibration and Acceptance of Icing Wind Tunnels

2.1.2 U.S. Department of Transportation, Federal Aviation Administration (FAA) Publications

Available from FAA, 800 Independence Avenue, SW, Washington, DC 20591, Tel: 866-835-5322, www.faa.gov. The FAA Icing Handbook is available through National Technical Information Service Springfield, Virginia 22161 (800)-553-6847 or (703)-605-6000.

Title 14 of the US Code of Federal Regulations, Federal Aviation Regulation Part 25 Airworthiness Standards: Transport Category Airplanes (14 CFR Part 25)

Title 14 of the US Code of Federal Regulations, Federal Aviation Regulation Part 29 Airworthiness Standards: Transport Category Rotorcraft (14 CFR Part 29)

DOT/FAA/CT-88/8-I, "Aircraft Icing Handbook, Volume 1 of 3" March 1991

2.1.3 NATO Advisory Group for Aerospace Research and Development (AGARD) Publications

Available from the North Atlantic Treaty Organization (NATO) office, at 7 Rue Ancelle, Neuilly-sur-Seine, France.

AGARD Advisory Report AR-304, Quality Assessment for Wind Tunnel Testing

2.1.4 Other Applicable Documents

Bragg, M. B., “A Similarity Analysis of the Droplet Trajectory Equation,” AIAA Journal, Vol. 20, no. 12, pp. 1681-1686, Dec. 1982.

Chigier, N., “Spray Science and Technology,” FED-Vol.178/HTD-Vol. 270, Fluid Mechanics and Heat Transfer in Sprays, ASME, 1993.

Chintamani, S., Delcarpio, D., and Langmeyer, G., “Development of Boeing Research Aerodynamic Icing Tunnel Circuit,” proc. AGARD Symposium on Aerodynamics of Wind Tunnel Circuits and Their Components, Moscow, Oct. 1996, AGARD CP-585, pp. 8.1- 8.27.

Gonsalez, J.C., Arrington, E.A., and Curry, R.M., “Aero-Thermal Calibration of the NASA Glenn Icing Research Tunnel (2000 Tests),” AIAA-2001-0233, Reno NV, Jan. 2001.

Ide, R. F. and Oldenburg, J. R., "Icing Cloud Calibration of the NASA Glenn Icing Research Tunnel," AIAA-2001-0234, Reno NV, Jan. 2001.

Kind, R.J., Potapczuk, M.G., Feo, A., Golia, C., and Shah, A.D., “Experimental and Computational Simulation of In-Flight Icing Phenomena,” Progress in Aerospace Sciences, Vol. 34, pp. 257-345, 1998.

Knezevici, D., Kind, R.J., and Oleskiw, M.M., “Determination of Median Volume Diameter (MVD) and Liquid Water Content (LWC) by Multiple Rotating Cylinders,” AIAA Paper 2005-0861, Reno NV, Jan. 2005.

Kreith, F., Principles of Heat Transfer, 2nd ed., International Textbook Co., Scranton, PA, 1965, ch. 9, 13.

Marek, C. J. and Bartlett, C. S.; “Stability Relationship for Water Droplet Crystallization with the NASA Lewis Icing Spray Nozzle,” AIAA-88-289, Reno, NV, Jan. 1988.

Miller, D.R., Potapczuk, M.P. and Langhals, T.J., “Preliminary Investigation of Ice Shape Sensitivity to Parameter Variations,” AIAA-2005-0073, Reno, NV, Jan. 2005.

Oleskiw, M.M., Hyde, F.H., and Penna, P.J., “In-Flight Icing Simulation Capabilities of NRC’s Altitude Icing Wind Tunnel,” AIAA-2001-0094, Reno NV, Jan. 2001.

Olsen, W., Takeuchi, D., and Adams, K., “Experimental Comparison of Icing Cloud Instruments,” AIAA Paper 83-0026, Reno NV, Jan. 1983. White, F.M., Viscous Fluid Flow, 2nd ed., McGraw-Hill Inc., 1991.

Schick, R.J., “An Engineer's Practical Guide to Drop Size,” Spraying Systems Co. (www.spray.com/lit/g_dropguid.asp).

Smolik, J., Dzumbovia, L., Schwartz, J., and Kulmala, M., “Evaporation of Ventilated Water Droplet: Connection Between Heat and Mass Transfer,” Journal of Aerosol Science, Vol. 32, pp. 739-748, 2001.

Strapp, J.W., Oldenburg, J., Ide, R., Lilie, L., Bacic, S., Vokovic, Z., Oleskiw, M., Miller, D., Emery, E. and Leone, G., “Wind Tunnel Measurements of the Response of Hot-Wire Liquid Water Content Instruments to Large Droplets,” Journal of Atmospheric and Oceanic Technology, Vol. 20., No. 6, pp. 791-806, 2003.

2.2 Related Publications

The following publications are provided for information purposes only and are not a required part of this SAE Aerospace Technical Report.

Wright, W.B., “User Manual for the NASA Glenn Ice Accretion Code LEWICE (Version 2.2),” Ch. 13.

2.3 Abbreviations and Symbols

A_c	Accumulation parameter
ASSP	Axial scattering spectrometer probe
CIRA	Centro Italiano Ricerche Aerospaziali
CD	Compact Disc containing a complete set of all test data (see Section 5)
CR	Contraction ratio
FAA	Federal Aviation Administration
FSSP	Forward scattering spectrometer probe
FSTL	Approximate freestream turbulence intensity in test section with atomizing air on
H	Test section dimension in the direction perpendicular to the model span
L	Approximate distance from spray nozzles to model mid-chord
LWC	Liquid water content
MPSA	Malvern particle size analyzer
MVD	Median volumetric diameter
PDPA	Phase Doppler particle analyser
S1	Upper horn height (in)
S2	Upper horn angle (deg)
S3	Lower horn height (in)
S4	Lower horn angle (deg)
S5	Ice area (sq. in)
S6	Leading edge minimum thickness (in)
S7	Upper icing limit (in)
S8	Lower icing limit (in)
α	Angle of attack
β	Collection efficiency
τ	Test-run duration

3. INTRODUCTION

Partly in response to the United States Federal Aviation Administration (FAA) Inflight Aircraft Icing Plan, the Facility Standardization Panel of the SAE AC-9C Aircraft Icing Technology Subcommittee initiated an activity involving tests of three models in various icing wind tunnels and comparison of the ice shapes produced on the models. The test results were discussed by test participants at a workshop held in August 2003 at Galaxy Scientific Corp. in New Jersey and again at a meeting of the Facility Standardization Panel held at the Italian Aerospace Research Center (CIRA) in Capua, Italy, in October 2003. This report presents an outline of the test results and a discussion of possible reasons for some features of the results. Included in Appendix C and Appendix D are reports which were prepared for that workshop and meeting, and which support the discussion contained in the main body of this AIR.

4. BACKGROUND

Each of the major icing wind tunnel facilities in North America and Western Europe were invited to participate in the Facility Standardization activity, with a deadline of March 31, 2003, for submission of initial test results. It was agreed at early meetings of the Facility Standardization Panel that test results would be kept anonymous so that the facility that produced any particular set of results could not be identified. Each participating facility would be identified only by a randomly assigned letter. However, once testing was completed and an initial review conducted, it was agreed that the facilities could be identified in the final report and the identifying letters are included in Table 1.

Six facilities (designated by the randomly assigned letters A, E, F, H, M, and P) performed tests. Table 1 lists these facilities and includes icing wind tunnel parameters and information regarding instrumentation used for the tests.

Three models were tested: a 36 in chord NACA 0012 airfoil at angle of attack α = 3 degrees, a 12 in chord NACA 0012 airfoil at α = 3 degrees, and a 1.5 in diameter circular cylinder. The same three models were shipped from facility to facility for use in each test. Nominal test condition parameters were specified as follows:

- freestream air static temperature: -7, -23 and -30 °C
- liquid water content (LWC): 0.5 and 1.0 g/m^3
- drop diameter (MVD): 20 and 40 μm
- freestream airspeed: 67 and 90 m/s

TABLE 1 - PARTICIPATING FACILITIES DATA

Tunnel Letter	H	P	F	A	E	M
Facility	AIWT, NRC (Oleskiw, et al [2001])	GKN ATS (formerly ACT), UK*	BRAIT, Boeing (Chintamani, et al [1996])	COX	Goodrich	IRT, NASA (Gonsalez, et al [2001])
H	22.5 in (57.2 cm)	30 in wide (76.2 cm)	72 in (182.9 cm)	46 in (116.8 cm)	44 in (111.8 cm)	108 in (274.3 cm)
L	13 ft (3.96 m)	16 ft (4.9 m)	20 ft (6.1 m)	19 ft (5.8 m)	21 ft (6.4 m)	44 ft (13.4 m)
CR	5.8	15.5	7.2	9.6	11.0	14.1
FSTL (%)	1.5	No details available at present	Less than 2%	1 to 1.25	3	<1.5
Instrumentation for LWC	Single Rotating Cylinder confirmed by Icing Blade.Multiple rotating cylinders and King Probe have also been used for some conditions.	Icing blade.	Icing Blade	Icing Blade	Rotating Cylinders	Icing Blade
Instrumentation for MVD	Malvern Spraytec (borrowed from Cox & Co.) and PDPA (borrowed from AEDC). Multiple rotating cylinders have been used for some conditions.	Malvern Insitec (Spraytec) Model No. OHD-EPCS-4.0	PDPA	Malvern Spraytec RTS 5214 (mainly), and FSSP+OAP	*TSI* PDPA	FSSP & OAP
Calibration Standards for LWC	Single Rotating Cylinder and Icing Blade.	LWC calibrated at 1 in or 2 in grid spacing (depending on test component size) for each new test installation / configuration or variation of airspeed and/or cloud drop MVD	Icing Blade	ARP5905	ARP5905	
Calibration Standards for MVD	Field calibration Reticule for Malvern (borrowed from Cox & Co.)	Malvern Insitec calibrated (verification) annually by manufacturer using standard reticule	Boeing Procedure utilizing mono-dispersed drop generator	Malvern Reticule	ARP5905	Glass beads (FSSP) Rotating Reticule (OAP) (Ide, et al [2001])
Test Date	7/02 & 7/04	2/03 & 5/04	11/98	9/02	10/02 & 10/03	11/98 & 9/00

* When required the Malvern instrument is used to confirm the cloud drop MVD just before the start of test. The measurements are made "in situ" just downstream of the tunnel contraction - immediately before entering the tunnel working section.

H = test section dimension in the direction perpendicular to the model span
L = approximate distance from spray nozzles to model mid-chord
CR = contraction ratio
FSTL = approximate freestream turbulence intensity in test section with atomizing air on

Up to three repeat runs were carried out for some cases and centerline and off-centerline ice-shape tracings were made by most of the facilities. The specified test matrix is shown in Table 2.

TABLE 2 - SPECIFIED TEST MATRIX

					Icing Time (min)				
Test Cond.	Static Temp °C/°F	LWC g/m^3	Drop Size µm	Speed m/s/mph	36 in NACA 0012	12 in NACA 0012	1.5 in Cylinder	Icing Type	Repeat Cond.
1	-7/20	0.5	20	67/150	25	20	15	Glaze	3
2	-7/20	0.5	20	90/200	20	15	10	Glaze	3
3	-7/20	1.0	20	67/150	20	15	10	Glaze	3
4	-7/20	1.0	20	90/200	15	10	10	Glaze	3
5	-7/20	1.0	40	67/150	20	15	10	Glaze	3
6	-7/20	1.0	40	90/200	15	10	10	Glaze	3
7	-30/-22	0.5	20	67/150	25	20	15	Rime	2
8	-30/-22	0.5	20	90/200	20	15	10	Rime	2
9	-23/-10	0.5	20	67/150	25	20	15	Rime	2
10	-23/-10	0.5	20	90/200	20	15	15	Rime	2
11	-30/-22	1.0	20	67/150	15	10	10	Rime	3

No standard was available to gauge which ice shapes were closest to the “truth.” The test results consist primarily of ice-shape tracings. Tracings obtained in the different facilities are compared to provide an indication of facility-to-facility variations.

In the original test plan (Appendix A), 12 test condition cases were proposed. Test condition 12 was nominally the same as test condition 2 except that the test facilities would adjust the air temperature to get a model temperature that was recorded when the first facility (NASA) ran the test. The intent was to evaluate any facility-to-facility differences in measured air temperature. Because of an inadequate explanation in the test plan of how to run test condition 12 and a confusion of the intent behind condition 12, that condition was not run consistently or widely at all. Therefore, condition 12 results are not included in this report.

The test matrix in Table 2 would involve 29 test runs for each model, for a total of 87 runs, if the specified number of repeats were carried out. Some of the facilities carried out a substantially smaller number of test runs, mainly by reducing the number of repeat runs. Note that glaze icing is expected for about half of the specified test conditions and rime icing for the remainder. The results were collected in the form of ice-shape tracings on cardboard templates, prepared using the techniques in normal use at each facility. Facility operators were encouraged to collect three tracings from each ice accretion, one at the centerline (i.e., mid-span), one some distance to the left and another some distance to the right. The spanwise distances between tracings were chosen by the operators.

The tracings are designated as *centerline, left,* and *right.* However, only one tunnel provided tracings with these designations. In order to facilitate comparison of the data, the designations provided by tunnel operators were mapped onto *centerline, left, and right*. Table 3 shows the designations provided by the tunnel operators and their mapping onto *left* and *right*. All centerline tracings were designated centerline by the tunnel operators, except for one which only provided one tracing for each test. These were assumed to be centerline.

TABLE 3 - LEFT/RIGHT MAPPINGS

LEFT	RIGHT
West	East
Starboard	Port
Outside	Inside
-	+
Below	Above

5. PROCESSING AND PRESENTATION OF RESULTS

All ice-shape tracings were digitized using a Calcomp digitizing tablet controlled by Didger 3® software created by Golden Software, Inc. The initial digitization typically yielded files containing several thousand coordinates for each tracing. The number of coordinates was reduced to about 200, using a process called *decimation,* and these coordinates were entered into an MS-Excel® spreadsheet. Checks showed that the number of coordinates retained was more than adequate to represent the tracings in detail.

A Cartesian coordinate system was used for the clean models and digitized ice-shape tracings. The origin is at the leading edge of the clean model and the x axis is coincident with the model's chordline. The x-axis points to the right which is the downstream direction in the plots. Coordinates of the model were entered sequentially, proceeding counterclockwise, starting at the trailing edge (*x/c, y/c* = 1.0, 0) of the model. However, coordinates of the ice shapes were entered in either clockwise or counterclockwise direction, depending on the complexity of the plot. Plots of the tracings and clean models were prepared in Excel®. The plots are in terms of non-dimensional coordinates, (*x/c, y/c*), where *c* is the chord length. Only selected results will be presented in the hard-copy version of this document, to illustrate the discussion. The complete results are stored on a CD-ROM (CD), which is available by request from the Flight Safety Branch, FAA William J. Hughes Technical Center. This CD contains directories for each participating facility, A, E, F, H, M, and P, as well as *Composites* directory and a directory using the THICK computer program written by W. Wright for NASA Glenn Research Center. Table 4, and also the file *Overview Matrix* on the CD, shows which test runs were done by each facility. The facility directories contain Excel® spreadsheets, including plots of all tracings, for every test condition provided by that facility. The *Composites* directory contains Excel® files with composite plots, i.e., overlaid plots of the centerline tracings from the various facilities for each test condition of Table 2. The plots in the *Composites* directory enable easy comparison of the results from the different facilities. See the *Read Me* file on the CD for details.

After the August and October 2003 workshop and meeting, several of the participating facilities carried out additional test runs. These were runs specified in the test matrix, Table 2, that the facility had either not done in its initial tests, or wished to repeat, because tunnel settings or icing times in the initial test runs had not corresponded with the specifications of Table 2. In cases where initial tests were re-run, only the results of the re-runs are included on the CD-ROM; that is the results of the corresponding earlier runs have been discarded. The final results comprise tracings from 340 runs, with 930 ice-shape tracings.

The following identification convention was adopted for the test runs:

first field [*model*]	*N36*, *N12* or *C15* for 36 in NACA 0012, 12 in NACA 0012 or 1.5 in Cylinder, respectively
second field [*test condition*]	*01* to *11* per left hand column of Table 2
third field [*repeat #*]	*R1, R2, or R3* corresponding to first, second or third run for the particular test condition; this field is omitted if reference is to more than one repeat run
final field [*facility*]	*A, E ,F, H, M*, or *P*

For example N12-05-R1E denotes the first run (R1) of the 12 in NACA 0012 for test condition 5 of Table 2, in Facility E. This convention is used in the computer filenames and spreadsheet headings.

The target test conditions are specified in Table 2. Settings in the actual test runs were often, of course, somewhat different from the values specified in Table 2. Usually the differences were small, but in some instances they were substantial. If the differences exceeded the tolerances given in Table 5, the results were still processed and are presented in the normal way, but notes drawing attention to the differences appear in the relevant plots, and the out-of-tolerance values are highlighted in the numerical sheets of the Excel® spreadsheets. Results recently presented in Miller, et al [2005] indicate that ice-shape variations due to parameter variations within the tolerances of Table 5 would be relatively minor, although those due to ±5% LWC variation and to ±1 °F/ ±0.5 °C temperature variation would be discernible.

TABLE 4 - OVERVIEW OF AVAILABLE TEST RESULTS

Run 1	NACA 0012 36"											NACA 0012 12"											Cylinder											Total Tracings	Total Runs
Tunnel/Run #	1	2	3	4	5	6	7	8	9	10	11	1	2	3	4	5	6	7	8	9	10	11	1	2	3	4	5	6	7	8	9	10	11		
A	3	3	2	3	3	3		3	3	3	3	3	3	3	3	3	3			3	2	3	3	3	3	2	3	3		2	3	3	3	83	29
E	3	3	3	3	3	3			3	3	3	3	3	3	3	3	3			3	3	3	3	3	3	3	3	3			3	3	3	81	27
F	3	3	3		3	3	3	3	3	3	3	3	3	3		3	3	3	3	3	3	3	3	3	3	3	3	3	3	3	3	3	3	90	30
H	3	1	3	3	3	3			3	3		3	3	3	3	3	3	3	3	3	3	3	3	3	3	3	3	3	3	3	3	3	3	88	30
M	3	3	3	3	3	3	3	3	3	3	3	3	3	3	3	3	3	3	3	3	3	3	3	3	3		3	3	3	3	3	3	3	96	32
P	1		1		1		1		1		1	1	1	1	1	1	1	1		1	1	1	1	1	1	1	1	1		1	1	1	1	26	26
Run 2	**NACA 0012 36"**											**NACA 0012 12"**											**Cylinder**												
Tunnel/Run #	1	2	3	4	5	6	7	8	9	10	11	1	2	3	4	5	6	7	8	9	10	11	1	2	3	4	5	6	7	8	9	10	11		
A	3	3	2	3		2				3			3	3	3	3	3			3	2					3					3			42	15
E	3	3	3	3	3				3	3		3	3	3		3	3			3	3	3	3	3	3	3	3	3			3	3	3	72	24
F	3	3	3		3	3	3	3	3	3	3	3	3	3		3	3	3	3	3	3	3	3	3	3		3	3	3	3	3	3	3	90	30
H	2	3	3	3	3	3			3	3		3	3	3	3	3	3			3	3	3	3	3	3	3	3	3			3	3	3	77	26
M	3	3	3	3	3	3	3	1	3	3	3	3		3		3		3	3	3	3	3	3	3	3		3	3	3	3	3			79	27
P	1		1						1		1	1	1		1										1	1	1				1	1	1	13	13
Run 3	**NACA 0012 36"**											**NACA 0012 12"**											**Cylinder**												
Tunnel/Run #	1	2	3	4	5	6					11	1	2	3	4	5	6					11	1	2	3	4	5	6					11		
A			3																															3	1
E			3																															3	1
F	3	3	3		3	3					3	3	3	3		3	3					3	3	3	3		3	3					3	54	18
H																																		0	0
M	3	3	3	3	3	3																		3	3	3		3	3					33	11
P																																		0	0
Shading denotes runs that should be made. "n" denotes the number of tracings that were made.																															**GRAND TOTALS**				
Total Tracings	37	34	42	27	34	32	13	13	29	30	23	32	32	34	20	34	31	16	15	31	29	31	34	34	35	19	35	34	15	18	32	26	29	930	340
Total Runs	14	12	16	9	12	11	5	5	11	10	9	12	12	12	8	12	11	6	5	11	11	11	12	12	13	8	13	12	5	7	12	10	11	930	340

TABLE 5 - PARAMETER TOLERANCE LIMITS

Parameter	Limits
Temperature	±1 °F/±0.5 °C
LWC	±5%
MVD	±2 µm
Speed	±2 mph/ ±1 m/s
Time	±2%

Figure 1 shows a sample plot of all results from a particular facility for one test case, in this example for three runs from Facility F for test condition 6 of Table 2 for the 12-in chord NACA 0012 airfoil model (N12-06-F). Figure 2 shows a sample composite plot for the same test case. Recall that the composite plots only include centerline tracings unless a centerline tracing was not provided.

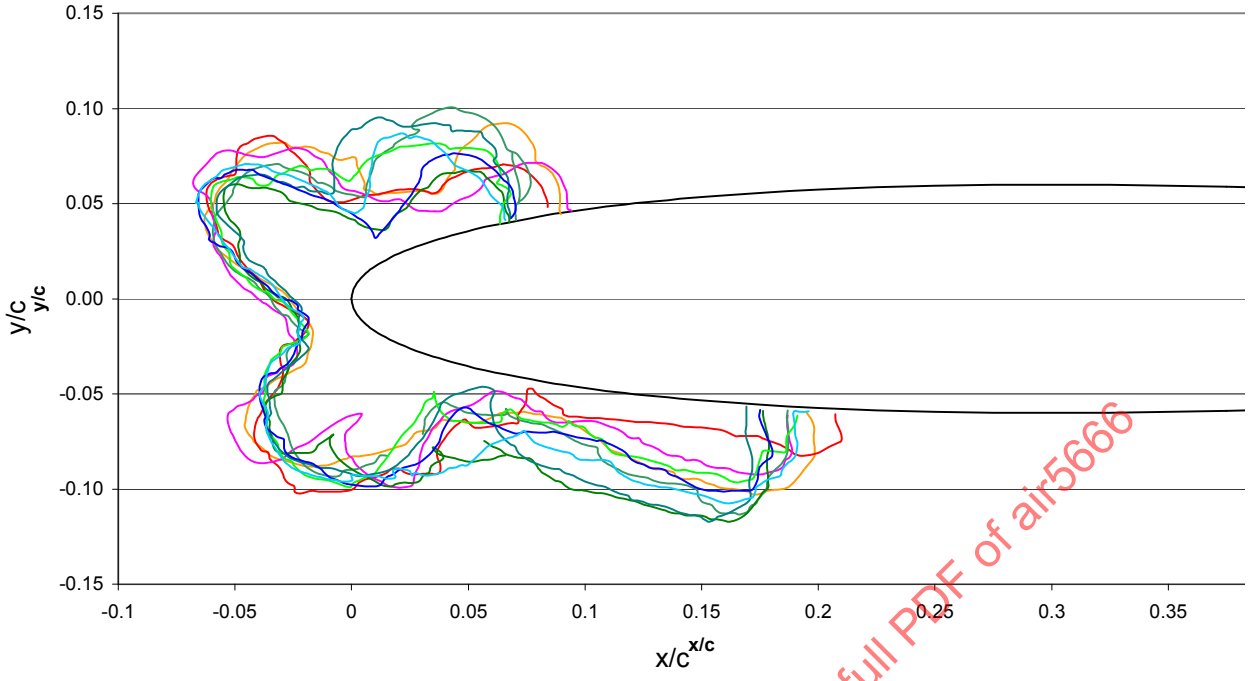

FIGURE 1 - SAMPLE PLOT OF ALL TRACINGS OBTAINED BY ONE OF THE PARTICIPATING FACILITIES FOR THE 12 IN NACA 0012 AIRFOIL, TEST CONDITION 6 OF TABLE 2

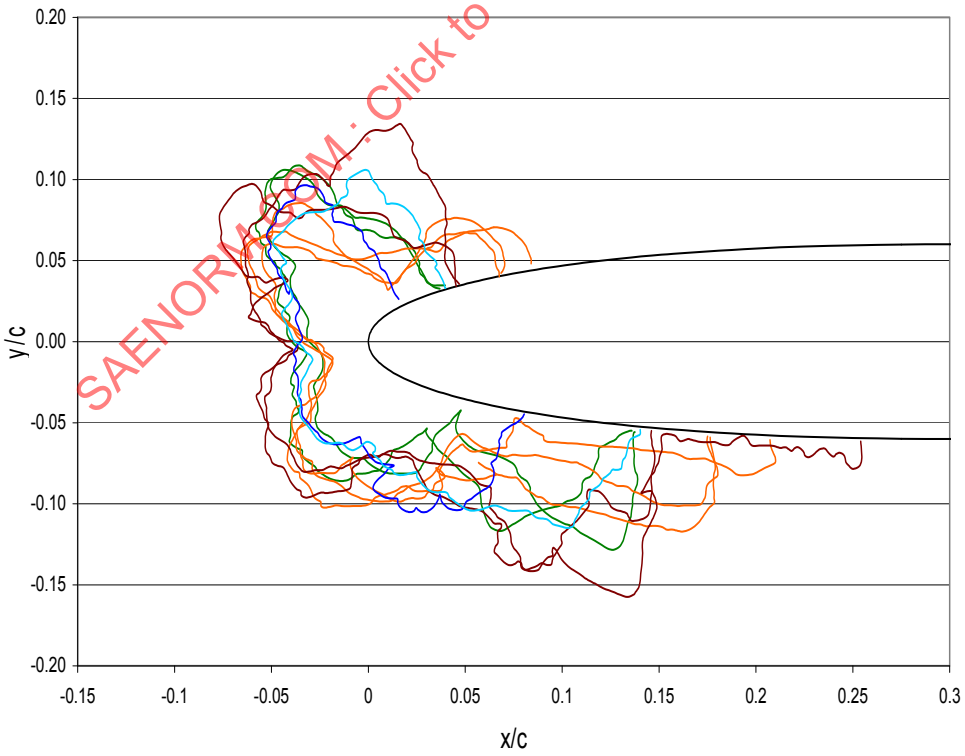

FIGURE 2 - CENTERLINE TRACINGS FROM ALL PARTICIPATING FACILITIES FOR THE 12 IN NACA 0012 AIRFOIL, TEST CONDITION 6 OF TABLE 2

In an effort to concisely quantify and summarize the results, the digitized centerline tracings were processed using the THICK computer code. For clean-body and ice-shape tracings input as x, y coordinates, THICK determines the following eight parameters: upper horn angle, lower horn angle, upper horn height, lower horn height, ice area, leading edge minimum thickness, upper icing limit, and lower icing limit. The definitions of the horn parameters are shown in Figure 3.

Of course some of these parameters are inappropriate for some ice shapes and in such cases THICK may return meaningless or unreasonable values. Both the wrapped plot (i.e., plots like those of Figures 1, 2, and 3) and the unwrapped plot (i.e., ice thickness as ordinate versus s/c as abscissa) produced by THICK for each tracing were examined to check the THICK results for reasonableness. Only the reasonable results are reported. Where THICK results were unreasonable, reasonable values selected from the plots are reported wherever possible.

The results of the processing with THICK are contained in three Excel® files, ThickSmry-RunID-12in.xls, ThickSmry-RunID-36in.xls, and ThickSmry-RunID-Cylinder.xls which are available on the CD (see Section 5). The Overview tab is the same in all three files as it shows which tunnels provided data for which runs. Samples of the results are shown in Tables 6 and 7. Detailed information on the processing with THICK is contained in Appendix B.

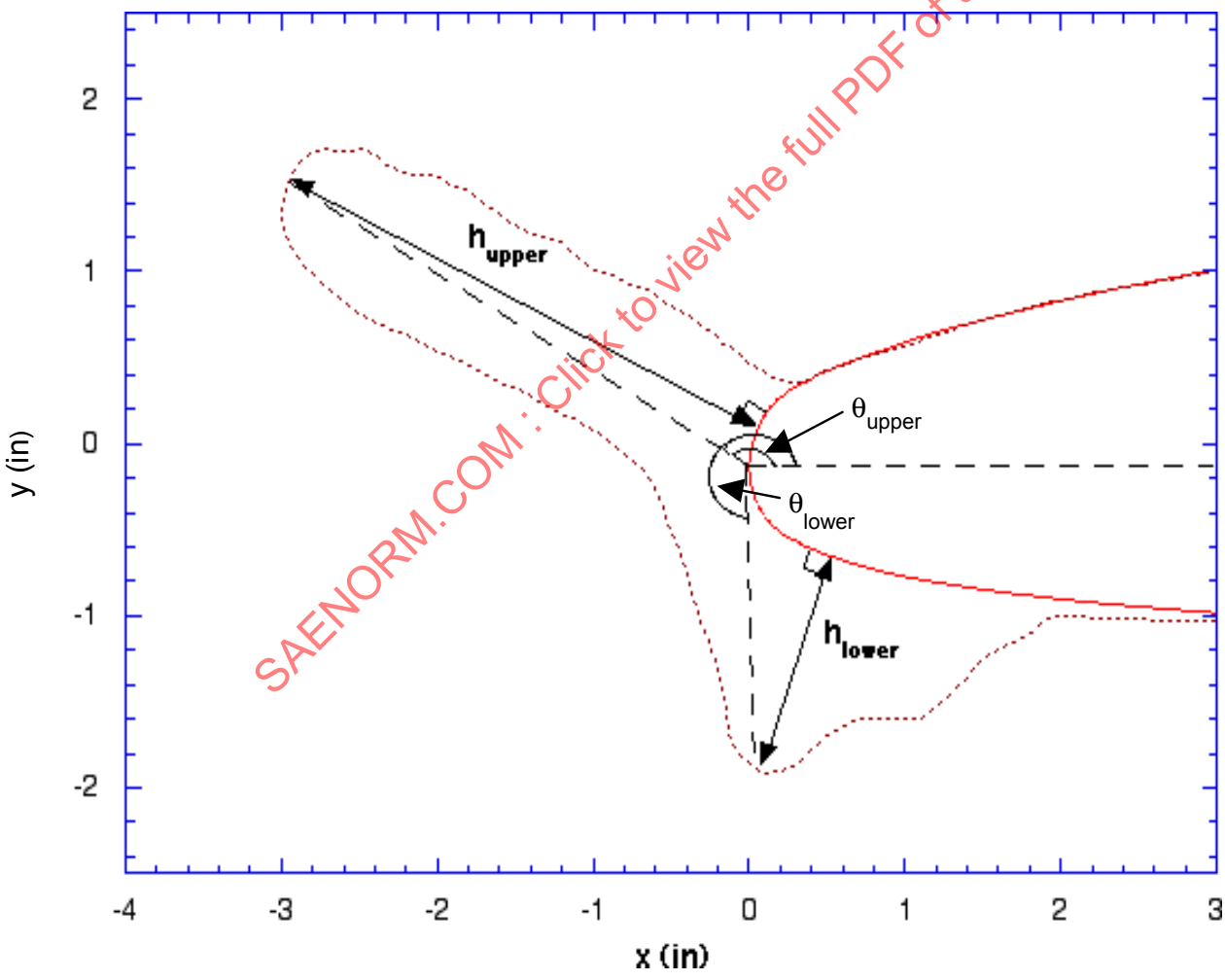

FIGURE 3 - DEFINITION OF HORN PARAMETERS GIVEN BY THICK

TABLE 6 - SAMPLE OF RESULTS PROVIDED BY THICK (FOR CENTERLINE TRACINGS, ALL FACILITIES, CASES N12-06) (FROM FILE \THICKSMRY-RUNID-12IN.XLS OF CD)

Tunnel	Run ID	S8 lower icing limit (in)	S7 upper icing limit (in)	S3 lower horn height (in)	S6 leading edge minimum thickness (in)	S1 upper horn height (in)	S5 ice area (sq. in)	S4 lower horn angle (deg)	S2 upper horn angle (deg)
A	N12-06CR1A	1.65	0.44	0.67	0.09	1.24	2.01	263	114
F	N12-06CR1F	2.49	1.01	1.08	0.25	1.02	2.21	257	121
H	N12-06CR1H	3.05	0.56	1.26	0.44	1.26	3.76	310	90
M	N12-06CR1M	0.96	0.19	0.90	0.60	1.08	1.56	280	110
P	N12-06CR1P	1.68	0.48	0.80	0.36	1.01	2.25	311	92
A	N12-06CR2A	1.63	0.48	0.87	0.28	1.23	2.18	256	117
F	N12-06CR2F	2.12	0.81	0.91	0.29	0.90	2.43	248	133
H	N12-06CR2H	1.75	0.54	1.15	0.47	1.30	2.94	300	127
F	N12-06CR3F	2.10	0.82	0.91	0.24	0.99	2.23	268	139

TABLE 7 - SAMPLE OF RESULTS PROVIDED BY THICK (FOR CENTERLINE TRACINGS, ALL FACILITIES, CASES C15-06) (FROM FILE \THICKSMRY-RUNID-CYLINDER.XLS OF CD)

Tunnel	Run ID	S8 lower icing limit (in)	S7 upper icing limit (in)	S3 lower horn height (in)	S6 leading edge minimum thickness (in)	S1 upper horn height (in)	S5 ice area (sq. in)	S4 lower horn angle (deg)	S2 upper horn angle (deg)
A	C15-06CR1A	0.51	0.50	1.05	0.33	1.00	2.18	260	107
E	C15-06CR1E	0.56	0.39	1.46	0.31	1.26	2.29	244	125
F	C15-06CR1F	0.70	0.54	1.23	0.17	1.08	1.98	239	131
H	C15-06CR1H	0.56	0.62	1.22	0.36	1.22	2.95	245	115
M	C15-06CR1M	0.40	0.40	1.17	0.33	1.16	1.93	256	112
P	C15-06CR1P	0.51	0.51	0.98	0.26	1.08	1.98	278	95
E	C15-06CR2E	0.70	0.73	1.23	0.28	1.28	2.26	236	130
F	C15-06CR2F	0.54	0.46	1.15	0.26	1.04	1.68	246	126
H	C15-06CR2H	0.61	0.59	1.27	0.35	1.23	2.89	242	113
M	C15-06CR2M	0.47	0.50	1.04	0.29	1.09	1.79	253	106
F	C15-06CR3F	0.66	0.62	1.20	0.22	1.18	2.44	236	135
M	C15-06CR3M	0.59	0.62	0.98	0.17	1.17	1.76	270	102

6. DISCUSSION

6.1 Comments on the Results

As mentioned earlier, the complete results are available on a CD-ROM (see Section 5). For discussion purposes only selected results are presented in the present document. The general characteristics of the results are the same for the three models, but the results selected to illustrate the discussion will be mainly for the 12 in NACA 0012 airfoil. This is because, as will be seen below, the 36 in NACA 0012 airfoil at 3 degrees angle of attack is subject to excessive wall interference effects in the smaller participating icing wind tunnels and because icing on circular cylinders is of more limited interest than airfoils.

Repeatability was generally good, as illustrated by the Facility F results for cases N12-06 and N12-02 in Figures 4 and 5, the Facility A results for the same cases in Figures 6 and 7, and the Facility M results for case C15-02 in Figure 8. Bear in mind that these ice accretions were clearly quite irregular, especially for N12-06, so that differences between tracings in Figures 4 to 7 would be due mainly to stochastic irregularities, not to any systematic lack of repeatability.

Agreement between centerline and off-centerline tracings was generally quite satisfactory indicating cloud uniformity over the measurement span. The agreement seen in Figure 1 is typical. Again the irregularity of the ice shapes must be kept in mind.

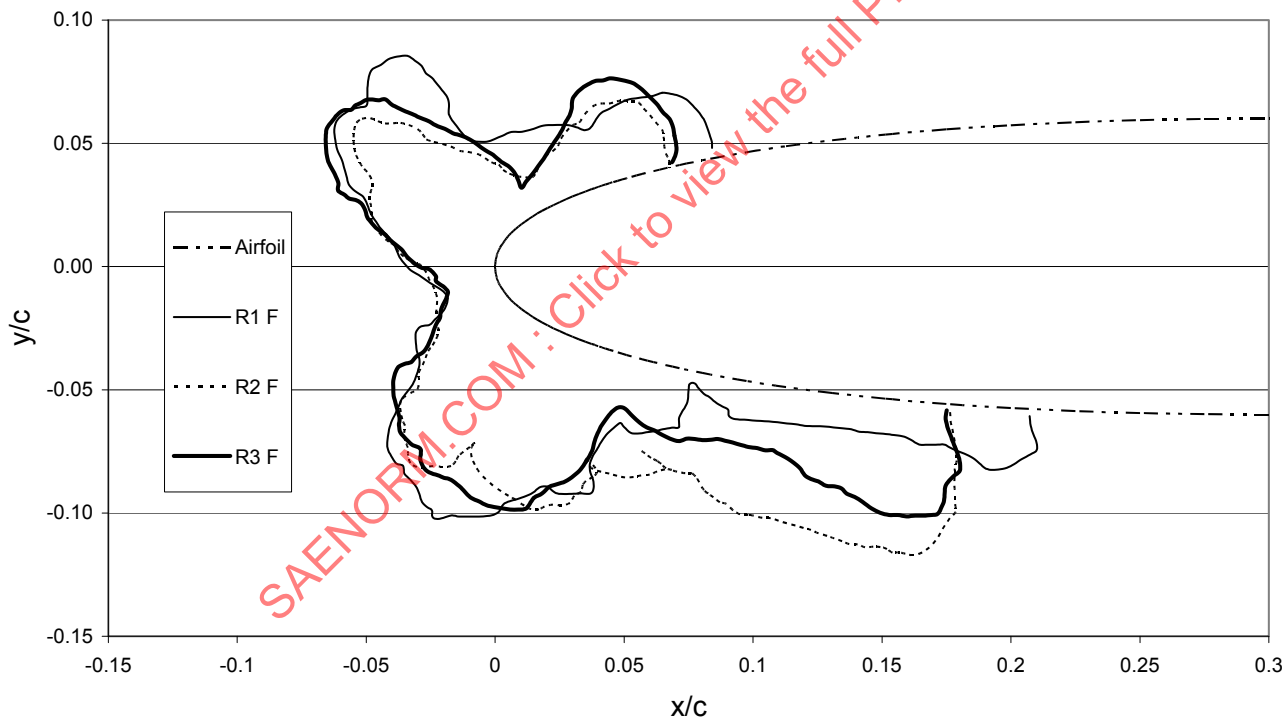

FIGURE 4 - ILLUSTRATION OF TYPICAL REPEATABILITY - FACILITY F CENTERLINE TRACINGS FOR CASE N12-06

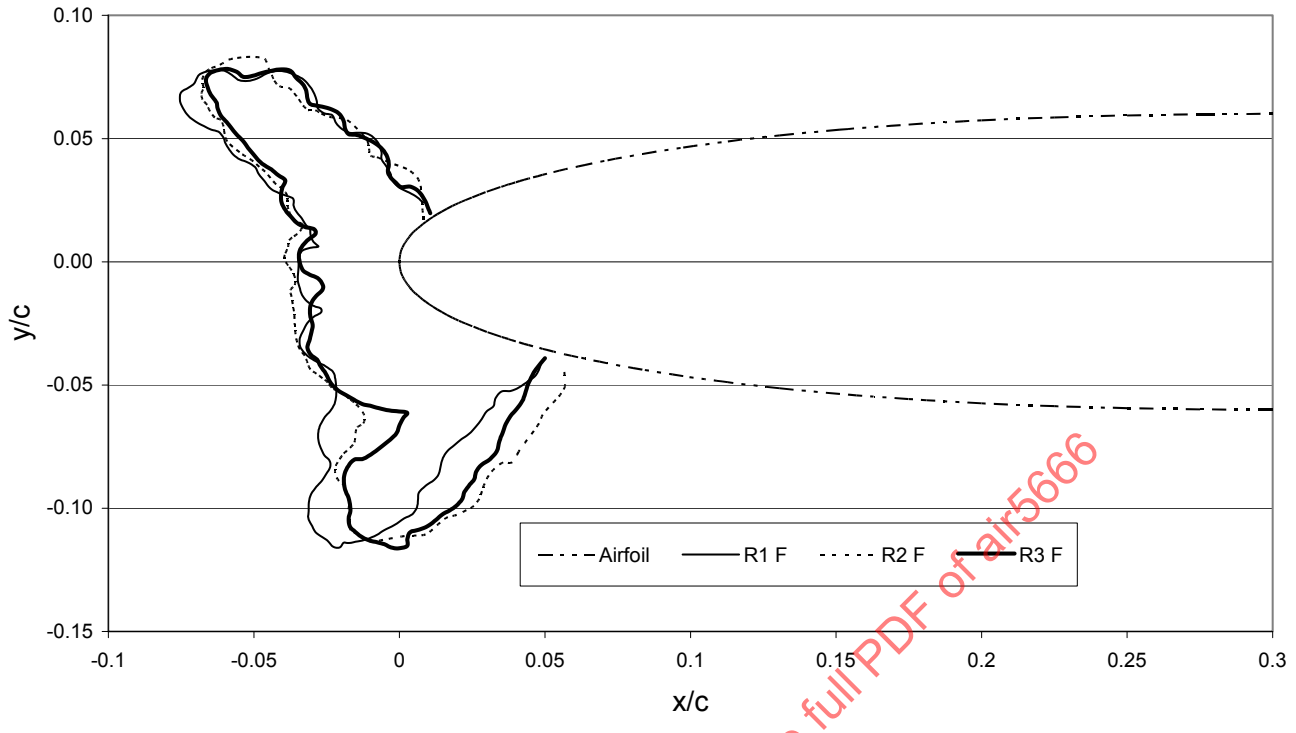

FIGURE 5 - ILLUSTRATION OF TYPICAL REPEATABILITY - FACILITY F CENTERLINE TRACINGS FOR CASE N12-02

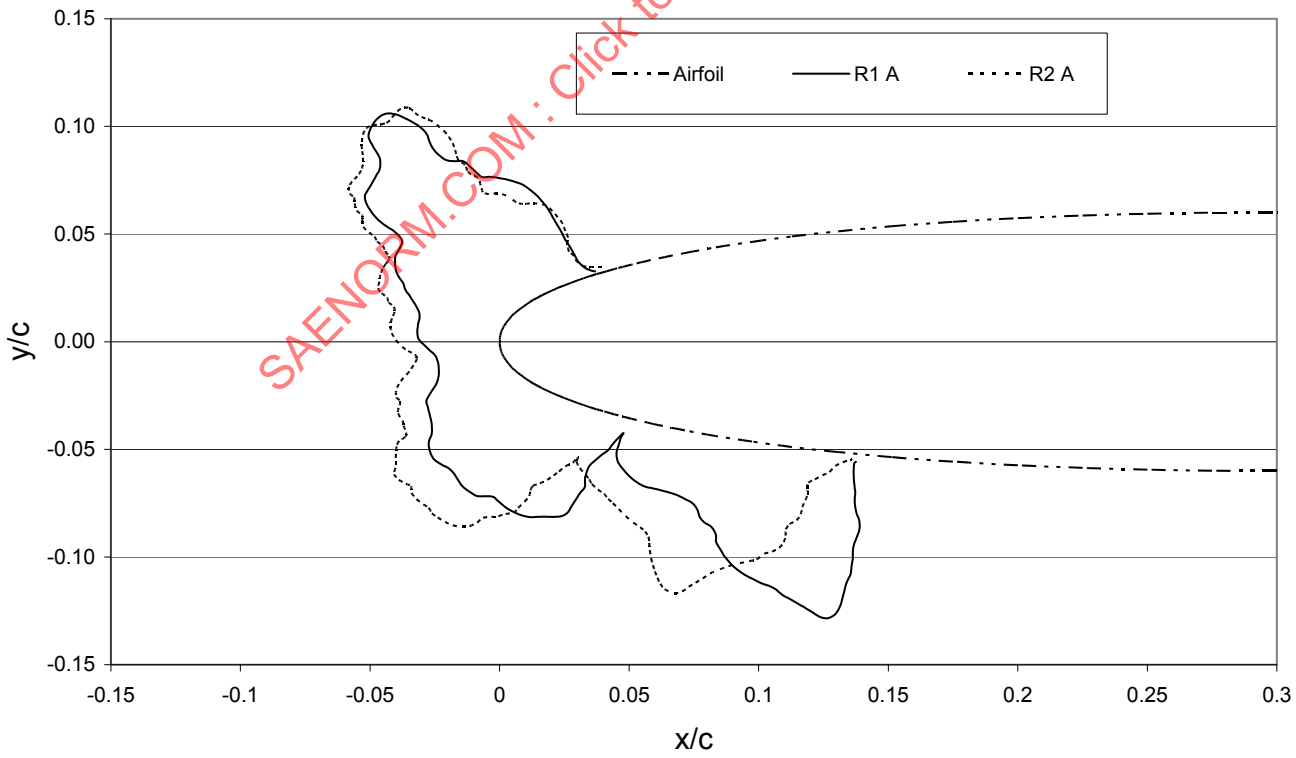

FIGURE 6 - ILLUSTRATION OF TYPICAL REPEATABILITY - FACILITY A CENTERLINE TRACINGS FOR CASE N12-06

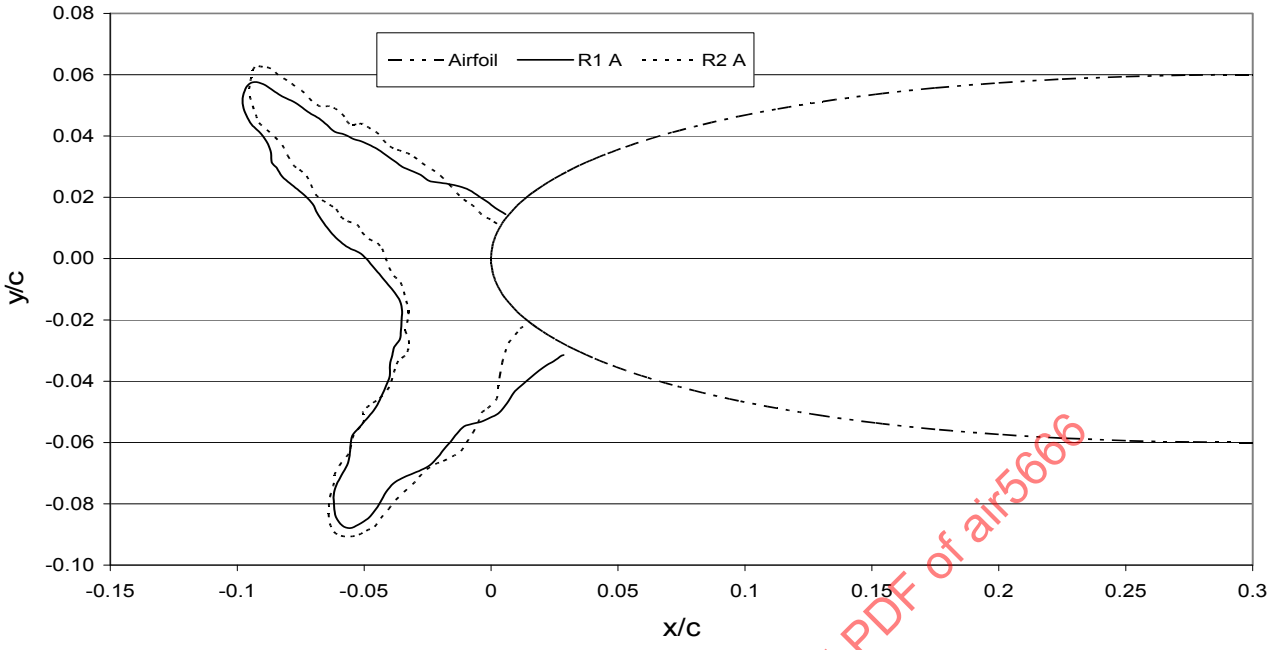

FIGURE 7 - ILLUSTRATION OF TYPICAL REPEATABILITY - FACILITY A CENTERLINE TRACINGS FOR CASE N12-02

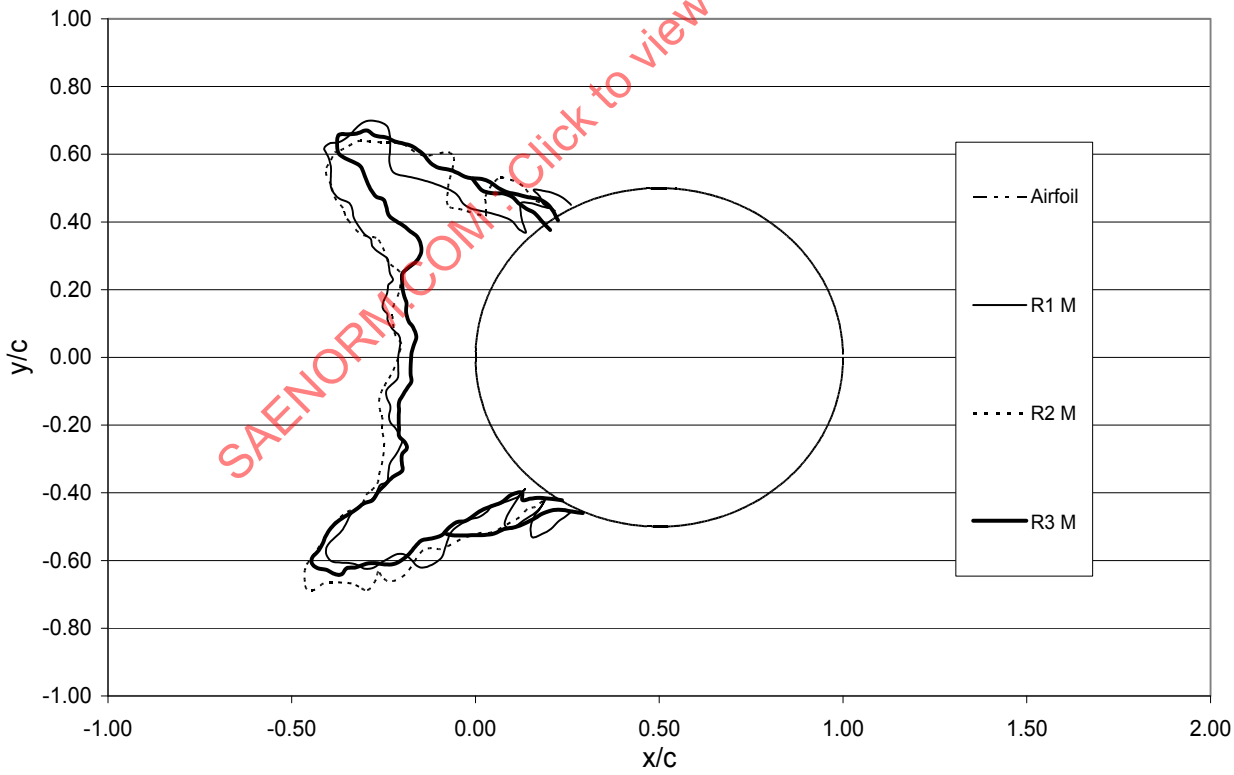

FIGURE 8 - ILLUSTRATION OF TYPICAL REPEATABILITY - FACILITY M CENTERLINE TRACINGS FOR CASE C15-02

The composite plots compare centerline tracings from all of the facilities. Figure 2 is an example of a composite plot and Figure 9 is another. It can be said that there is a broad resemblance between the ice shapes from the various facilities for a particular test-condition specification. However, from Figures 2 and 9 and the other composite plots it is clear that there are substantial differences between ice shapes from the various facilities for the same test-condition specifications. Not only do the ice shapes, but even the ice areas vary substantially, with the areas enclosed by the tracings, varying by up to a factor of two. The numerical ice-shape parameters evaluated for the tracings by THICK reflect these facts, as can be seen from the sample THICK results in Tables 6 and 7 and in Figure 10. The facility-to-facility differences substantially exceed the typical variations between repeat runs in any one facility. This is true not only for the glaze cases, but also for most of the rime cases (e.g., Figure 11) and for the three models (e.g., Figures 11, 12, 13, and 14). On a more positive note, some of the rime results for the cylinder showed quite good agreement between the participating facilities, as exemplified in Figure 15. The overall situation revealed by the results is, however, one of substantial facility-to-facility differences in ice shapes and amounts of accreted ice. The remainder of this discussion will attempt to identify possible causes of the discrepancies.

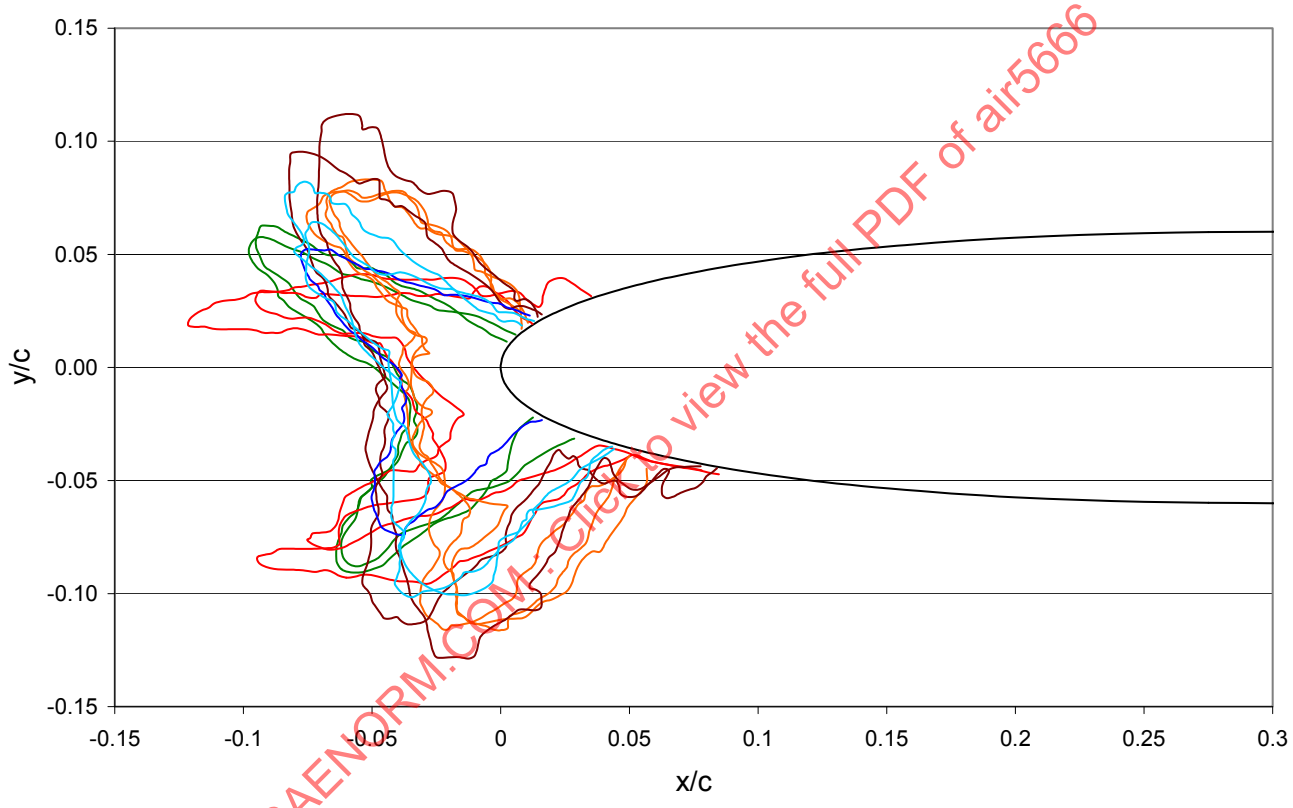

FIGURE 9 - CENTERLINE TRACINGS FROM ALL PARTICIPATING FACILITIES FOR THE 12 IN NACA 0012 AIRFOIL FOR TEST CONDITION 2 OF TABLE 2

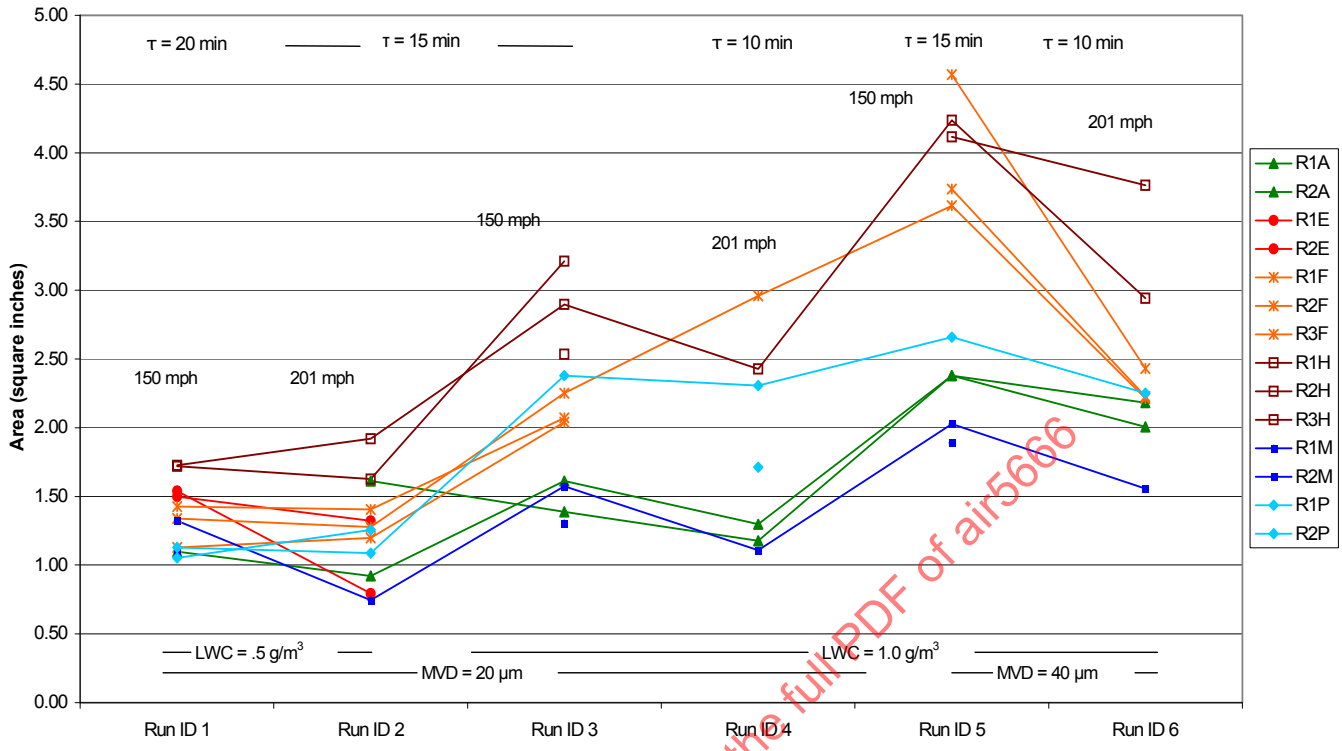

FIGURE 10A - 12 IN NACA 0012, GLAZE CASES (I.E., CASES 1 TO 6 OF TABLE 2)

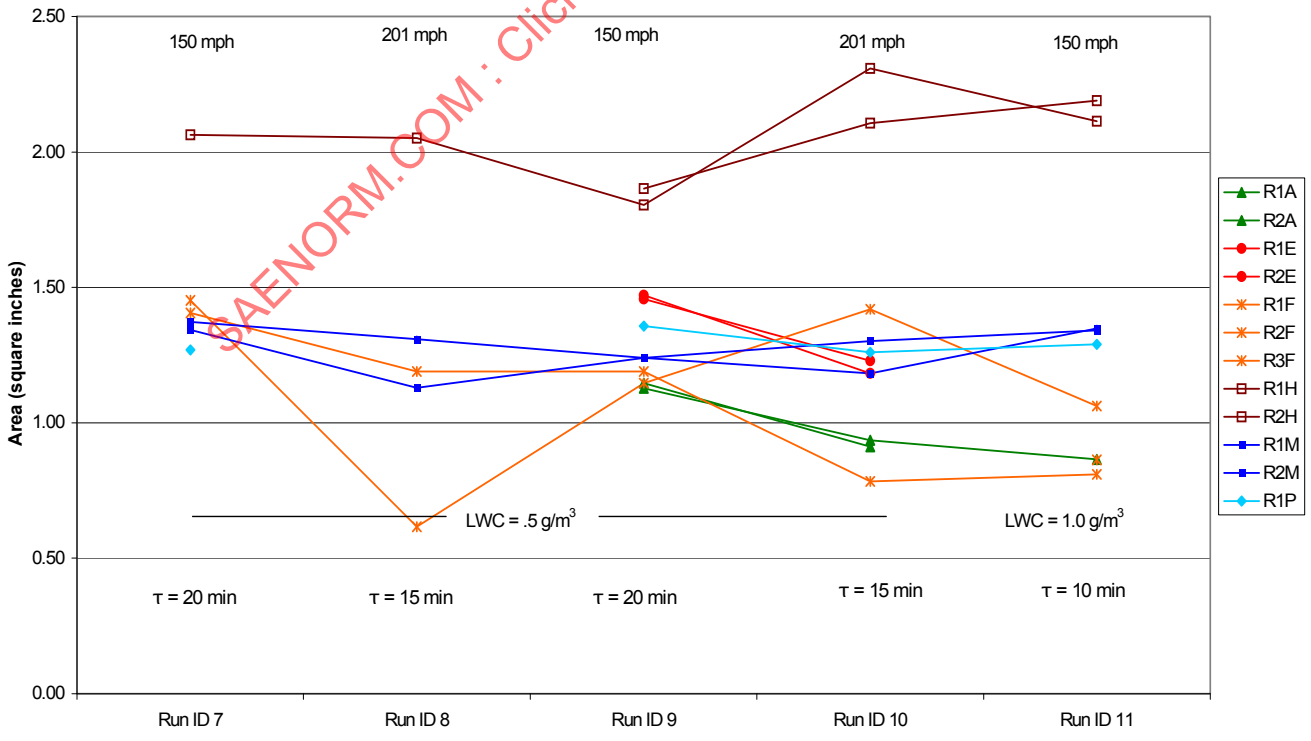

FIGURE 10B - 12 IN NACA 0012, RIME CASES (I.E., CASES 7 TO 11 OF TABLE 2)

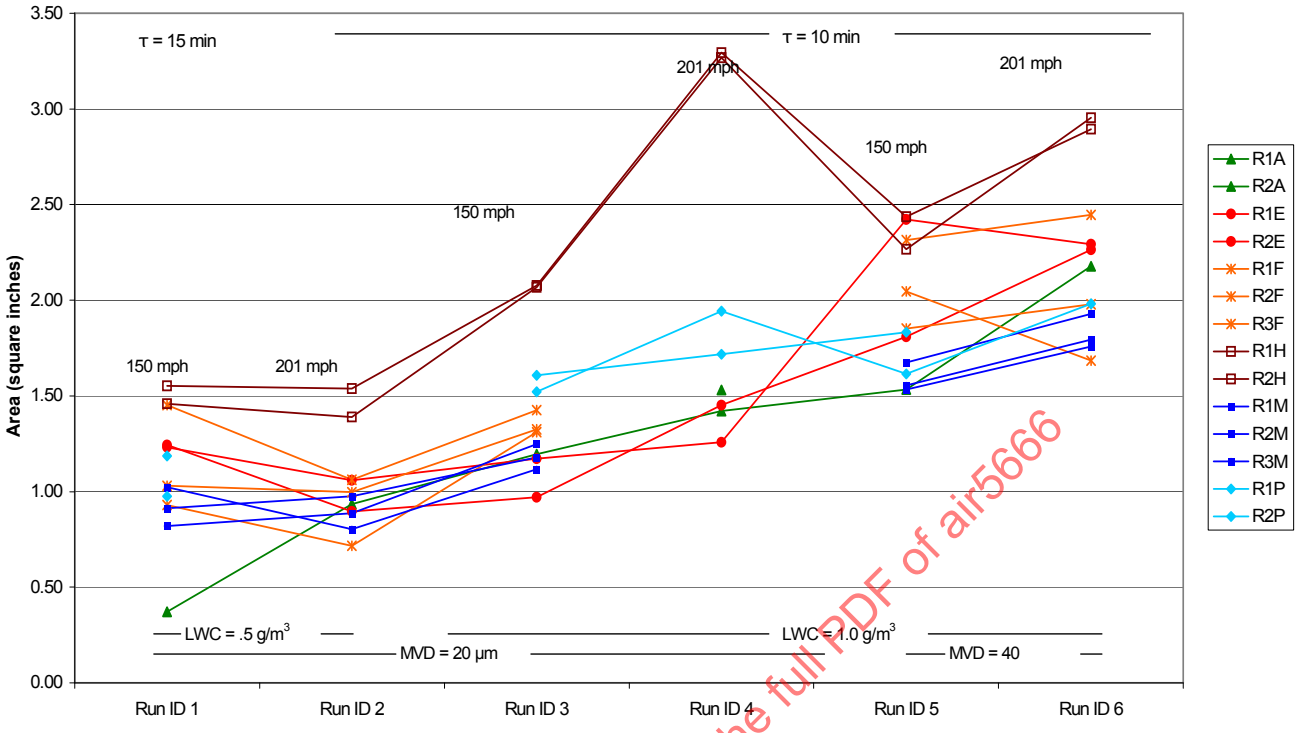

FIGURE 10C - 1.5 IN CYLINDER, GLAZE CASES (I.E., CASES 1 TO 6 OF TABLE 2)

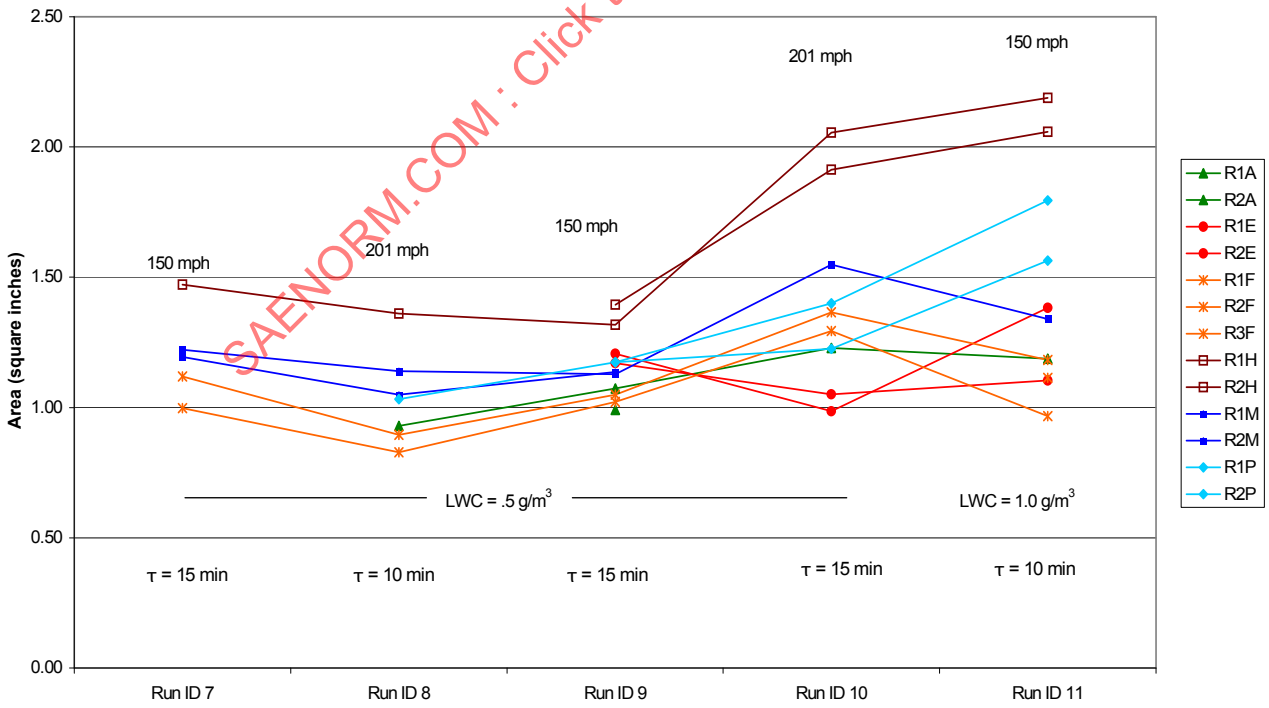

FIGURE 10D - 1.5 IN CYLINDER, RIME CASES (I.E., CASES 7 TO 11 OF TABLE 2)

FIGURE 10 - TOTAL ICE AREA VALUES EVALUATED USING THE THICK CODE FOR THE CENTERLINE TRACINGS SUBMITTED BY PARTICIPATING FACILITIES FOR THE 12 IN NACA 0012 AND 1.5 IN CYLINDER MODELS

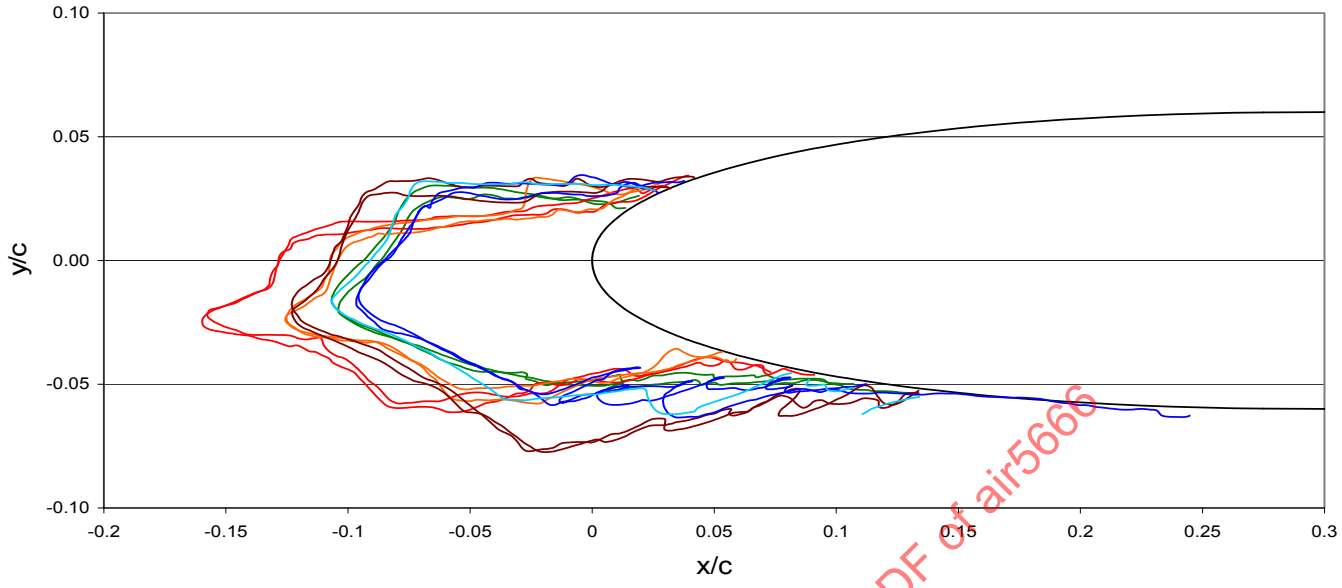

FIGURE 11 - CENTERLINE TRACINGS FROM ALL PARTICIPATING FACILITIES FOR THE 12 IN NACA 0012 AIRFOIL FOR TEST CONDITION 9 OF TABLE 2

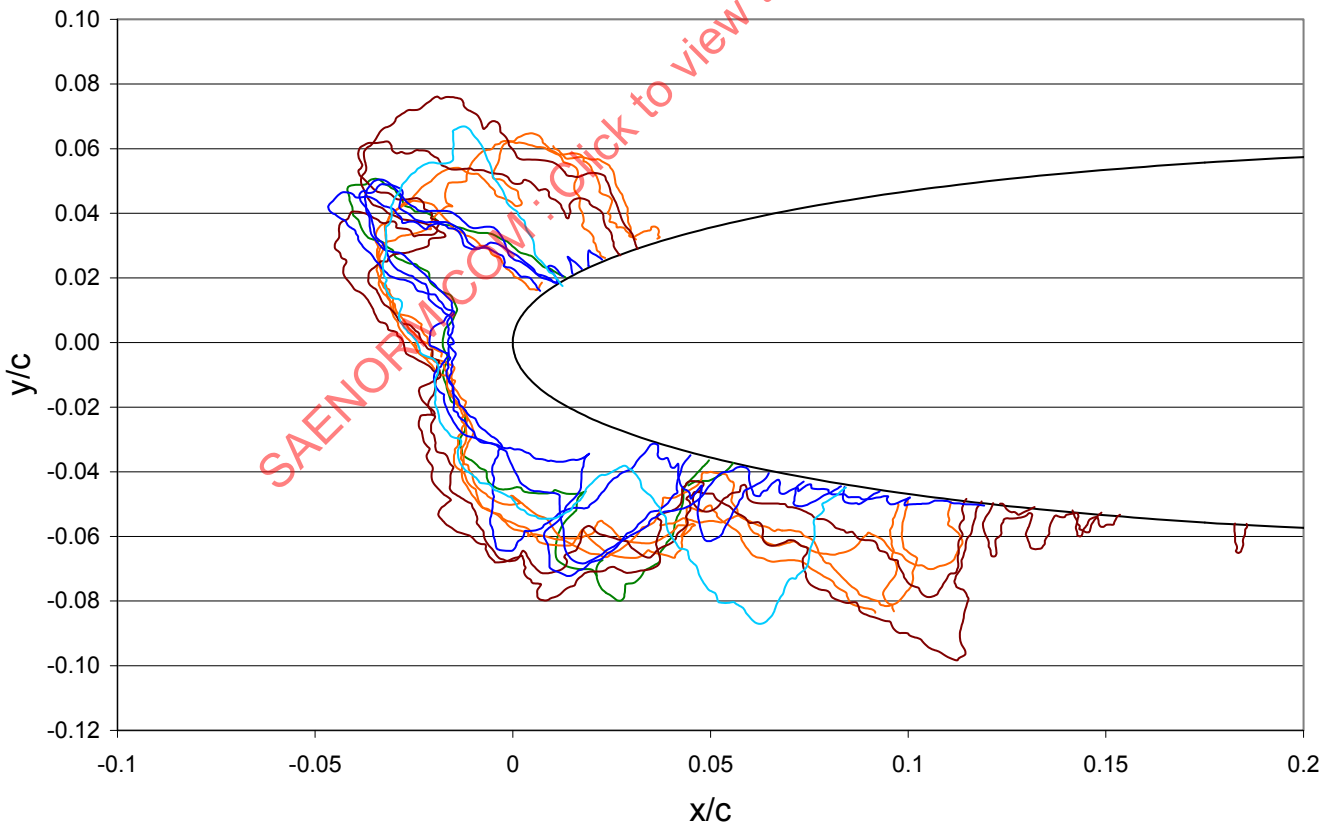

FIGURE 12 - CENTERLINE TRACINGS FROM ALL PARTICIPATING FACILITIES FOR THE 36 IN NACA 0012 AIRFOIL FOR TEST CONDITION 5 OF TABLE 2

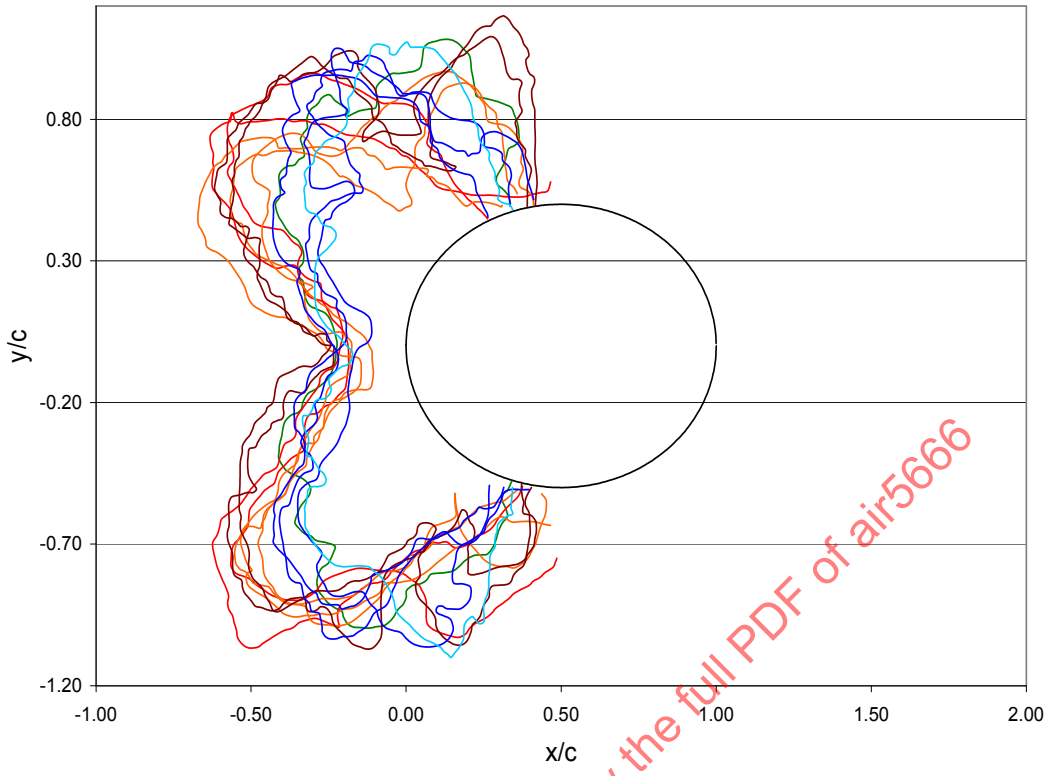

FIGURE 13 - CENTERLINE TRACINGS FROM ALL PARTICIPATING FACILITIES FOR THE 1.5 IN CYLINDER-FOR TEST CONDITION 6 OF TABLE 2

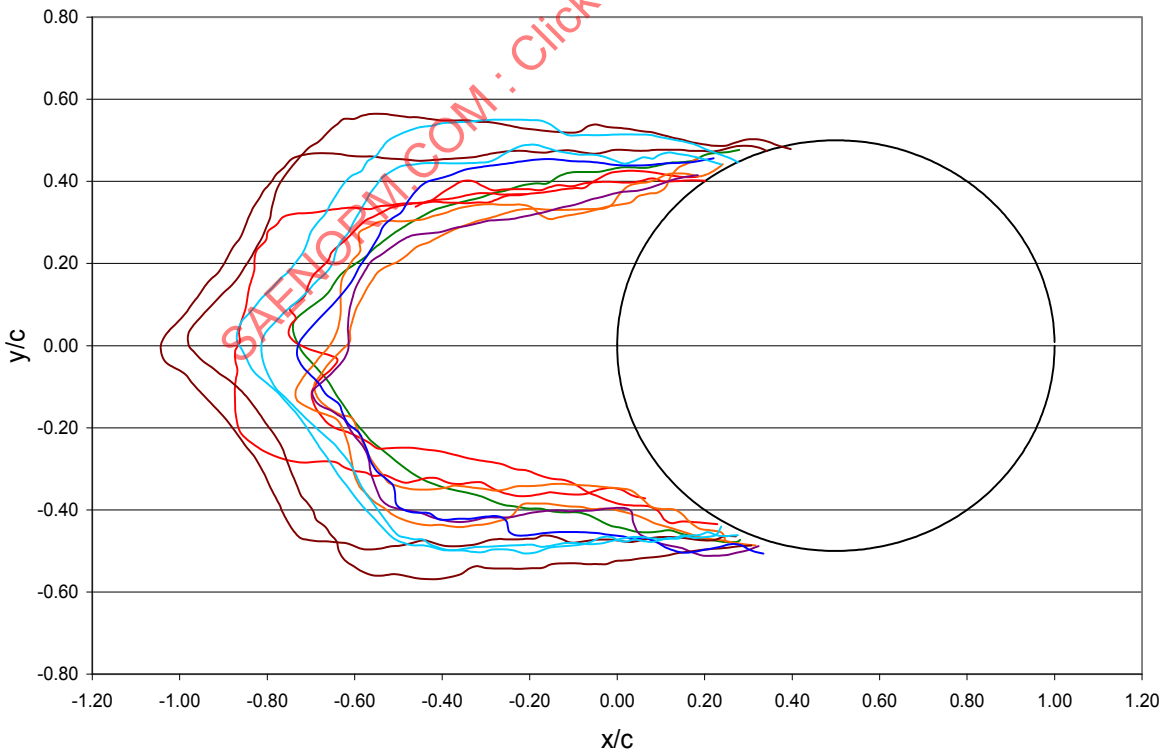

FIGURE 14 - CENTERLINE TRACINGS FROM ALL PARTICIPATING FACILITIES FOR THE 1.5 IN CYLINDER-FOR TEST CONDITION 11 OF TABLE 2 (MVD OF R1F, R2F AND R3F = 24 MM)

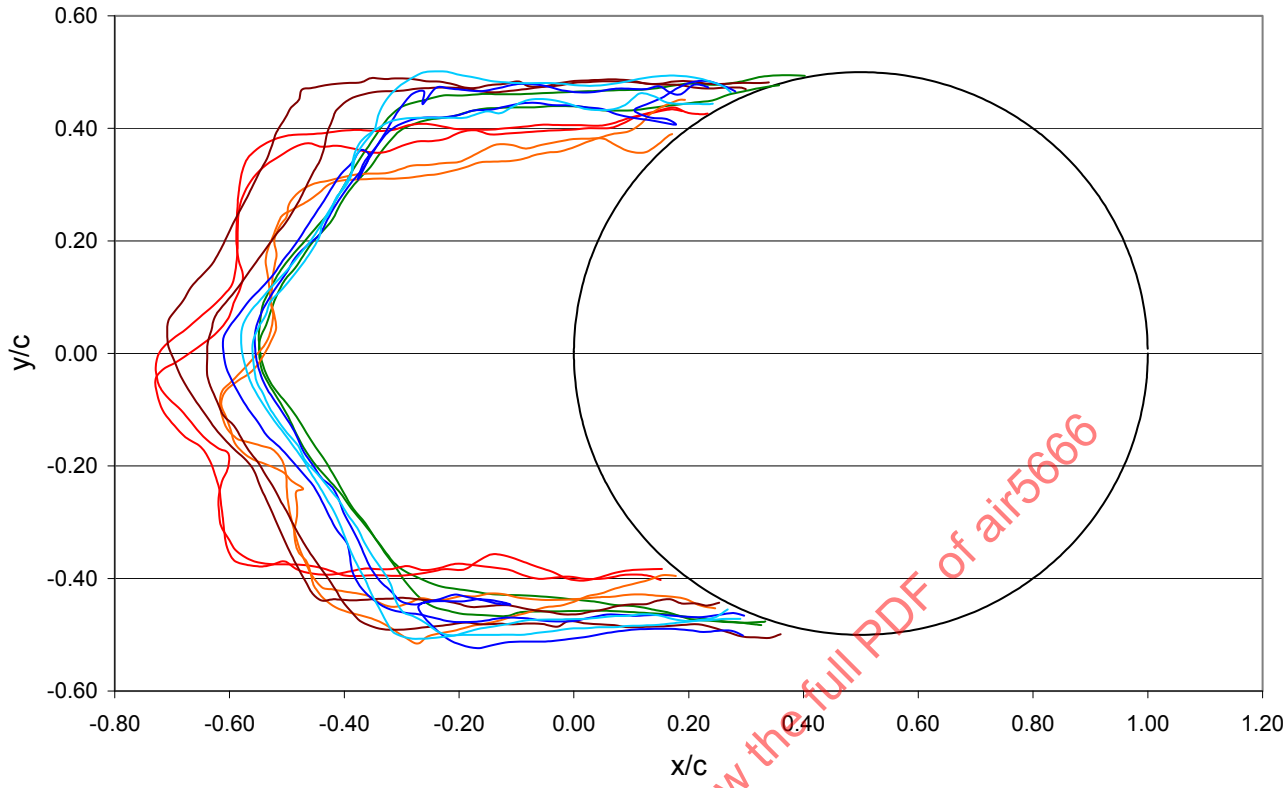

FIGURE 15 - CENTERLINE TRACINGS FROM ALL PARTICIPATING FACILITIES FOR THE 1.5 IN CYLINDER-FOR TEST CONDITION 9 OF TABLE 2

6.2 Identification of Probable Problem Areas

As seen in Table 1, there are substantial differences in the size of the participating facilities. Facility size could conceivably affect results by virtue of wall interference effects and by virtue of effects on velocity and temperature equilibrium between spray drops and the tunnel air, as well as on evaporation from the drops. Figure 16 shows estimated wall interference effects for the three models used in the present tests as a function of height of the icing wind tunnel test section. The figure shows the percent error in the air velocity at the point of maximum velocity (suction peak) for each model, calculated using a potential flow code. Wall interference effects are acceptably small for the 12 in NACA 0012 at three degrees incidence and for the 1.5 in cylinder models in all participating tunnels, but they may be a concern in the smaller tunnels for the 36 in chord NACA 0012 airfoil at three degrees incidence.

A time-integrating code was developed in Excel® to compute drop velocity, temperature, and diameter as drops moved from the spray nozzles to the model along the tunnel centerline. Bragg's drag law, Bragg [1982], and a convective heat transfer relation from Smolik, et al [2001], valid for Reynolds numbers in the range $0 < Re < 100$, were used. The usual analogy between convective mass and heat transfer (Kreith [1965]) was used to estimate evaporation rate and evaporative heat transfer. The results were found to be insensitive to the heat transfer correlation, provided it had the correct theoretical limiting value of 2.0 for Nusselt number for Reynolds numbers below about 1.

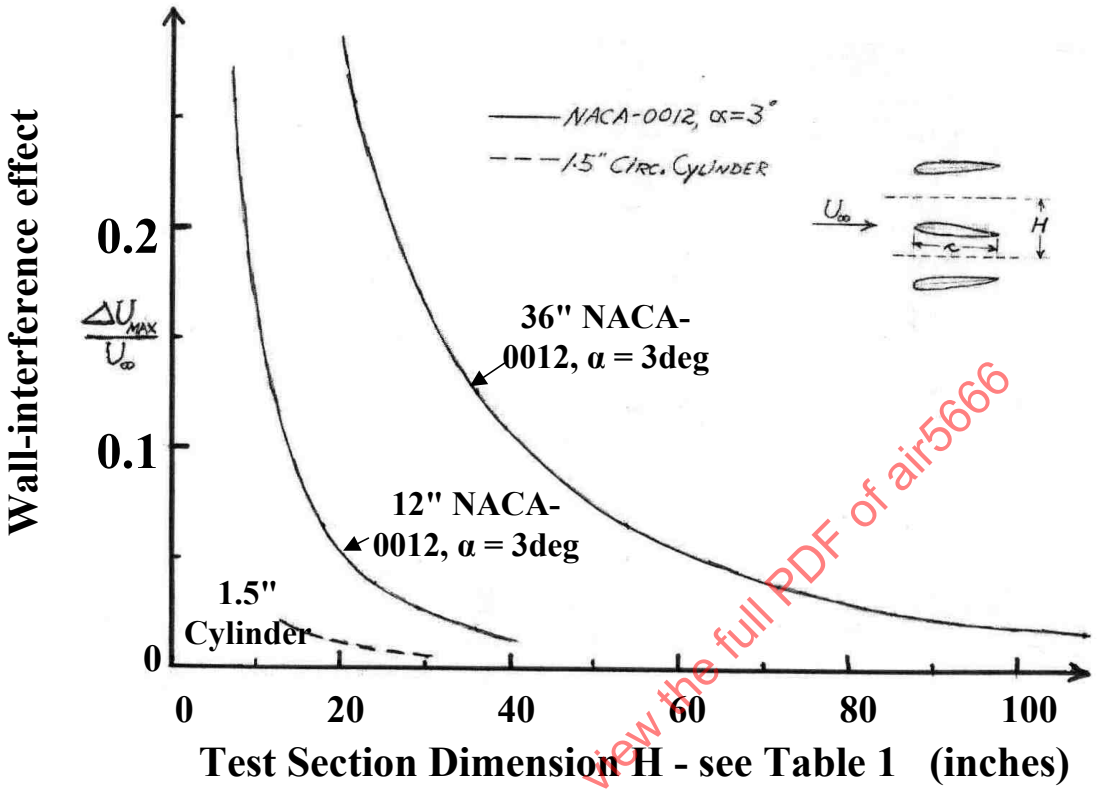

FIGURE 16 - ESTIMATED WALL INTERFERENCE EFFECTS FOR THE THREE MODELS AS A FUNCTION OF TEST SECTION HEIGHT; THE ORDINATE GIVES THE ERROR IN THE NON-DIMENSIONAL AIR VELOCITY AT THE SUCTION PEAK OF THE CLEAN MODELS

Figure 17 shows results for 20 and 40 µm drops in a hypothetical small tunnel having a contraction ratio of 6 and a contraction length of 3 m (10 ft). For these plots the tunnel air temperature and the initial temperature of the drops are assumed to be -7 ºC (20 ºF) and +20 ºC (68 ºF), respectively. Initial drop velocity at the nozzles is assumed to be 10 m/s (22 mph) and the airspeed in the test section is assumed to be 90 m/s (200 mph). The graphs show that the temperature and velocity of the drops and of the air are virtually identical from about 0.5 m (1.7 ft) aft of the contraction exit. This is true for any reasonable values of initial drop temperature, velocity, and contraction ratio. Also, even with a tunnel air relative humidity of 70% the diameter of the 20 µm drops decreases only about 4% by 8 m (26 ft) downstream of the spray nozzles. The decrease is only 1% for a more realistic relative humidity of 100%. It can be concluded that neither non-equilibrium of temperature and velocity nor excessive evaporation are problems for the size range of the participating tunnels for the test conditions of Table 2.

Assuming that uniformity of dynamic pressure and flow angularity are within generally accepted limits in all of the participating facilities, quality of the time-average flow in the tunnels need not be a significant concern in this discussion.

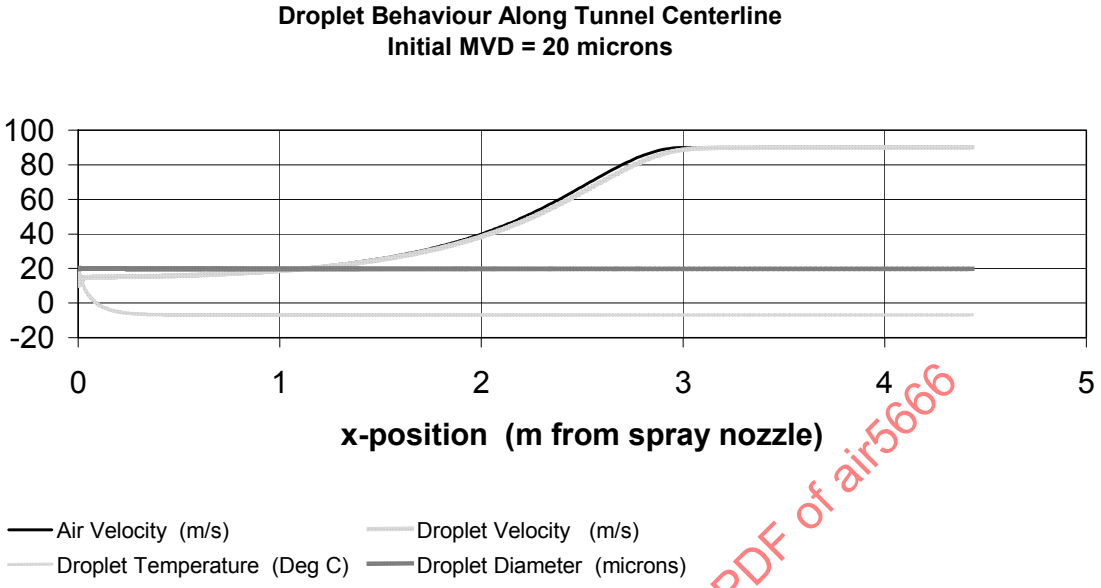

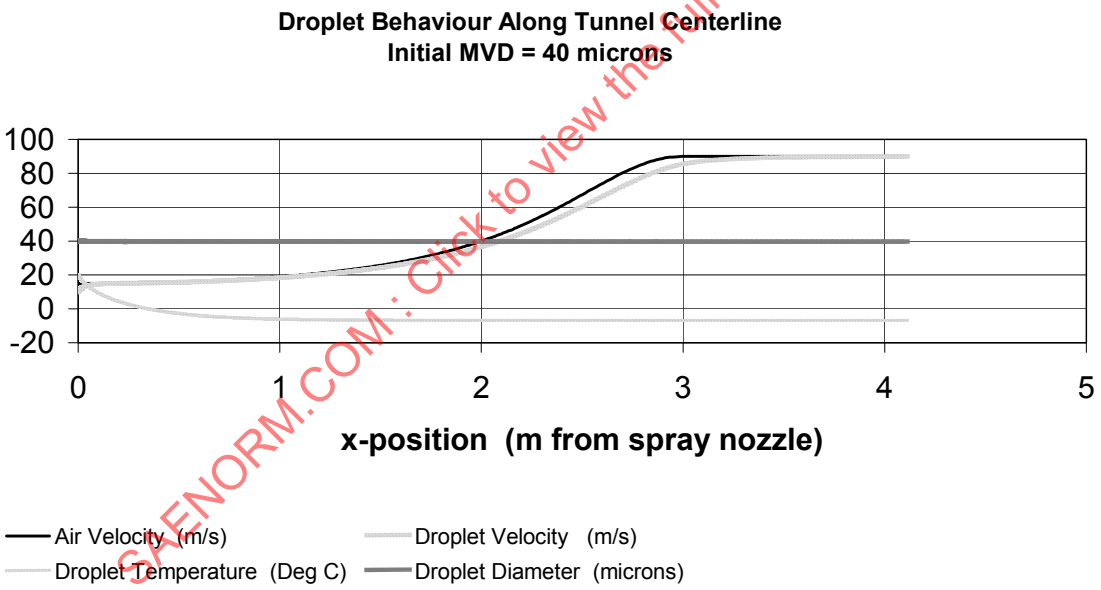

FIGURE 17 - DROP BEHAVIOR ALONG TUNNEL CENTERLINE, RELATIVE HUMIDITY OF TUNNEL AIR = 70%

Turbulence characteristics, vibrations, and acoustic phenomena in the vicinity of the spray nozzles are known to affect the atomization process (Chigier [1993]) and thus the eventual drop size distribution. However, provided that they are repeatable, these effects will be accounted for in the facility calibration.

Freestream turbulence intensity and/or scale might conceivably affect the ice accretion process. There is, however, little information available on this. In one-phase airflows, the freestream turbulence characteristics can affect transition, boundary-layer development, separation positions, and convective heat transfer rates (White [1991]). The effects are somewhat similar to those of surface roughness. In the case of icing, especially glaze icing, the surface of the accreting ice is rough and separation positions tend to be fixed by abrupt changes of the surface slope. Thus it seems reasonable to expect that potential effects of freestream turbulence are largely overwhelmed by the effects of roughness and abrupt geometry of the accreting ice. Furthermore, the freestream turbulence intensity in the test section will tend to be similar in all of the participating icing wind tunnels, because all have approximately the same contraction ratio (see Table 1), all have spray bars and air-blast atomizing nozzles a short distance upstream of the contraction, and none have any flow conditioning devices between the spray bars and the test section. It seems unlikely that facility-to-facility differences in freestream turbulence characteristics are a major cause of the observed differences in ice accretion shape and size.

With the elimination of basic tunnel characteristics as probable major causes of the observed facility-to-facility differences, attention must turn to characteristics of the icing spray clouds at the model position in the icing tunnel test sections. Recall that both ice shapes and amounts of accreted ice differed substantially from facility to facility for the same specified test conditions. This is evident from both the plots of the tracings (e.g., Figures 2, 9, 11, 12, 13, and 14) and from the THICK results (e.g., Tables 6 and 7 and Figure 10). In particular, ice areas sometimes differ by a factor of roughly two. The discussion will focus on possible causes of the large discrepancies in ice area, which is proportional to the amount of ice accreted on the model during a test run. The same causes may well also be responsible for the discrepancies in ice shape, especially in glaze icing cases, where differences in liquid water impingement rates result in differences in freezing fraction and runback.

A measure of the mass of liquid that impinges onto the model during a test run is given by the product of the accumulation parameter, A_c, and the collection efficiency β. That is, e.g., Kind et al. [1998]:

$$A_c\beta = [LWC * V * \tau /(L\ \rho_w)]\beta \qquad \text{(Eq. 1)}$$

where:

LWC = the liquid water content of the spray cloud in the test section

V = the freestream airspeed

τ = the test-run duration

L = a measure of model size

ρ_w = the density of liquid water

If we are interested in the total mass of ice, the average collection efficiency is used for β. If we are interested in the spatial distribution of impinging water the local collection efficiency is used for β clearly the distribution of this β has an effect on the ice accretion shape. In the present context, barring operator errors, the facility-to-facility variations of V, τ, L, and ρ_w will be negligible. It is straightforward to measure and control V and τ reliably within the tolerances of Table 5; also model size, L, is identical and ρ_w is a virtually constant physical property. That leaves LWC and β as possible sources of discrepancies in mass of impinged water.

Discrepancies in LWC and β would translate directly into discrepancies in ice area, provided that aerodynamic stripping of liquid water is either negligible or the same in all facilities, and provided that the density of accreted ice is approximately the same in all facilities. In view of the discussion of flow quality, aerodynamic shear and pressure forces acting on liquid water accumulations on the ice surface should be approximately the same in all facilities so that the proviso regarding aerodynamic stripping should be satisfied. It is also reasonable to expect only small facility-to-facility variations of ice density, especially for the glaze icing cases.

It can be concluded that problems with LWC and/or collection efficiency are the most probable causes of the facility-to-facility discrepancies in ice areas. Of course the collection efficiency, β, is directly related to the diameter of the water drops in the spray cloud, i.e., the MVD, as well as to other parameters. Appendices C and D present extensive analysis and discussion of the test results that supports the conclusion that problems with LWC and/or MVD are a key factor in the facility-to-facility discrepancies. The analyses in these appendices give some indications of the particular facilities in which LWC and/or MVD discrepancies may be most problematic.

Having decided that problems with LWC and/or MVD are amongst the most probable causes of the substantial facility-to-facility discrepancies in ice areas, the discussion must now turn to consideration of the possible nature of the problems. Icing wind tunnels are normally calibrated using procedures similar to those outlined in ARP5905. Basically the calibration process consists of measuring the LWC and drop size spectrum or MVD in the tunnel test section over the full range of tunnel operating conditions and spray-system settings such as water pressure, temperature, and flowrate, and atomizing-air pressure and temperature. Graphical and/or analytical calibration relations between LWC and MVD and the tunnel and spray-system settings are then established on the basis of the calibration data. This would appear to ensure that, within a facility's capability envelope, specified values of LWC and MVD can readily be obtained in the test section simply by using the corresponding settings indicated by the calibration relations. At least in principle, however, two types of problems can occur.

First the LWC and/or MVD measurements during the calibration process could be inaccurate so that use of settings aimed at achieving certain specified values produces different actual values, resulting in different actual LWC and MVD in different facilities. Second, there might be unknown factors which affect the relationships between LWC and MVD and the various system settings in some haphazard way so that the calibration relationships may be seriously wrong for some or all test runs. Problems of the second type would cause deficiencies in repeatability. Potential problems of both types will be considered next, first for LWC and then for MVD.

6.3 Potential Accuracy and Repeatability Problems with LWC

ARP5905 recommends use of an icing blade, rotating cylinder, or calibrated hot-wire instrument for LWC calibration. Details on each method are provided in the Appendix of ARP5905, where the hot-wire instrument is specifically a King probe. The appendix suggests that an LWC calibration accuracy of better than ±10% can be achieved with careful use of a rotating cylinder or King probe and implies a similar accuracy for an icing blade. A recent paper by Strapp, et al [2003] contains much valuable information on the accuracy of both LWC and particle-sizing instrumentation. The icing blade and rotating cylinder can be considered as primary instruments for LWC measurement and Strapp, et al [2003] indicates an absolute accuracy of roughly ±5% for them. It also indicates that random tunnel variations can be expected to contribute an additional dispersion of about 3.5% to calibration points giving an overall accuracy consistent with the ±10% suggested by ARP5905, Strapp, et al. [2003] show evidence both from their own experiments and others that the response of the King probe rolls off for MVD values above about 30 μm. The LWC indicated by a King probe when MVD = 50 μm is only about 70% of that when MVD = 20 μm, for the same reference LWC. Thus unless appropriate calibrations are used for each MVD value, a King probe could give LWC readings that are roughly 25% low at the MVD = 40 μm values specified for Test Conditions 5 and 6 of Table 2. Inaccuracies of LWC calibrations could thus account for about a 25% ice-area discrepancy for test conditions 5 and 6 if LWC values are established using a King probe that has not been calibrated at an MVD of about 40 μm. The maximum observed discrepancies are however much larger, roughly 100%. Moreover the large discrepancies in ice area also occurred when the specified MVD was 20 μm. Assuming that the LWC calibrations of the participating facilities were carried out with due care, it can be concluded that inaccuracies in LWC calibration are probably not a major cause of the observed facility-to-facility discrepancies in ice area or ice shape.

If the water flowrate supplied to the spray nozzles is monitored during testing and is consistent with values during facility calibration, it is unlikely that the total water content in the test section will be substantially different from calibration values. However the liquid water content, LWC, could differ substantially if the amount of water that freezes out, rather than remaining supercooled, varies in some haphazard way. It is known, that if the temperature of the atomizing air drops too low upon expansion, drop crystallization occurs (Marek and Bartlett [1988]). That is, some of the spray drops freeze rather than remaining liquid and becoming supercooled. This, of course, results in lowered LWC. Appendix B of ARP5905 outlines how the possibility of freezeout should be dealt with during the tunnel calibration process; it basically involves determining acceptable temperature ranges for the atomizing air and spray water for all operating conditions. Provided that freezeout behavior is repeatable over medium and long periods of time, this should ensure satisfactory determination of actual LWC values from the calibration data. If, on the other hand, freezeout behavior is unstable over time, repeatability of results from the facility will suffer.

This could be a significant contribution to the observed facility-to-facility discrepancies in ice areas and ice shapes. While discussion at the August and October 2003 workshop and meeting indicated that current opinion does not support this speculation, it is inescapable that there are large unexplained facility-to-facility discrepancies in the ice-accretion results. The possibility of variations in drop freezeout due to haphazard variations in spray-water or atomizing air characteristics should not be completely dismissed at this stage as a potential contributing factor, although it is probably more applicable to rime ice conditions than glaze ice conditions.

6.4 Potential Accuracy and Repeatability Problems With MVD

ARP5905 gives some guidance on MVD calibration of icing wind tunnels, but does not consider accuracy of the drop-sizing instruments that are of course central to the procedure. Instruments commonly used for this purpose for drop sizes below about 60 μm are the forward scattering spectrometer probe (FSSP), the Malvern particle size analyzer or equivalent (MPSA) and the phase Doppler array probe (PDPA). The FSSP shines a laser beam through a tube through which a portion of the particle-laden airflow passes. As tested in these wind tunnels, the MPSA is not exposed to the moist airstream and is only suitable for use with small tunnels; it shines a laser beam through the entire test-section flow and thus deduces a transverse average of the particle size spectrum from the scattering of the laser beam. The PDPA splits a laser beam into two and uses the Doppler shift frequency and spatial frequency of the interference pattern produced when a particle crosses the small volume where the two laser beams intersect. More detailed descriptions of these and other instruments are available in Schick and AIR4906. AIR4906 explicitly considers their application in icing test facilities and discusses accuracy in qualitative terms. It gives quantitative estimates of repeatability, but not of absolute accuracy, for some of the instruments.

Strapp, et al [2003] includes a discussion of the accuracy of drop-sizing instrumentation. Several FSSP probes were tested in the NASA IRT in the study of Strapp, et al [2003]. The authors found the icing wind tunnel to be a particularly challenging environment for FSSPs, because of the high number-density or concentration of small particles in the spray cloud, a feature not typical of natural clouds where FSSPs are widely used. Only with “much remedial effort” were they able to obtain stable data at an airspeed of 67 m/s and no useful data was obtained at 100 m/s. This suggests that FSSP measurements during calibration of icing tunnels could be highly inaccurate unless suitable steps, for example operation of a reduced number of spray nozzles, are taken during calibration. An earlier study, Olsen, et al [1983], had more success with FSSPs and ASSPs, a somewhat similar drop sizing instrument that is no longer in use. Olsen, et al [1983] found that repeatability of individual FSSP/ASSP instruments was good with an uncertainty (for 95% confidence or two standard deviation limits) of about ±3%, but that MVD indications from different instruments differed widely with about ±30% overall uncertainty. On the other hand, Strapp, et al [2003] concluded that an accuracy of about ±10% was attainable with a PDPA in cases where all of the drops in the distribution were less than 62 μm, as may be the case for the 20 μm study cases. They did not report any results for an MPSA which is more suitable than FSSPs for high density sprays {AIR4906).

Calibration of FSSPs, MPSAs, PDPAs, and other optical particle-sizing instruments relies on scattering or other optical theory, (AIR4906). Strapp, et al [2003] states that there is no true MVD reference standard, making rigorous error estimates impossible. The oil slide technique (AIR4906) would appear to be useful as an MVD reference standard, but it is cumbersome and tedious and thus not well suited for MVD calibration of instruments or facilities. Knezevici, et al [2005] reports considerable success in adapting the rotating multicylinder method, previously used only in meteorological icing work, for measurement of LWC and MVD in icing tunnels. Four separate rotating cylinders having diameters ranging from 2.1 to 40 mm are inserted, one after the other, into the icing tunnel test section and the mass of ice accreted on each cylinder is determined by weighing. Since collision efficiency depends on MVD as well as on cylinder diameter, MVD can be determined together with LWC by a regression analysis procedure. The method appears to have good potential for use as a reference standard for calibration of both LWC and MVD instrumentation.

It would appear that instruments presently available for particle sizing are complex, relatively difficult to use, and subject to errors from a variety of causes. In the words of AIR4906 none of them can be considered 'turnkey' systems. Moreover their absolute accuracy is difficult or impossible to quantify. Table 1 includes information on what particle-sizing instruments were used in the MVD calibration of the facilities participating in the present facilities standardization study. Strapp, et al [2003] tentatively suggests an uncertainty of ±10 to ±30% MVD values within the range of this study. As already mentioned, Olsen, et al [1983] found a ±30% scatter of MVD measurements from different FSSP/ASSP instruments. The ±30% uncertainty is for a confidence level of 95% which corresponds to two standard deviations; that is, 95% of measured values can be expected to be within two standard deviations, or in this case ±30%, of the true value (AGARD AR 304). Assuming that the probability density distribution is normal or Gaussian, about 1% of values can be expected to fall beyond 2.6 standard deviations, or about ±40%, from the true value. It is thus plausible that for the same specified value of MVD the highest actual MVD value in one of the six participating facilities was roughly twice that in another participating facility (140% versus 60%).

Figure 18 shows LEWICE 2.0 computational results for collection efficiency and ice shape for case N12-07, for the specified MVD of 20 μm and also for MVD values of 13 μm and 27 μm. Note the large differences in areas under the collection-efficiency distribution curves and the directly corresponding differences in ice areas. Clearly uncertainties of order ±30% in true MVD values could account for a substantial part of the observed facility-to-facility differences in ice areas. The differences in the distributions would also cause differences in ice shape in both rime and glaze icing cases.

If non-repeatability of drop freezeout were indeed a problem, as discussed in 6.3, MVD would most probably also be subject to non-repeatability since the larger drops are more prone to freezeout. This is because, for thermodynamic reasons, larger drops are less stable in the liquid state at sub-freezing temperatures. For a given initial drop-size distribution, MVD will thus tend to decrease as more freeze out occurs. The lower attendant values of collection efficiency would tend to aggravate somewhat the effects of decrease in LWC in the tunnel test section.

6.5 Potential Problem Areas of Secondary Importance

As discussed above, the main probable causes of the observed facility-to-facility discrepancies are problems with LWC and/or MVD of the spray clouds. However a few additional issues may be possible contributing factors of secondary importance. These are briefly mentioned here.

At the August 2003 Facility Owners Workshop it was suggested that erosion of developing ice accretions by ice particles circulating in the tunnel circuit may be responsible for discrepancies in ice area in rime conditions. It is surmised that the circulating ice particles are shed from tunnel components in some facilities under some conditions. This deserves investigation.

Another possible contribution to systematic differences in ice tracings between facilities is differences in operator tracing technique. Examples of different tracing techniques can be found in Run 2 of the N12-01-Composite-SAE and N12-03-Composite-SAE files found on the CD. In these cases, Facility H compared the results of their standard tracing technique (using a specialized tracing instrument) to those obtained using a pencil. While discernible differences can be noticed in comparing the techniques, the magnitude of the differences in these cases appears to be smaller than that noted in comparing tracings from different facilities.

Miller, et al [2005] recently presented results for change in total mass of accreted ice when the LWC is changed by about ±15% and all other parameters are held constant. The measured changes in ice mass were not usually directly proportional to the changes in LWC, as one would expect from Equation 1, if aerodynamic stripping was negligible. This would suggest that aerodynamic stripping of liquid water from the surface of the accreting ice may be significant, at least in glaze icing conditions, and that factors, such as model vibration, that might affect it should be monitored. One can speculate that facility-to-facility differences in model vibration may have contributed somewhat to the observed discrepancies in ice shape. However this would not be an issue in rime icing conditions, Cases 7 to 11 of Table 1, for which facility-to-facility discrepancies in accreted ice area were also substantial.

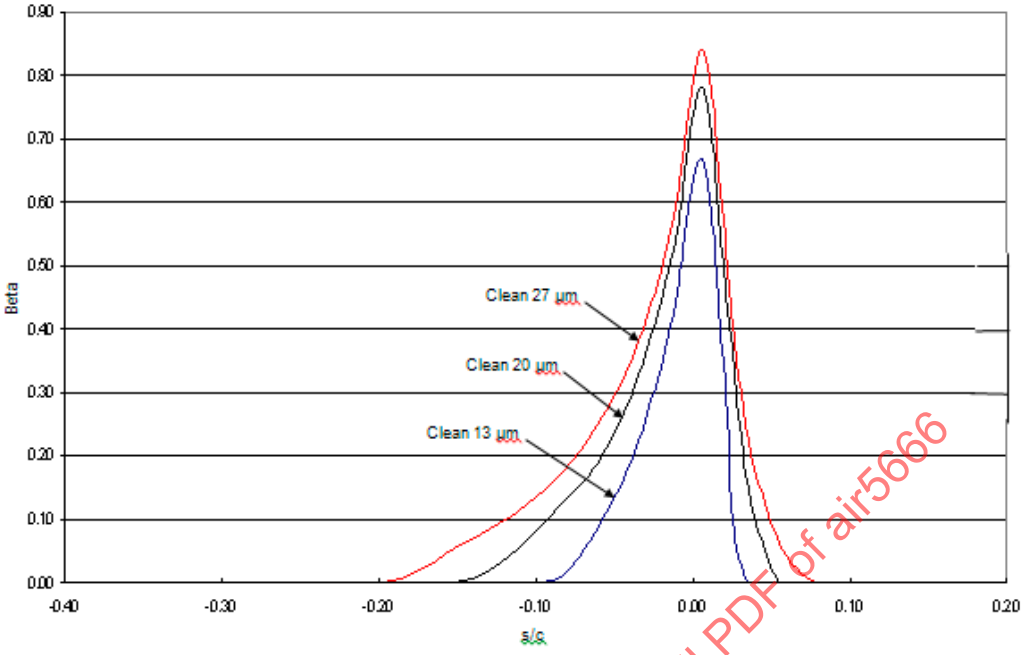

FIGURE 18A - LEWICE 2.0 COMPUTED COLLECTION EFFICIENCIES

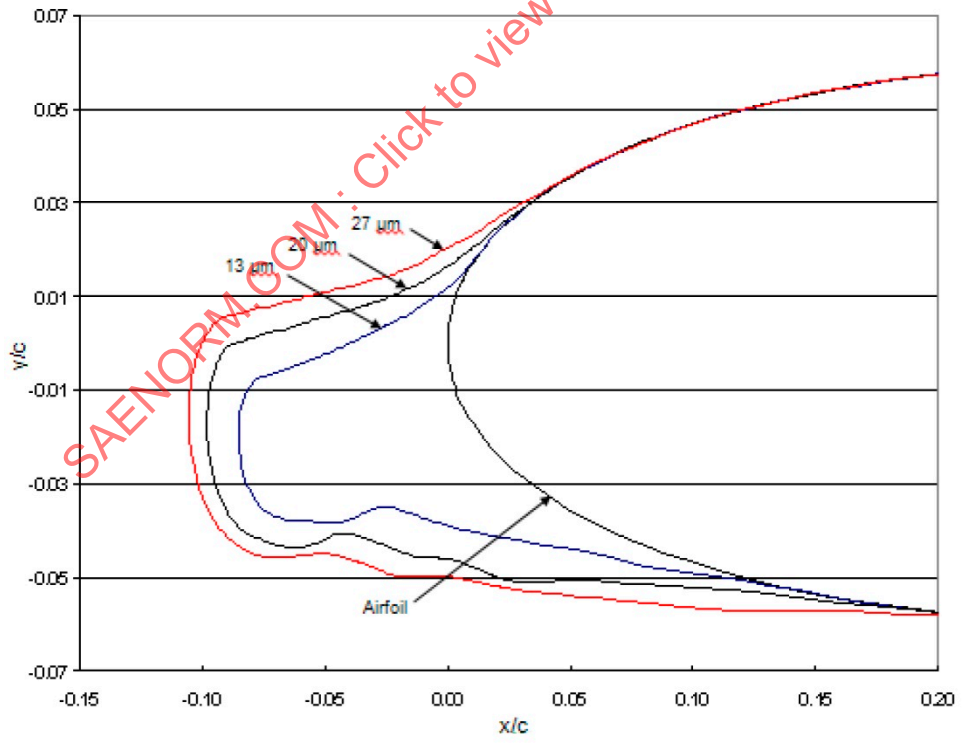

FIGURE 18B - LEWICE 2.0 ICE SHAPES

FIGURE 18 - LEWICE 2.0 COMPUTED COLLECTION EFFICIENCIES AND ICE SHAPES FOR MVD = 13, 20 AND 27 MICROMETERS FOR 12 IN NACA 0012 AT 3 DEGREES INCIDENCE, - 30 °C, V = 67 M/S, LWC = 0.5 G/M^3, 20 MINUTE EXPOSURE

7. CONCLUSIONS AND RECOMMENDATIONS

Icing tests using the same models have been done in six tunnels for a number of specified test conditions. For any particular target test-conditions the ice accretions produced in all of the participating facilities bore a broad resemblance to one another, but there were substantial facility-to-facility differences in ice shape and ice area or volume of accreted ice. Ice areas varied by a factor of roughly two for the three models (36 in and 12 in NACA 0012 airfoils at 3 degrees incidence and a 1.5 in diameter circular cylinder) and for both rime and glaze icing conditions.

Repeatability at each facility was good, with a few exceptions. The exceptions, although limited, may be indicative of problems of a somewhat sporadic nature.

Possible causes of the observed facility-to-facility differences are discussed. Wall interference, adjustment of drop velocity and temperature to tunnel air values, and drop evaporation are estimated to be acceptable in all participating facilities and are ruled out as probable causes of the differences. Difficulties with actual LWC and MVD are identified as the most probable causes of the substantial facility-to-facility discrepancies in ice areas and ice shapes.

The usual techniques of measuring LWC for calibration purposes are judged to be sufficiently accurate. It is somewhat plausible, however, that actual LWC values may occasionally vary substantially in a haphazard way from calibration values, due to variations in drop freezeout associated with variations of water-quality and perhaps also of atomizing-air quality.

The uncertainty of techniques normally used to determine MVD for calibration purposes is difficult to quantify and may well be rather large, of order ±30%. Actual MVD values could then differ by a factor of roughly two at different facilities for the same target value of MVD. Collection efficiency would then also differ greatly, giving rise to substantial differences in ice area and ice shape.

The basic reasons for the problems with LWC and/or MVD can probably only be identified by comparative experimental work. It is recommended that facility owners occasionally run one or more of the test cases of Table 2 (e.g., cases 2 and 6) to monitor long term repeatability in their facility. A replica of the cylinder model would be simple to make and suitable for this purpose. Informal interfacility comparison of the observations may provide some insights. It is also recommended that the aforementioned multiple rotating cylinder apparatus of Knezevici, et al [2005], which belongs to the NRC/AIWT facility, be circulated to other facilities and that the measured ice masses accreted on each of the four cylinders for a few sets of target conditions be compared. Simultaneous, or nearly simultaneous, measurements of LWC and MVD in the test section of one or more facilities using different instruments is also recommended. Facility owners should also be alert to the possible significance of the potential secondary problem areas mentioned in the discussion.

8. ACKNOWLEDGMENTS

The significant investments made by the participating facility owners and the United States Federal Aviation Administration are gratefully acknowledged.

9. NOTES

9.1 A change bar (l) located in the left margin is for the convenience of the user in locating areas where technical revisions, not editorial changes, have been made to the previous issue of this document. An (R) symbol to the left of the document title indicates a complete revision of the document, including technical revisions. Change bars and (R) are not used in original publications, nor in documents that contain editorial changes only.

PREPARED BY SAE SUBCOMMITTEE AC-9C, AIRCRAFT ICING TECHNOLOGY OF
COMMITTEE AC-9, AIRCRAFT ENVIRONMENTAL SYSTEMS

APPENDIX A - TEST PLAN

The following is the original test plan for the facilities standardization test program. This plan has evolved and may not have been followed in its entirety. It has been modified to conform to SAE format.

ICING GROUND SIMULATION FACILITY
ICE SHAPE COMPARISON TEST
WORK PLAN (REV. 4, 7-JAN-00)

A.1 INTRODUCTION & BACKGROUND

An acceptable icing ground simulation facility is one that credibly simulates conditions from the 14 CFR Part 25 and 14 CFR Part 29 Appendix C aircraft/rotorcraft icing envelope.

The SAE AC-9C Aircraft Icing Subcommittee chartered the “Icing Facility Characterization Panel” in 1989 to better understand and improve the quality of ground ice accretion testing. The tangible accomplishment of this panel is the publication of AIR5320, “Summary of Icing Simulation Test Facilities." This AIR is the first step to the goal of improving ground ice accretion testing.

At the Spring ’97 SAE AC-9C meeting held in Minneapolis, MN, the Facility Standardization Panel was chartered. The purpose of this Panel is to define standards for icing simulation facilities with respect to icing cloud and aerothermodynamic characteristics. The need arises from a requirement to comply with the above listed 14 CFR Part 25 and Part 29, i.e., the need of the airframe, propulsion systems, ice protection systems and other OEMs to use acceptable ground simulation facilities for designing, building, and certifying safe aircraft.

The approach presented and agreed to at the Fall ’97 SAE AC-9C subcommittee meeting, held in Pittsburgh, PA, was a four phase program leading to the development of an Icing Facility Standard. The four-phased program is shown schematically in Figure 1. The first phase of this program includes the facility comparison test described herein. The purpose of the first phase is to conduct a controlled experiment to quantify the comparison of ice shapes created in different icing facilities. This is accomplished by measuring the predominant features of glaze, mixed and rime ice accretions and using the data analysis techniques described in A.9 of this work plan to compare ice shape similarities/differences. The second phase of the Facility Standardization program is to characterize the ground simulation facility “independent” variables including aerothermodynamic and icing cloud characteristics and to establish uniform or translatable cloud calibration methodology, measurement (instrumentation) methods and data processing techniques. The third phase of the program will include establishing facility-to-facility relationships or characterization of the “dependent” variables. These include defining ice shape similitude criteria and the measurements of ice shape induced aerodynamic effects on airfoil lift and drag. Phase four is the completion of an “Icing Ground Simulation Standard.” The need for phases 2 and 3 of this program is dependent upon the results of phase 1.

Concurrent with the SAE sponsored Facility Comparison Test, the FAA has formed a working group 11A to address simulation validation requirements issues that are documented in the FAA Icing Plan. The work of the SAE Facility Standardization Panel supports the efforts of the FAA 11A Simulation Validation Requirements working group. The icing ground facilities subgroup of the 11A working group is authoring an “Icing Ground Simulation Standard.” This is being done concurrent with this Facility Comparison Test program with the understanding that Facility Comparison Test results may have an impact on the content of the “Icing Ground Simulation Standard.”

A.2 PROJECT OBJECTIVE & APPROACH

This work plan describes the Facility Comparison Test being sponsored by the SAE AC-9C Aircraft In-flight Icing Subcommittee. The objective of the test is to compare ice accretion shapes from various icing ground simulation facilities to validate the similarities that exist between these facilities.

The proposed approach is to use two NACA 0012 airfoils (36-in chord and 12-in chord) and one 1.5-in diameter cylinder. The participating facilities in this facility comparison test are identified in A.3. The test conditions are defined in A.4. The similarities and/or differences in ice accretion shapes produced by each facility will be quantified using the methodology described in A.9. Each participating facility should have their facility calibration report on record prior to the start of the Facility Comparison test and will make this available to the Facility Standards Panel if necessary.

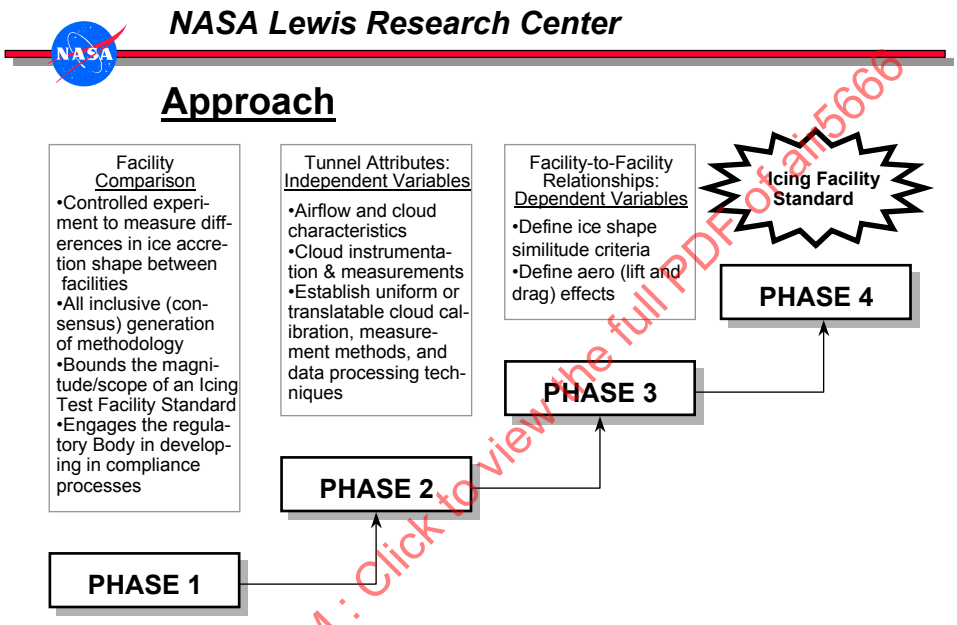

FIGURE A1 - FOUR STEP APPROACH TO ICING GROUND SIMULATION FACILITY STANDARDIZATION

A.3 FACILITIES ASSIGNED TO THE PROJECT

The list of tentative participating facilities is provided in Table A1.

TABLE A1 - TENTATIVE LIST OF PARTICIPATING FACILITIES

Org/Facility	Location	Contact	Test Section Size	Max Speed
NASA GRC Icing Research Tunnel	Cleveland, OH U.S.A.	John R. Oldenburg	6 ft X 9 ft X 20 ft	430 mph
Boeing Research Aerodynamic Icing Tunnel	Seattle, WA U.S.A.	Gene Cain	6 ft X 4 ft X 20 ft	288 mph
BF Goodrich Icing Tunnel	Uniontown, OH U.S.A.	Dave Sweet	3.7 ft X 1.8 ft X 5 ft	200 mph
Cox & Co. LeClerc Icing Wind Tunnel	New York, NY U.S.A.	Kamel Al-Khalil	3.8 ft X 2.3 ft X 6.5 ft	220 mph
AEDC R-1D	Tullahoma, TN U.S.A.	Tom Tibbals	3 ft. (dia.) X 9 ft	615 mph
NRC Icing Tunnel Facility	Ottawa, Ontario Canada	Myron Oleskiw	1.9 ft X 1.9 ft X 6 ft	201 mph
ONERA S1MA Wind Tunnel	Modane, France	Joseph Prieur	20.2 ft (dia.) X 46 ft	224 mph
ACT Artington Icing Wind Tunnel	Artington, England	Dave Armstrong	1.5 ft X 1.5 ft X 5.5 ft	410 mph
CEPr S1 and R6	Paris, France	Sophie Le Berre	0.7 ft X 0.7 ft X 1.64 ft	418 mph
CIRA IWT	Capua, Italy	Ludovico Vecchione	7.1 ft x 6.8 ft x 21.2 ft	300 mph

A.4 RANGE OF TEST CONDITIONS, CONFIGURATIONS, AND DETAILED TEST MATRIX

Three test articles are to be used in this test. They include a 36-in chord NACA 0012 airfoil, a 12-in chord NACA 0012 airfoil and a 1.5-in cylinder. Design details of the test articles are found in the following section. The test matrix for all models is shown in Table A2.

TABLE A2 - DETAILED TEST MATRIX

					Icing Time (min)				
Run ID	Static Temp. °C/°F	LWC g/m^3	Droplet Size µm	Speed m/s/mph	36 in NACA 0012	12 in NACA 0012	1.5 in Cylinder	Icing Type	Repeat Cond.[3]
1	-7/20	0.5	20	67/150	25	20	15	Glaze	3
2	-7/20	0.5	20	90/200	20	15	10	Glaze	3
3	-7/20	1.0	20	67/150	20	15	10	Glaze	3
4	-7/20	1.0	20	90/200	15	10	10	Glaze	3
5	-7/20	1.0	40	67/150	20	15	10	Glaze	3
6	-7/20	1.0	40	90/200	15	10	10	Glaze	3
7	-30/-22	0.5	20	67/150	25	20	15	Rime	2
8	-30/-22	0.5	20	90/200	20	15	10	Rime	2
9	-23/-10	0.5	20	67/150	25	20	15	Rime	2
10	-23/-10	0.5	20	90/200	20	15	15	Rime	2
11	-30/-22	1.0	20	67/150	15	10	10	Rime	3
12	-7[1]/20	0.5	20	90/200	20	15	10	Glaze	1

NOTES:
[1]. For run ID 12 the temperature is a model indicated temperature.
[2] Icing times were determined using LEWICE calculations as a guide to establishing run times. Final run times were rounded up in increments of 5 min.
[3] Repeat conditions defines the minimum number of times, or replications, that each icing condition should be run.

The run times were determined by running the LEWICE computer program and establishing the time necessary to accrete a large enough ice shape in order to make accurate measurements of the ice shape features necessary to use the comparison methodology described in A.9. For the rime conditions, this is a 1-in buildup of accreted ice and for the glaze conditions, the times correspond to 1 in horn length ice accretion. The aerodynamic angle-of-attack for both NACA 0012 airfoils shall be 3 degrees. Preliminary calculations indicate that the model blockage in the smaller facilities may limit airspeed to less than specified in the test matrix.

The detailed test procedure to be followed in conducting the test is as found in Appendix AA. The entire set of conditions should be completed prior to doing repeats. The test sequence, using the Run ID from the table above shall be 6, 4, 2, 1, 3, 5, 10, 9, 8, 11, and 7 during the first set of icing sprays for each model. The second set test sequence shall be 7, 11, 8, 9, 10, 5, 3, 1, 2, 4, and 6. The third set test sequence shall be 6, 4, 2, 1, 3, 5, 11, and 12. Repeat conditions should be run hot to cold, cold to hot and then hot to cold. If a facility is unable to reproduce the specified test condition, then that point should be eliminated from the test matrix and the sequence continued with the next doable condition. Under no circumstances should repeat conditions be run back-to-back.

Participants have been tasked with calculating and defining their facility capabilities with regards to the test conditions specified above. Test participants are instructed to eliminate any test point that cannot be reproduced in their facility.

A.5 TEST HARDWARE DEFINITION

Assembly drawings of the 36-in chord and 12 in chord models were completed by Boeing and distributed at the Spring 1998 AC-9C meeting, held in Las Vegas, Nevada. The span (length) of both models is 22 in.

The drawings numbers and titles of the 36 in chord and 12 in chord models are as follows (all numbers are Boeing numbers):

218X0148 (Rev B) Structure, Test Article - 36 in Icing Model (Lab Test Only)

218X0149 (Rev B) Skin, Leading Edge - 36 in Icing Model (Lab Test Only)

218X0150 (Rev B) Skin, Upper/Lower - 36 in Icing Model (Lab Test Only)

218X0151 (Rev New) Structure, Adapter - 36 in Icing Model (Lab Test Only)

218X0152 (Rev New) Skin, Leading Edge - 36 in Icing Model (Lab Test Only)

218X0153 (Rev New) Skin, Upper - 36 in Icing Model (Lab Test Only)

218X0157 (Rev A) Structure, Test Article - 12 in Icing Model (Lab Test Only)

218X0158 (Rev B) Skin, Leading Edge - 12 in Icing Model (Lab Test Only)

218X0159 (Rev New) Skin, Upper/Lower 12 in Icing Model (Lab Test Only)

218X0160 (Rev New) Adapter - 12 in Icing Model (Lab Test Only)

218X0161 (Rev New) Skin, Leading Edge - Adapter, 12 in, Icing Model (Lab Test Only)

The drawing of the 1.5-in diameter cylinder was competed by NASA Glenn Research Center. The drawing number and title is:

7509M77A003 Shaft, FAA - Model Support - Ice Tunnel

A single set of models has been fabricated and assembled to these design drawings. The fabrication and assembly of the airfoils has been completed by the Boeing Company and upon completion and acceptance by the FAA and by NASA, will become government (NASA) owned equipment. NASA will be responsible for maintaining FAA conformity of the models and for all logistics associated with shipping models to the participating organizations for their tests. Procedures for pre- and post-test inspection of the models have been written by and will be performed by the NASA Glenn Research Center's Office of Safety, Environment and Mission Assurance (OSEMA).

A.6 INSTRUMENTATION NEEDS

The airfoil measurements to be taken include static pressure measurements, at up to 29 locations and model temperatures taken at 7 internal locations. Three measurements will be taken on the backside of the leading edge surface skin and 4 measurements will be taken on internal structures (rib/stringer). Temperature measurements only will be taken on the cylinder at three internal locations.

The static pressure taps on both the 12-in chord and 36-in chord airfoils will be located at the chord-wise locations on both sides of the symmetric airfoils as shown in Figure 2A, Figure 2B and Table A3.

All taps are to be located at the model span-wise centerline. Pressure taps will also be located at ±6 in above and below the centerline (span wise dimension) at the 30% and 60% chord locations. Thus, there will be four off-centerline taps on each side of the model. The delta between these off-centerline taps and the centerline location taps will be used as indicators of end, or wall, effects in the various facilities.

The model pressure measurements are to be acquired via a stand-alone data acquisition system. This will be a PC based data acquisition system that consists of two 16-channel pressure modules and a 20 channel A-D that can acquire both thermocouple and voltage inputs. The description of the Data Acquisition System is found in Appendix AB. Participants are required to setup this data acquisition system by making all necessary instrument connections.

The temperature measurements to be taken on the airfoils are as previously described. The actual T/C locations are shown on the airfoil drawings given in A.5. Photographs of the 12-in chord, 36-in chord, and cylinder models are found in Figs. 4A, 4B, and 4C respectively.

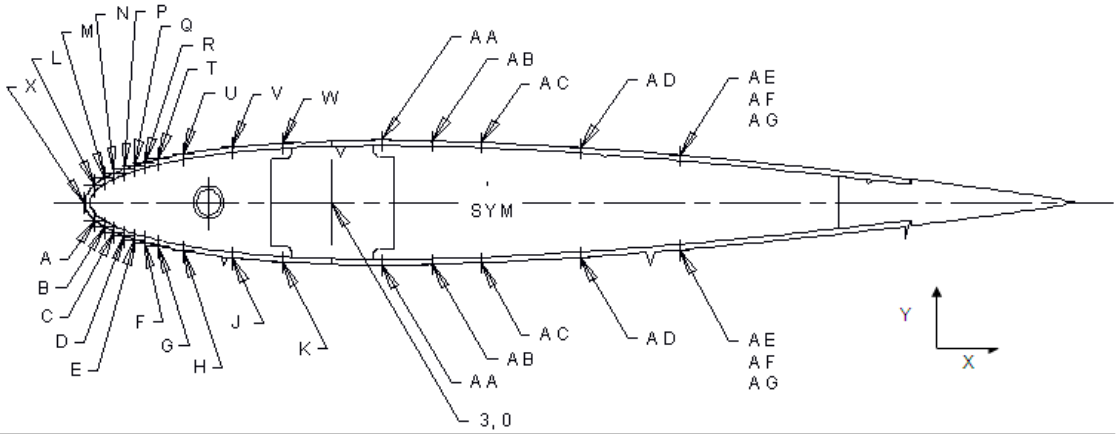

LEADING EDGE PORTS			LEADING EDGE PORTS			UPPER/LOWER SKIN PORTS		
POINT DEFINITION	COORDINATE VALUE 'X' (INCHES)	'Y' (INCHES)	POINT DEFINITION	COORDINATE VALUE 'X' (INCHES)	'Y' (INCHES)	POINT DEFINITION	COORDINATE VALUE 'X' (INCHES)	'Y' (INCHES)
A	0.120	- 0.204	M	0.240	0.283	AA	3.602	0.721
B	0.240	- 0.283	N	0.360	0.341	AB	4.203	0.714
C	0.360	- 0.341	P	0.480	0.387	AC	4.804	0.696
D	0.480	- 0.387	Q	0.600	0.427	AD	7.005	0.635
E	0.600	- 0.427	R	0.720	0.461	AE	8.207	0.547
F	0.720	- 0.461	T	0.900	0.504	AF	8.207	0.547
G	0.900	- 0.504	U	1.200	0.562	AG	8.207	0.547
H	1.200	- 0.562	V	1.800	0.641			
J	1.800	- 0.641	W	2.400	0.689			
K	2.400	- 0.689	X	0.000	0.000			
L	0.120	0.240						

FIGURE A2 - 12 IN MODEL CROSS SECTION - PRESSURE TAP LOCATIONS

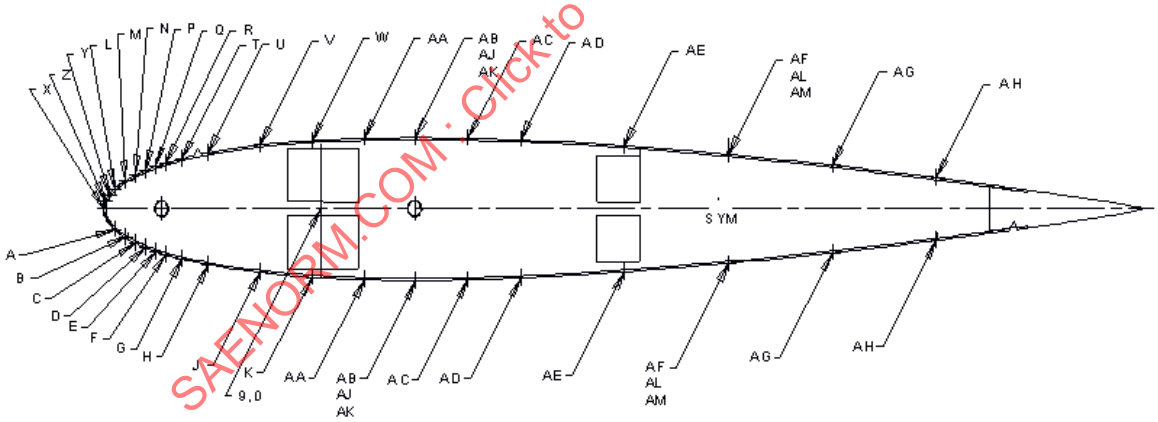

LEADING EDGE PORTS			LEADING EDGE PORTS			UPPER/LOWER SKIN PORTS		
POINT DEFINITION	COORDINATE VALUE 'X' (INCHES)	'Y' (INCHES)	POINT DEFINITION	COORDINATE VALUE 'X' (INCHES)	'Y' (INCHES)	POINT DEFINITION	COORDINATE VALUE 'X' (INCHES)	'Y' (INCHES)
A	0.360	- 0.613	L	0.360	0. 613	AA	10.500	2.138
B	0.720	- 0.850	M	0.720	0.850	AB	12.300	2.164
C	1.080	- 1.022	N	1.080	1.022	AC	14.100	2.141
D	1.440	- 1.162	P	1.440	1.162	AD	15.900	2.089
E	1.800	- 1.280	Q	1.800	1.280	AE	19.500	1.906
F	2.160	- 1.382				AF	23.100	1.643
G	2.700	- 1.512				AG	26.700	1.319
H	3.600	- 1.686				AH	30.300	0.944
J	5.400	- 1.924				AJ	12.300	2.164
K	7.200	- 2.086				AK	12.300	2.164
						AL	23.100	1.643
						AM	23.100	1.643

FIGURE A3 - 36 IN MODEL SECTION CUT - PRESSURE TAP LOCATIONS

NOTE: See samples of ice tracings supplied for guidance on ice documentation.

TABLE A3 - STATIC PRESSURE TAP LOCATIONS

Tap No.	Location
1	Stagnation Line
2	1% chord
3	2% chord
4	3% chord
5	4% chord
6	5% chord
7	10% chord
8	15% chord
9	30% chord
10	60% chord
11	80% chord

The cylinder temperature measurements are to be taken at three locations along the length of the cylinder. The thermocouples are to be mounted behind the leading edge of the cylinder. The locations are shown on the cylinder drawing referenced in A.5.

FIGURE A4A - 12 IN CHORD
NACA 0012 MODEL PLAN VIEW

FIGURE A4B - 36 IN CHORD
NACA 0012 MODEL ASSEMBLY

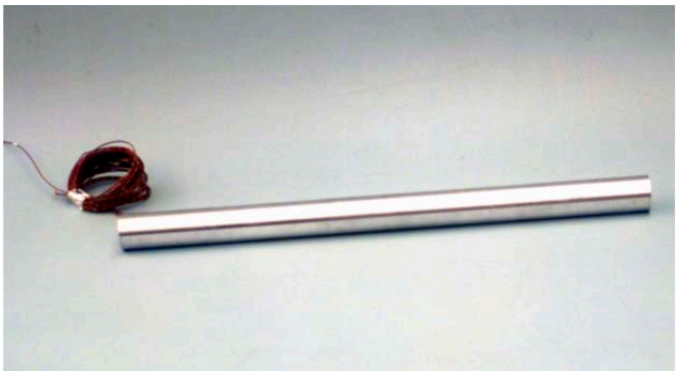

FIGURE A4C - 1.5 IN DIAMETER CYLINDER MODEL ASSEMBLY

FIGURE A4 - MODEL PHOTOGRAPHS

A.7 MODEL INSTALLATION AND CLEANING

Each participating organization is responsible for adapting the models to their facility. The costs associated with facility modification, end plate modification or support struts shall be the responsibility of the participant. The installation procedure is facility dependent and therefore a generic procedure cannot be specified. Each participant should install the models consistent with the design of their support structure and by following their own internal procedures for model installation and removal. FAA conformance of the installation is not required for this test. Procedures for establishing model system angle-of-attack are found in 8.A.1.

After installation of the model, but prior to the start of testing, the model shall be cleaned with an alcohol-based solvent to remove any debris/foreign substances (e.g., packing material debris,

A.8 DATA SYSTEM CONFIGURATION

A.8.1 Model System Data

The model pressure measurements are to taken during model installation and setup in order to establish angle-of-attack. Measured pressures should be used to establish an aerodynamic 0 degree angle-of-attack. The model is then geometrically rotated +3 degrees to establish a relative (to the aero 0 degree angle-of-attack) +3 degrees angle-of-attack. A comparison should then be made using the measured pressure distribution to the theoretical +3 degrees pressure distribution. The participating organizations should use engineering judgment to determine if the measured and theoretical pressure distributions agree or do not agree. If they agree, then proceed with testing. If they do not agree, then do not proceed with testing until the cause of the discrepancy has been successfully resolved. After this is completed, the pressure taps should be disconnected at the base of the model to avoid entrapment of moisture in the tubing. The tubing inside the model will be purged at the conclusion of testing.

The temperature measurements are taken to ensure model temperature stability and uniformity, prior to the start of each icing spray test point. A reading of the model temperature should be recorded prior to each icing spray. No model temperature data is to be acquired during icing sprays. For the case where temperature is being controlled to model indicated temperature (i.e., test ID 12), the facility temperature will be set prior to the icing spray and held constant. The procedure used to establish test section temperature shall be described in writing and provided as part of the data submittal.

A.8.2 Ice Shape Tracings

Ice shape tracings will be taken at the span-wise centerline location of all models. NASA Glenn Research Center will be responsible for providing templates on to which to record the ice shapes. The NASA Glenn authored procedure to follow for making the ice tracings is described in Appendix AC.

A.8.3 Model Deicing

Deicing of the model between icing sprays is to be accomplished by a using a combination of a plastic scrapper (supplied with the model by NASA), by using forced hot air or steam to remove all ice which is not removed by the scrapping, and by “cleaning” the model by wiping away the excess water. Participants may wish to use an alcohol-based solvent to thoroughly clean the model and to ensure removal of any residual ice not melted by the hot air system or steam. The intent is to avoid or minimize damage to the model.

If forced hot air is used, then the heater/blower or heater/compressed air source which will be used to de-ice the model between sprays is the responsibility of each facility operator. It is understood that this capability is available in all participating facilities. Any model support equipment (struts, end plates, etc.) should be designed and built to accommodate the hot air deicer. The model tube or duct through which the hot air will flow is nominally 0.5 inches in diameter for the 36-in chord airfoil and 0.375 in diameter for the 12-in chord airfoil. The support strut or attachment hardware hot air duct shall be designed to align with the model opening. No special attachment is required. The temperature of the hot air de-icier should be limited to 90 °C (195 °F) at the model in order to protect the thermocouples and their bond.

A.9 DATA ANALYSIS AND REDUCTION

The only data to be analyzed from these tests are the ice accretion shapes. The model data taken before or during testing, including model pressures and temperatures are taken for purposes of setting and documenting model angle-of-attack and to ensure temperature uniformity and stability, respectively.

Participant responsibilities with regards to data analysis and reduction include making ice accretion shape tracings and accurately documenting the icing spray conditions associated with each tracing. The actual data reduction and analysis of the ice shapes will be performed by Prof. Gary Ruff from Drexel University using the procedure described in paper AIAA-98-0195, presented at the Aerospace Sciences Meeting in Reno, Nevada. Details of the ice shape comparison methodology were discussed at the Fall 1998 meeting of the SAE AC-9C Subcommittee held in Bridgeport, CT. Boeing presented an alternate method of ice shape comparison at that time. The proposed method takes two ice feature measurements (upper horn angle and upper horn thickness) which most significantly affect aerodynamic performance. No final decision on the use of one or both of these methodologies has been made.

A.10 SCHEDULE

NASA Glenn will maintain the schedule.

A.11 PROJECT TASK ASSIGNMENTS AND RESPONSIBILITIES

The responsibility for planning, coordinating, and conducting the tests described in this document is the responsibility of each participating organization. The Boeing Commercial Airplane Company performed the model design and fabrication. The responsibility for the model attachment hardware is the responsibility of each participant. The detailed test procedures for model data system integration and checkout, the pre-defined test conditions and procedures, e.g., order of tests, will be documented and distributed by NASA. Test logistics such as scheduling and shipping will be coordinated by NASA. Data reduction and analysis will be the responsibility of Drexel University.

A.12 SUMMARY OF RESOURCES REQUIRED

The costs associated with test setup and running of the test will be the responsibility of each participating organization. The data reduction and analysis will be the responsibility of Drexel University, working under a grant from the NASA Glenn Research Center.

APPENDIX AA - TEST PROCEDURE

1. The model pressure measurements are to taken during model installation and setup in order to establish angle-of-attack. Measured pressures should be used to establish an aerodynamic 0 degree angle-of-attack. The model is then mechanically rotated +3 degrees to establish a relative (to the aero 0 degree angle-of-attack) +3 degrees angle-of-attack. A comparison should then be made using the measured pressure distribution to the theoretical +3 degrees pressure distribution. [The participating organizations should use engineering judgment to determine if the measured and theoretical pressure distributions agree or do not agree. If they agree, then proceed with testing. If they do not agree, then do not proceed with testing until the cause of the discrepancy has been successfully resolved.]

2. Disconnect the pressure taps at the base of the model to avoid entrapment of moisture in the tubing. The tubing inside the model will be purged at the conclusion of testing.

3. Stabilize the facility airspeed and air temperature at the specified values for the first test point.

4. Record the pressure port outputs and the thermocouples on the model.

5. Initiate water spray for the required time.

6. After icing is completed, shut off facility airspeed.

7. Photograph the ice shape from the side (~90 degrees) and from the front.

8. Cut or melt slices through the ice at the marked locations on the model, making sure to go all the way to the model surface. Do not drag knife across the model surface so as not to scratch the model skin.

9. Insert a template into a slot and trace the ice shape with a No. 2 pencil, attempting to trace as accurately as possible, following the provided ice tracing procedures.

10. On the template mark and note regions of clear ice, white (rime) ice and ice feathers or discontinuous icing.

11. Insert the clear gridded plastic template into the slot and take pictures of the ice at locations of 0, +45 and -45 degrees as referenced to the airfoil or cylinder cord line.

12. Document each ice tracing and picture with the test point number, date and time.

13. Turn on model heat until all ice is melted. Wipe the model dry with a soft, clean cloth. An alcohol-based solvent can be used if necessary or desired. The soft plastic IRT scrappers supplied with the models may also be used to clear ice from the model surfaces in order to minimize damage.

14. Go to next test condition, repeating steps 2 through 14.

APPENDIX AB - PRESSURE AND TEMPERATURE DATA ACQUISITION SYSTEM

A small portable pressure measurement system has been constructed to acquire and record the model pressure distributions and the model temperature.

The pressure measurement system consists of two Pressure Systems, Inc. Model 9016 Ethernet Intelligent Pressure Scanners and supporting hardware and software. Each module provides 16 silicon piezoresistive pressures sensors (32 total) which have an accuracy of ±0.05% full scale. Pressure data in engineering units is sent to the host computer through an Ethernet interface using TCP/IP protocol. A LabView program is used to display and record the pressure data.

The model pressure system is only intended to be used for the initial installation and set-up of the model angle-of-attack.

The model temperatures are measured using a small A/D system that can read up to 5 channels. This system uses a USB (Universal Serial Bus) interface to the host computer. Software to display and record the model temperature is included with the hardware.

APPENDIX AC - ICE TRACING PROCEDURE

1. Pre-warm the ice knife. Care should be taken to avoid overheating the knife. An overheated knife will melt away desired ice features. The larger the ice shape, the more heat energy will be required to make a clean cut. For most ice shapes, heating the knife with a trouble light is sufficient.

2. Make the first cut in the ice at the lowest tracing location on the model. This is done because ice melted from the cut runs down along the ice shape and re-freezes, destroying the original ice shape at the lower location.

3. Ensure the cut is clear of ice all the way to the model so that the template fits all the way onto the model.

4. Assistance is usually required to hold the template steady while tracing. For especially large templates, specially made tables or stands are needed to hold the template during tracing.

5. During tracing, hold the pencil normal to the template with the lead point close to the ice. A pencil is used because ink runs when it comes into contact with the melted ice. A No. 2 pencil is recommended.

6. Trace along the tops of features that have crevices or voids too small to accommodate the pencil. For digitization purposes, it is best to have one, easily distinguishable, continuous line for the ice tracing. This line must intersect with the model cutout in the template in two places: at the ice limit on both the suction and pressure surfaces of the model.

7. Before removing the template, annotate important ice features on the template not depicted by the ice tracing. A list of commonly observed ice features is found in Appendix D.

8. Immediately after finishing the ice tracings, review the tracings in the control room. Do this even if some run time is lost. This ice tracing information is important.

    - Ensure that the tracing intersects the edge of the model cutout in two places, such that the ice shape limits are well defined. In instances where large freestanding feathers or nodules can be traced to their intersection with the edge of the model cutout, be aware that these features will need to be digitized by hand.

    - Ensure that the primary ice tracing is one continuous, clearly marked line. Remove errant pencil marks.

    - Ensure your printed annotations are legible. Provide further explanation if needed.

    - Include not only the test run number, but also airspeeds, LWC, MVD, total and static temperature, spray time, and model serial number along with any other important information.

APPENDIX AD - LIST OF COMMONLY OBSERVED ICE FEATURES

Definitions for terms to be used on Ice Shape Tracing Templates:

Ice Type - ice formed under aircraft icing conditions can usually be classified as on of several different types:

beak - ice accretion formed at the suction peak of the clean airfoil when the free stream total temperature is above freezing. Predominately seen on rotor blades.

glaze - transparent or translucent ice formed by liquid water droplets at near freezing conditions. Typically has horns.

mixed - ice containing both glaze and rime characteristics. Usually is glaze at the stagnation line region with rime feathers at the sides.

rime - a milky and opaque ice formed at low temperatures and low LWC.

scallop/lobster tail - ice accretion that appears only on swept wings at meteorological conditions that favor glaze ice formations, and at certain velocities and sweep angles. The scallops are characterized by a particular pointed shape, height, and spacing. The area around the attachment line is called the base of the scallop, the pointed part is called the tip of the scallop.

Feathers - individual structures of ice formed as part of an overall ice shape. They tend to grow upstream and are usually one of two different types:

glaze feathers - ice feathers that grow significantly in width as they grow in height; they can grow together and become what appears on the surface to be a large continuous mass of ice.

rime feathers - ice feathers that have a distinctive crystalline structure, often similar to a bird's feather.

Ridge - a step ice accretion; it can be formed either naturally or by the activation of an ice protection system; several different types of ice ridges have been identified:

boot ridge - ice that remains on an airfoil aft of the active area of the deicing system, after the deicing system has been activated. It occurs when ice has accreted on the airfoil over a larger area than that covered by the deicing system.

runback ridge - water that has flowed aft on the airfoil to a specific zone where conditions for ice formation are optimum due to temperature and heat transfer. Predominately observed in conjunction with thermal ice protection system operation.

feather ridge - a line of glaze ice feathers that have grown together to form a continuous surface.

stall bar ridge - a narrow strip of ice running span wise on a wing. Normally occurs on the suction surface.

Bumps - part of glaze ice formations that show a non-uniform rounded shape. It may be covered by roughness elements.

Bead - roughness element formed away from the main ice accretion, it stands isolated on the airfoil surface.

Horn - the dominant ice growth feature of some glaze ice accretions.

Frost - a covering of minute ice crystals formed from the sublimation of water vapor; often observed in the IRT after an icing spray on the aft portion of an airfoil, away from the direct and indirect impingement zones.

Nodules - smooth, individual ice structures similar to glaze ice feathers, however, they grow nearly perpendicular to the general airflow direction; they are usually found on the surface of an airfoil away from the direct impingement zone, in the area of 20 to 50% chord.

Roughness element - deformed hemispherical frozen water droplet that covers all or parts of ice accretions. For theoretical studies it can be idealized as a frozen water droplet having a perfect hemispherical shape covering an ice substrate (the ice accretion proper), and characterized by diameter D, and height H. The ratio H/D has been measured experimentally to be approximately 0.5. The experimentally measured diameters show an upper bound of about 2 mm.

Rivulet - surface water that has coalesced on an airfoil, and flows some distance aft on the airfoil. It commonly leaves a streak of ice along its path.

Void - air filled pockets normally found in glaze ice.

APPENDIX B - THICK PROCESSING OF FACILITIES STANDARDIZATION CYLINDER DATA

B.1 BACKGROUND

It was decided to try to understand the cylinder data better by comparing results for quantitative ice-shape parameters. This appendix outlines the methods used in this effort and presents the results.

The quantitative ice-shape parameters are those selected as being most useful by the SAE AC-9C Codes panel in their deliberations leading to ARP5903 and are defined in that document. These parameters are not the only way the ice shapes can be characterized, but it was decided to use them since they were identified in the ARP. These parameters are:

S1 - Upper Horn Peak Thickness

S2 - Upper Horn Angle

S3 - Lower Horn Peak Thickness

S4 - Lower Horn Angle

S5 - Total Ice Area

S6 - Leading Edge Minimum Thickness

S7 - Upper Icing Limit

S8 - Lower Icing Limit

This effort was automated by using the THICK computer program. Although there are alternatives to using THICK, it was decided to use it because it automates the calculation of the eight parameters of interest. The version of THICK used for this work was the version provided on the LEWICE 2.2.2 CD. An Excel® file was built to receive the THICK output data. It contains a data sheet into which are copied the results from the THICK output files clean.dat, iced.dat, echo.dat, and total.txt. It also contains two charts: “wrapped” which shows the ice shape on the airfoil and “unwrapped” which shows the ice thickness at each point along the airfoil. Data from the echo.dat file are used to identify the peak locations on the wrapped plot. In addition, the peaks.dat data can be added to another worksheet if THICK has chosen the peaks badly.

B.2 THICK INPUT

THICK requires two input files: the clean airfoil and the iced shape. The ice shape may include the trailing edge of the airfoil or it may simply be the iced shape itself (as might be digitized from an experimental tracing). Current versions of THICK expand the given airfoil coordinates so that the airfoil shape used by THICK contains 5000 points.

The data may be entered in any self-consistent set of units. THICK will return the data in the same units.

B.3 THICK OUTPUT

THICK produces five output files: clean.dat, iced.dat, echo.dat, peaks.dat, and total.txt.

Echo.dat should be checked for error messages. (None were observed in this data.) All of the S1 through S8 parameters can be found in echo.dat, but it is easier to use the values as tabulated in total.txt instead.

The locations of the upper and lower peaks can be copied from echo.dat to identify the peaks on the ice shape. When these peak locations are plotted on the wrapped ice shape, the user can determine if THICK has chosen the appropriate peak locations. If the user disagrees with the peaks chosen by THICK, the peaks.dat file can be used to choose alternate peaks and their associated angles and thicknesses. THICK identifies a peak by a change in the slope of the ice shape. The locations identified by THICK might better be referred to as local maxima.

B.4 EXCEL® FILE FOR RESULTS

It was necessary to review the results provided by THICK because it does not always choose the upper and lower horns appropriately and it may introduce anomalies into the unwrapped plots of ice shapes. It was determined that an Excel® file would be the easiest way to review the data. These Excel® files are available on the CD-ROM that forms part of this document. In general, three tabs are used in this file: one worksheet for data and two plots, Wrapped and Unwrapped. A second worksheet is added if the wrapped plot shows that THICK has chosen the horns badly.

The data from clean.dat are copied into the worksheet starting in cell A9. Columns A and B are used to plot the airfoil on the Wrapped plot and columns D and C are used to plot the ice on the Unwrapped plot.

The data from iced.dat are copied into the worksheet starting in cell F9. Columns F and G are used to plot the ice shape on the Wrapped plot. Column H is not used.

The data from echo.dat are copied into the worksheet starting in cell J7. None of these data are plotted as copied from echo.dat because of the format: text and numbers are commingled. To get the data to plot the peak locations, the Max Thickness Ice Locations x and y values are copied into cells J2 and K2 for the lower peak and J4 and K4 for the upper peak. These locations then show up on the Wrapped plot as red squares to identify the horn maximum thicknesses.

The total.txt data are copied into the worksheet starting in cell A3.

B.5 SELECTION OF VALUES FOR S1 THROUGH S8 PARAMETERS

The user should verify that the data being plotted in the Wrapped and Unwrapped plots are complete. Usually the airfoil and the data in the Wrapped plots will be correct as THICK always puts out 5,000 data points. However, the number of data points on the ice shape varies from input to input. It is therefore necessary to check the data being plotted on the Unwrapped ice shape for completeness.

The user could blindly accept the data in total.txt for the S1 through S8 parameters; however, this is risky. The xlo and xhi points can be taken from the unwrapped plot or from the data used to produce it: column F. If they are taken from column F, the first and last points are used unless there was overlap of experimental data. xhi is the x-value corresponding to the end point with the positive y-value. xlo is the x-value corresponding to the end point with the negative y-value.

The Percent of Chord differences are provided because it was decided to flag the results if the differences in the xhi and xlow values between the THICK results and the endpoint results were greater than 1% of the chord.

The upper and lower horns are identified by the red squares on the Wrapped plot. If these are incorrect, the user needs to look at the peaks identified in the peaks.dat file. Plotting these peaks allows the user to choose the correct peaks and their associated angles. These data can replace the data provided by THICK for the maximum forward thickness (MFT)/lower max, upper max, MFT Ang/l. horn ang, and u. horn ang.

If the user chooses a different peak than one or both of those provided by THICK, the leading edge minimum thickness may also need to be changed.

The total ice area is determined by integrating the area in the airfoil and the area in the iced airfoil and subtracting the airfoil area from the iced airfoil area, so anomalies in the unwrapped plot do not affect the ice area calculations. However, the ice area may be inaccurate in cases where the iced shape includes the trailing edge of the airfoil - such as the outputs of some ice accretion codes. If the un-iced portions of the iced airfoil do not match exactly the clean airfoil, THICK may mistake it for ice, affecting the computed total ice area.

B.6 SAMPLE PLOTS

Figure B1 is an example of a “wrapped” plot. The cylinder coordinates are plotted from the clean.dat THICK output file. (This file is an expansion of the input file and generally contains 5000 data points.) The ice shape is plotted from the iced.dat THICK output file. (This file is essentially an echo of the input ice shape and contains the same number of data points as the input file.)

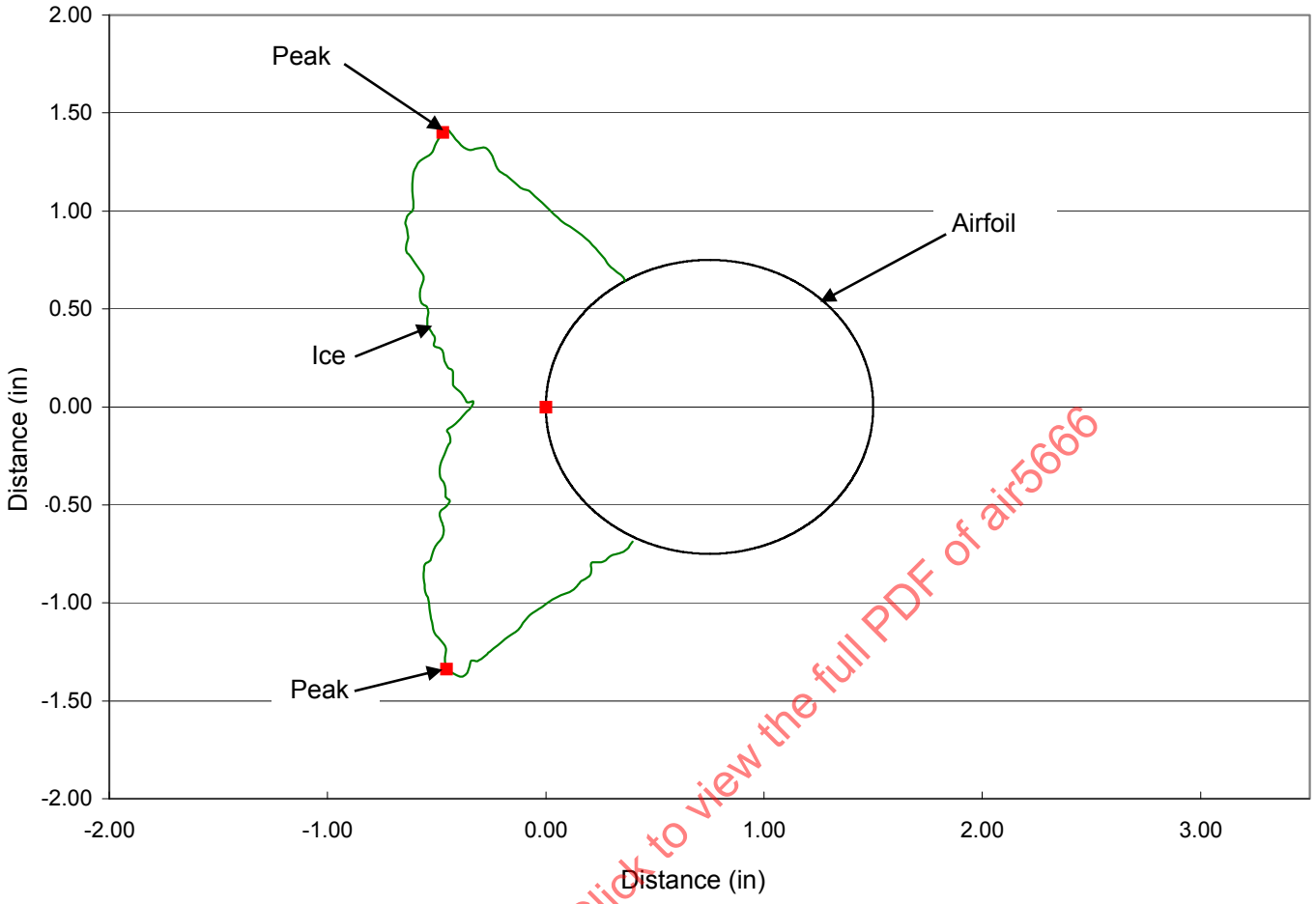

FIGURE B1 - EXAMPLE OF WRAPPED PLOT

The squares denote the leading edge and the positions chosen by THICK for the upper and lower horn locations on the ice shape. These are plotted to facilitate decisions as to whether THICK has chosen the correct horns.

Figure B2 is an example of an “unwrapped” plot. The ice shape is plotted from the clean.dat THICK output file. THICK projects a normal out from each of the 5000 data points on the cylinder. The distance from the cylinder to the ice shape along this normal is plotted for each cylinder data point. (If there is more than one such intersection, the outermost is plotted.) Occasionally, because of the differences in the number of points on the cylinder and the number of points on the ice shape (50:1), anomalies are introduced.

Figure B3 is an example of the anomalies which can be introduced by THICK. Anomalies tend to show up when there are few iced data points compared with the number of points in the underlying portion of the airfoil. In some cases, the anomalies cause the ice thickness to drop to zero (i.e., no ice) in places where the wrapped plot shows ice to be. None of the cylinder tracings shows that particular kind of anomaly. The case shown in Figure B3 was the only cylinder case to give an erroneous leading edge thickness. Figure B4 is a wrapped plot of the same ice shape shown in Figure B3. As can be seen from Figure B4, the anomalies seen in Figure B3 do not show up on the wrapped plot.

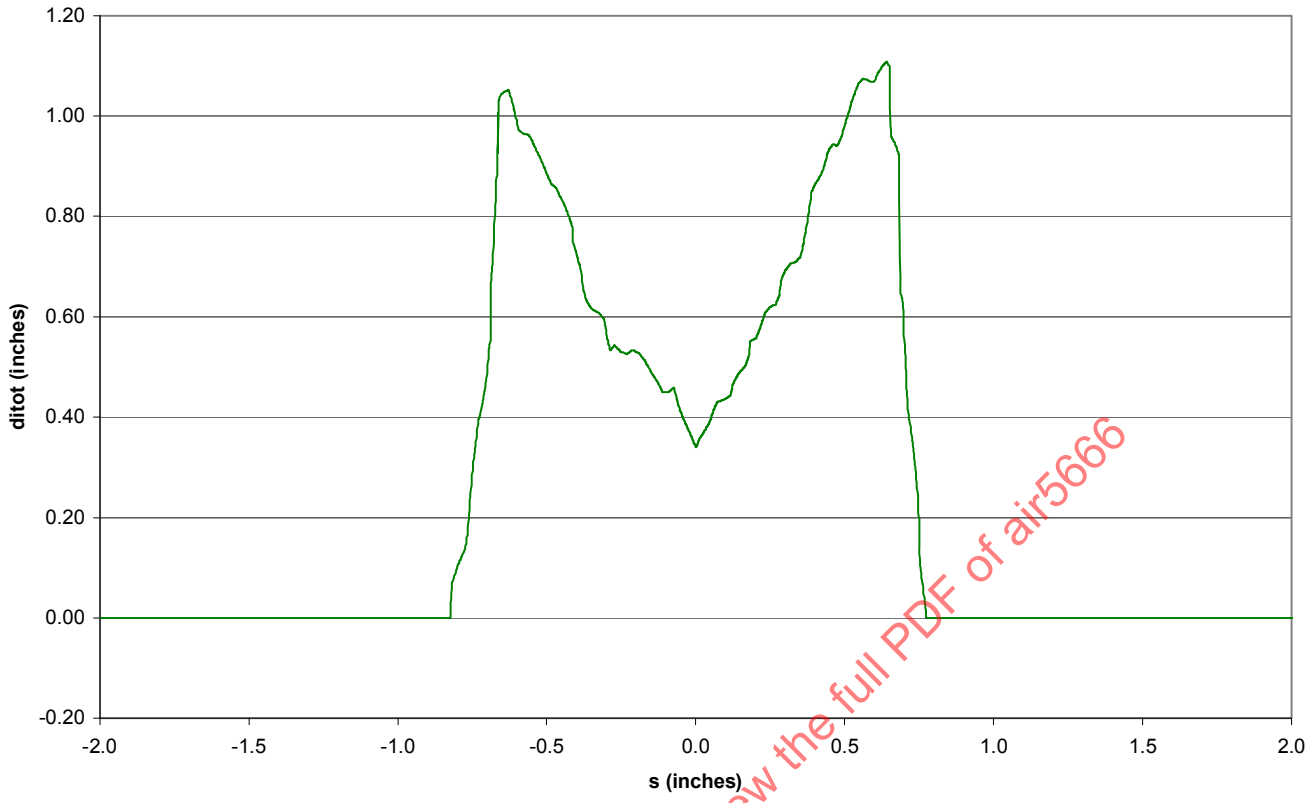

FIGURE B2 - EXAMPLE OF UNWRAPPED PLOT

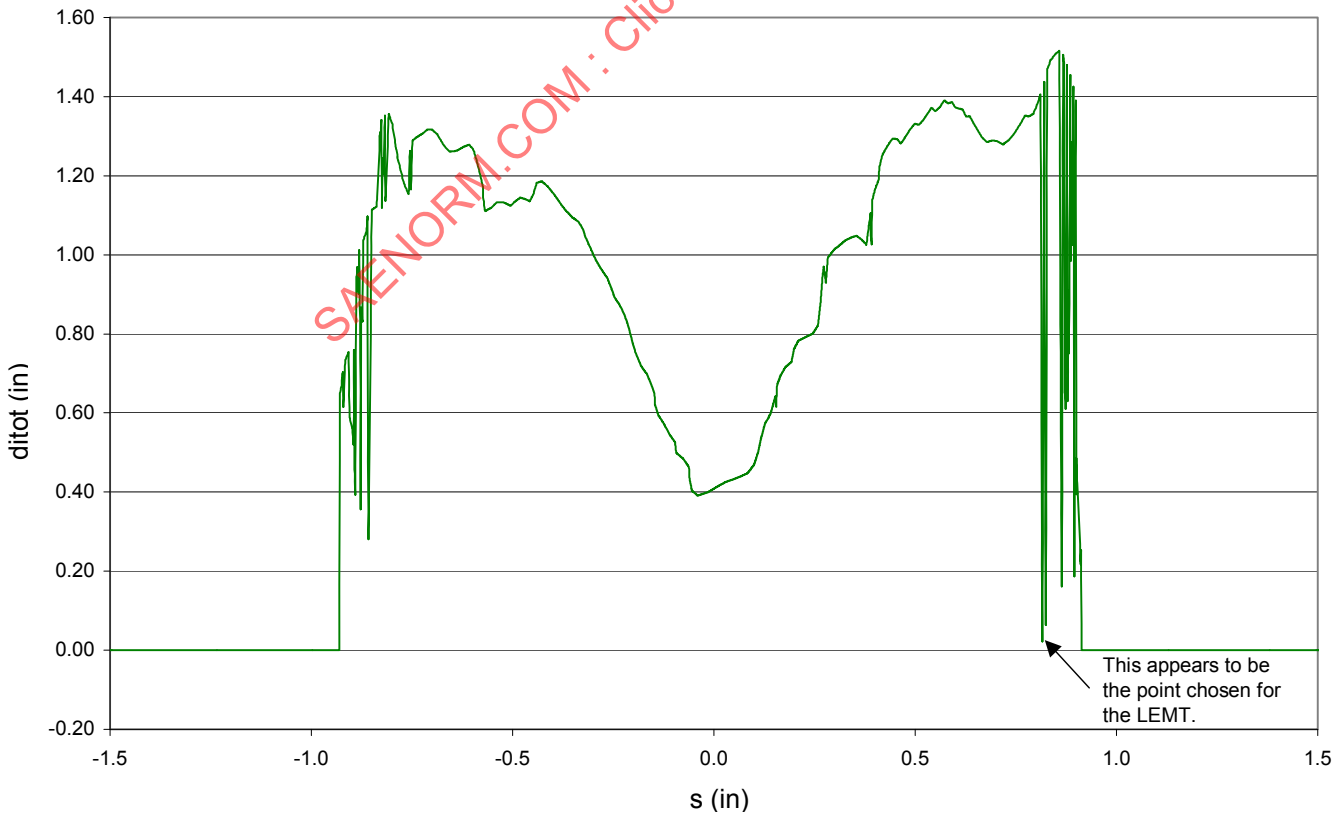

FIGURE B3 - EXAMPLE OF UNWRAPPED PLOT WITH ANOMALIES

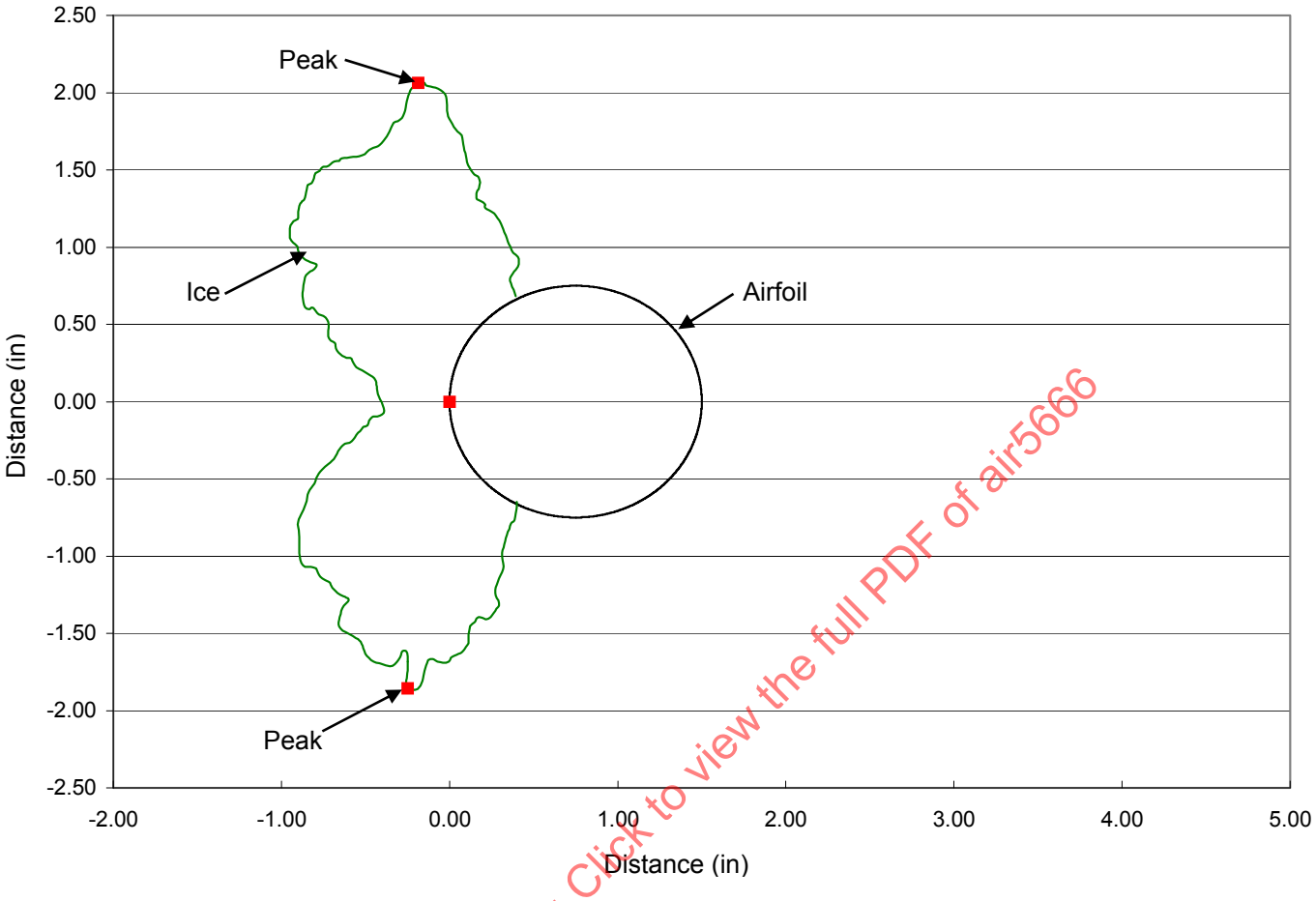

FIGURE B4 - WRAPPED ICE SHAPE CORRESPONDING WITH UNWRAPPED PLOT SHOWN IN FIGURE B3

B.7 DISCUSSION OF RESULTS

B.7.1 S1 and S3 - Upper and Lower Peak Thicknesses

The upper peak is identified at the location with the greatest height above the airfoil surface. The lower peak is identified at the location with the greatest height below the airfoil surface. THICK finds these peaks by locating changes in the slope of the ice shape. These locations may be in error if a non-zero angle of attack is used for an airfoil. They may also be in error if there are more than two horns with approximately the same height. In that case, the user might prefer the horn closer to the leading edge, while THICK may choose one that is more aft.

It was decided to compare the cylinder results with an estimate of the maximum thickness derived from equations in DOT/FAA/CT-88/8-I. An estimate of ice thickness at the stagnation point is given by Equation B1:

$$EstMax = A_c c \beta_0 n_0 \quad \text{(Eq. B1)}$$

For the cylinder, d replaces c. In addition, assuming that $\beta_0 = 1$ and $n_0 = 1$ gives Equation B2, which may be used for the estimated maximum. Since this formula ignores runback, it is possible for horn thicknesses to exceed the estimated maximum.

$$EstMax = A_c d \quad \text{(Eq. B2)}$$

A_c, the accumulation parameter is expressed by Equation B3,

$$A_c = (LWC \times V \times t)/(d\rho_i) \quad \text{(Eq. B3)}$$

where:

LWC = liquid water content

V = velocity

t = time

ρ_i = ice density

d = cylinder diameter

Multiplying EstMax by β_0 provides an approximation to ice thickness at the stagnation point for rime ice and may provide an approximation of horn thickness for glaze ice. (See the paragraph on Approximate Two-dimensional Icing Formulas in the Aircraft Ice Accretion Section in DOT/FAA/CT-88/8-I.) This justifies the use of this equation for cases 7-11, which are rime cases. In addition, for glaze cases, due to runback and other physical processes, ice which would have built up at leading edge now builds up further back. Since mass is conserved, the formula may give an ice thickness roughly on same order as that of horns.

Figure B5 shows the S1 (Upper Peak Horn Thickness) Values for Run ID 1 through 6 - the Glaze Cases - with the Estimated Maximum Thickness Included for each case. (In this and subsequent figures, the estimated maximum thickness curve is included as an additional point of reference in assessing trends in the data. The formula should NOT be regarded as providing "truth.") The results are in inches.

All tests were run for 10 minutes except run ID 1, which is for 15 min, as indicated on the plot. The Tunnel H results are generally larger than those from the other tunnels. It is interesting to note that the estimated maximum for the LWC = 0.5 g/m^3 cases is somewhat lower than most of the test cases, but for most of the LWC = 1.0 g/m^3 cases the estimated maximum is significantly higher than the test results.

Figure B6 shows the S3 (Lower Peak Horn Thickness) values for run ID 1 through 6 - the glaze cases - with the estimated maximum thickness included. Unlike the Upper Peak Horn Thicknesses, the Tunnel E results here are frequently greater than the Tunnel H results.

Again, it is interesting to note that the estimated maximum for the LWC = 0.5 g/m^3 cases is somewhat lower than most of the test cases, but for most of the LWC = 1.0 g/m^3 cases the estimated maximum is significantly higher than the test results.

Figure B7 shows the S3 parameter for run ID 7 through 11 - the rime cases - with the estimated maximum thickness included. This parameter has been relabeled as the maximum forward thickness because rime cases typically do not exhibit horns. MVD = 20 um for all runs. The Tunnel H results are generally the highest.

For these rime cases (for which the estimate should be most accurate), the estimated maximum is lower than all the test cases for run ID 7 and 8, but just about in the middle of the test results for run ID 9, 10, and 11.

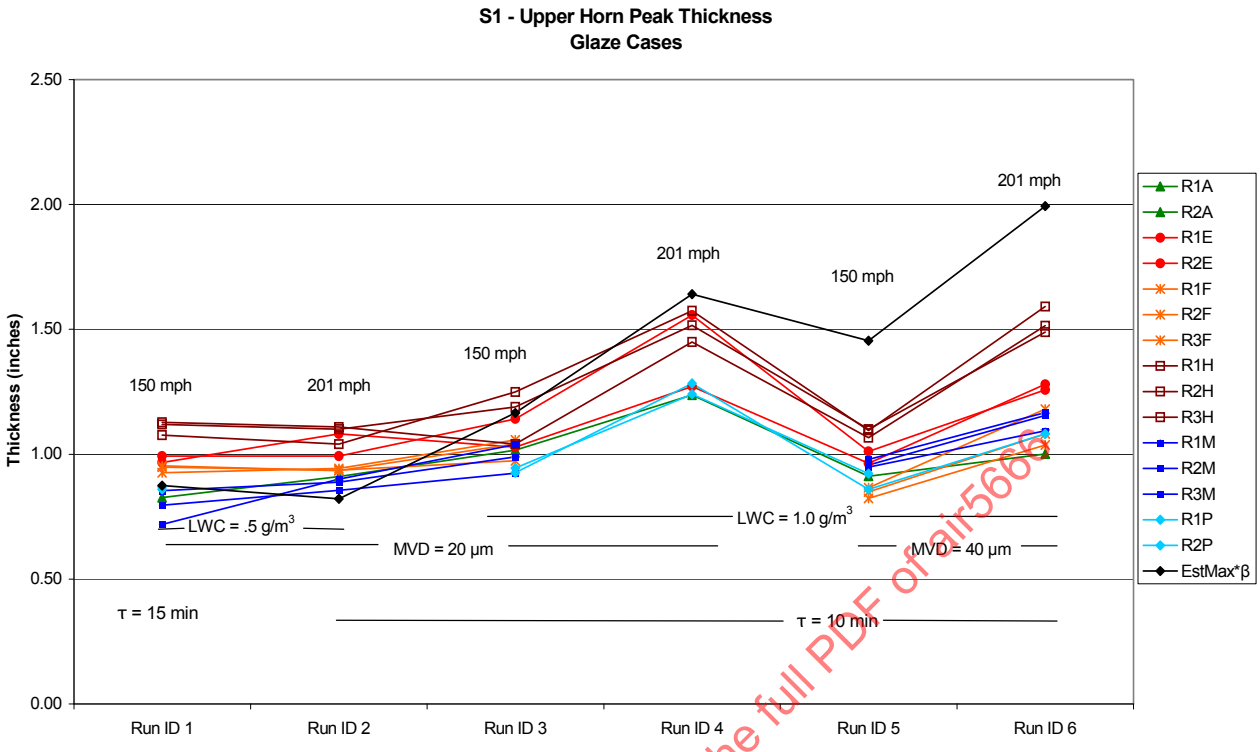

FIGURE B5 - S1 - GLAZE CASES

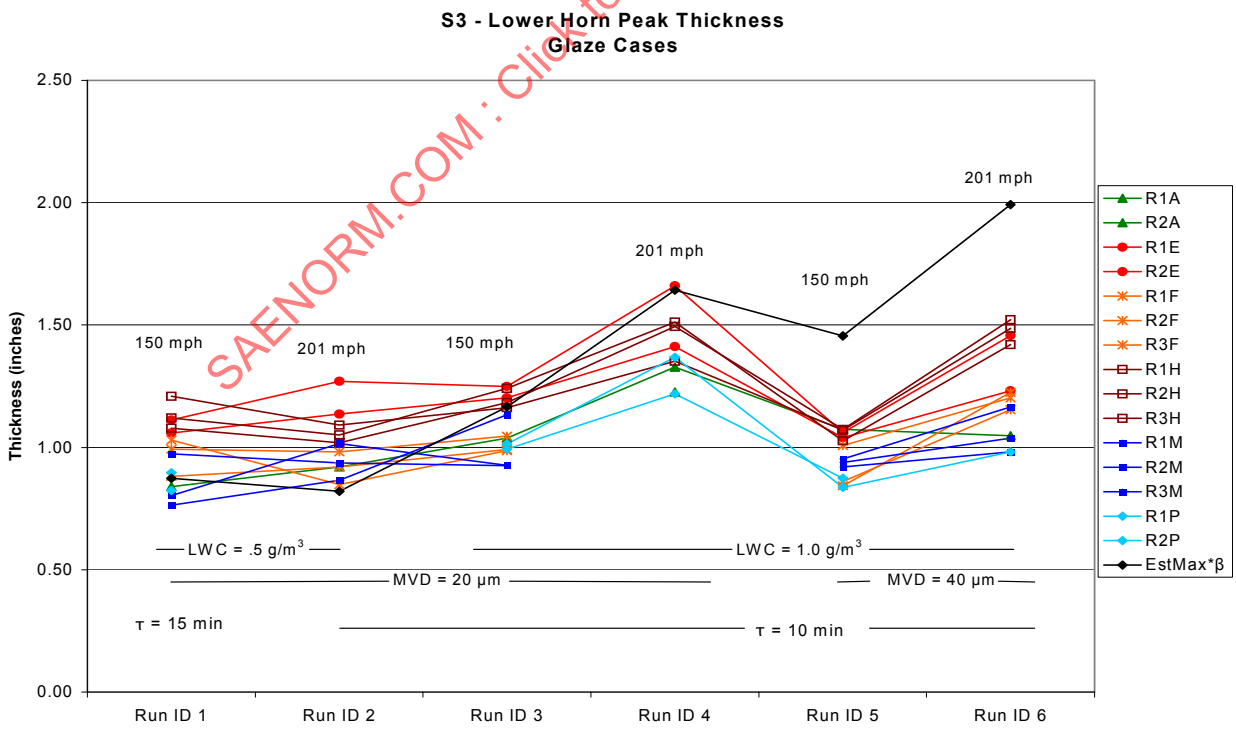

FIGURE B6 - S3 - GLAZE CASES

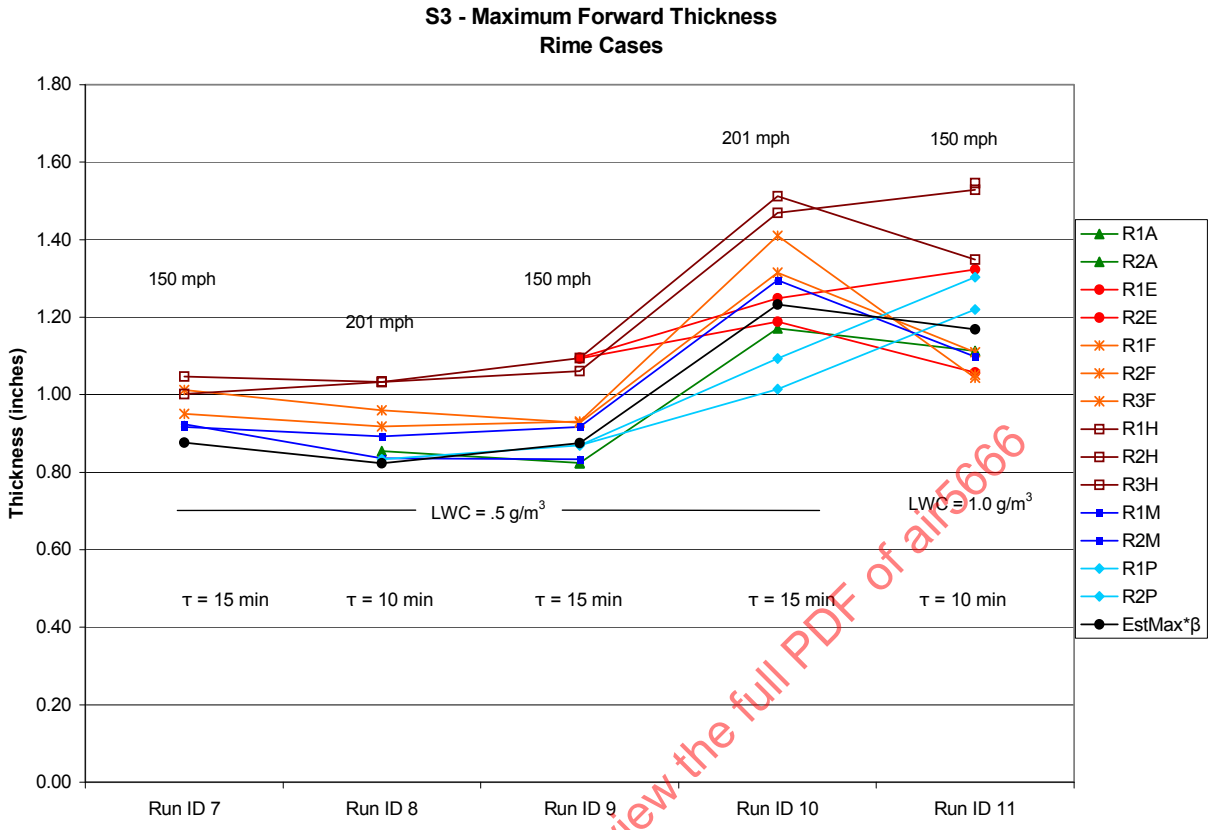

FIGURE B7 - S3 - RIME CASES

B.7.2 S2 and S4 - Upper and Lower Horn Angle

The horn angle is the angle made by a line drawn from the leading edge to the peak thickness point as shown in Figure B8. A horn angle of 180 degrees would be a 'horn' pointing directly upstream. Angles for the cylinder cases may be in error because there was no reference mark on the test cylinder to indicate the horizontal, so it may be that the template was rotated with respect to the horizontal for some of the ice shape tracings.

Figure B9 shows the S2 (Upper Horn Angle) values for runs ID 1 through 6 - the glaze cases. Higher angle numbers indicate more forward horns and vice versa. Again, template rotation may have affected horn placement.

Figure B10 shows the S4 (Lower Horn Angle) parameter for runs ID 1 through 6 - the glaze cases. Lower numbers indicate more forward horns and vice versa. Template rotation may have affected horn placement.

Figure B11 shows the S4 parameter for runs ID 7 through 11 - the rime cases. This parameter has been relabeled "Maximum Forward Thickness Angle" because the rime shapes don't have real horns. An angle of 180 degrees marks the horizontal position. Angles greater than 180 degrees are below the stagnation point and vice versa. Template rotation may have affected these results.

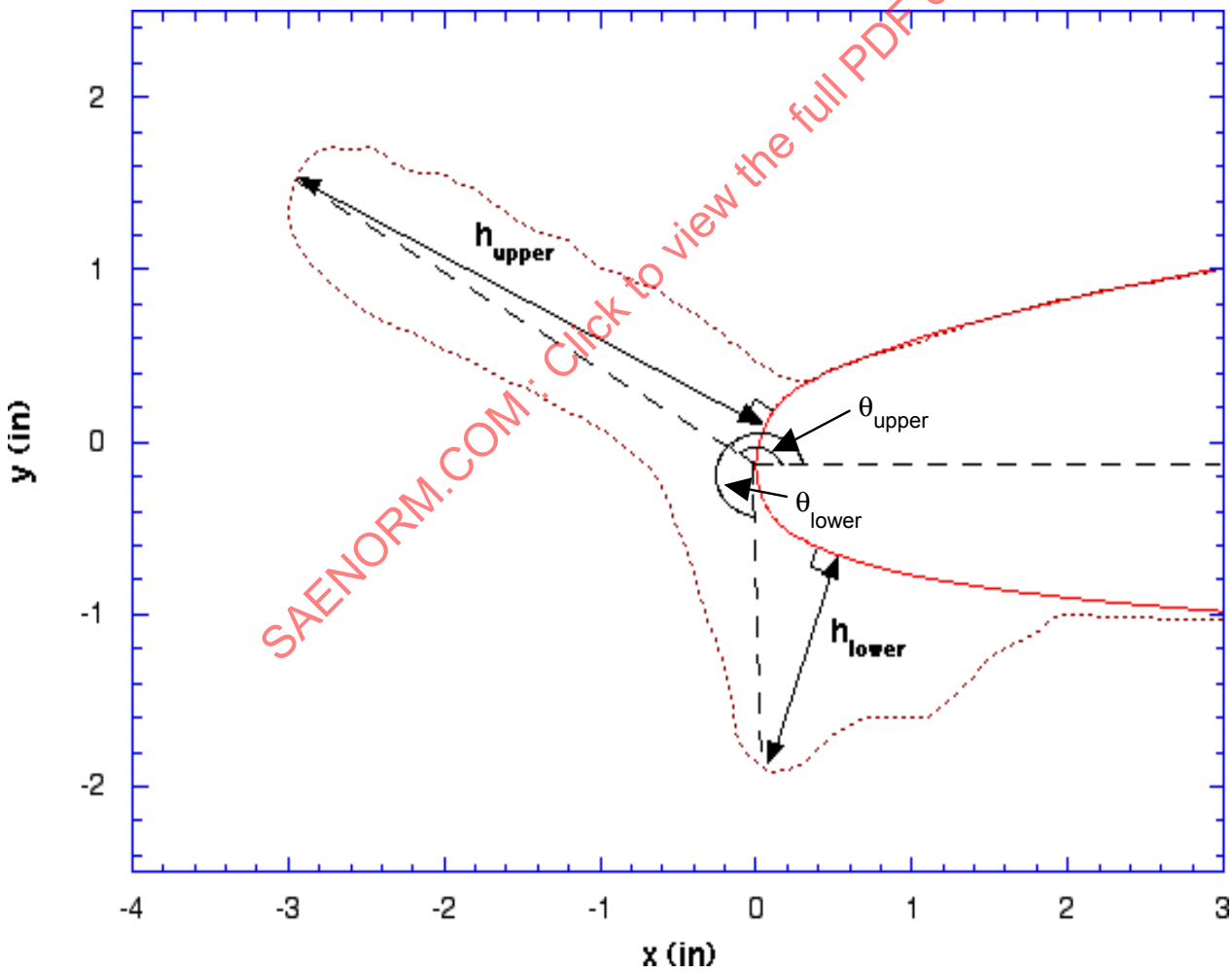

FIGURE B8 - HORN ANGLE DEFINITION

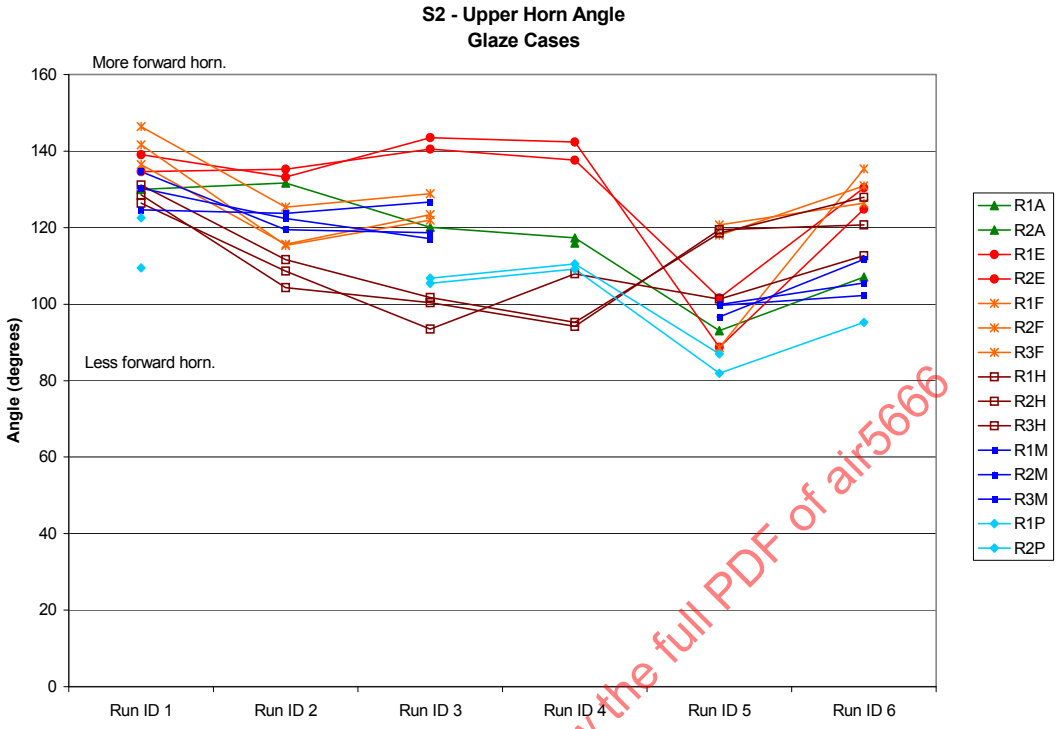

FIGURE B9 - S2 - GLAZE CASES

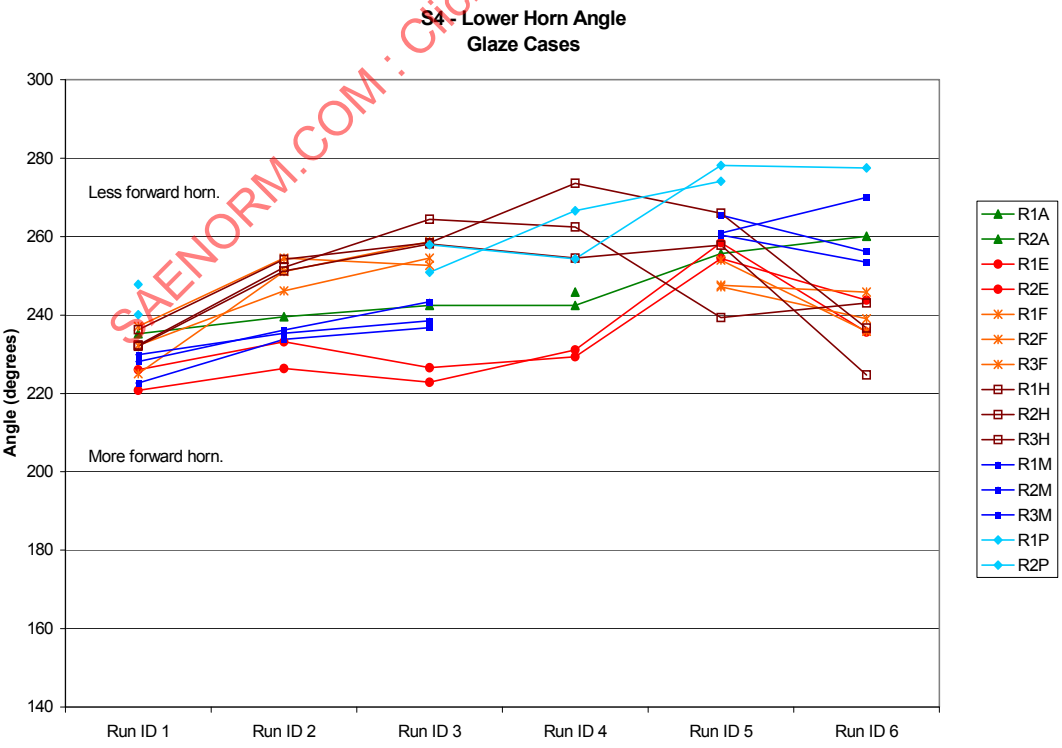

FIGURE B10 - S4 - GLAZE CASES

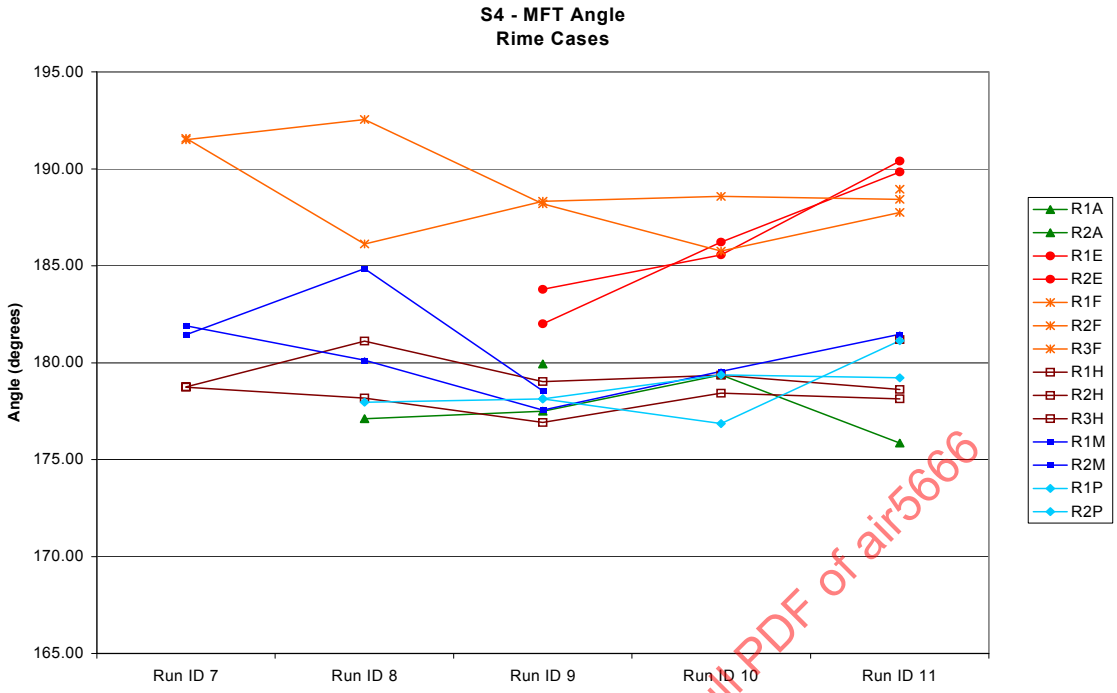

FIGURE B11 - S4 - RIME CASES

B.7.3 S5 - Total Ice Area

The total ice area is found by integrating the area of the airfoil plus ice shape and subtracting the airfoil area. The ice area is found from the wrapped plots, so anomalies in the unwrapped plots do not affect these values.

An estimate of the ice area can be obtained from Equation B4.

$$\text{Estimated Area} = A_c E d^2 \qquad \text{(Eq. B4)}$$

where:

A_c = the accumulation parameter given by Equation B3

E = the total collection efficiency

d = the cylinder diameter

Although E can be obtained from programs such as LEWICE, the values used in the present work were derived from the plot of K_0 vs. E in DOT/FAA/CT-88/8-I, Aircraft Ice Accretion Section.

Figure B12 shows the S5 (Total Ice Area) parameter for run ID 1 through 6 - the glaze cases - with the estimated area given by Equation B4 included. (In this and subsequent figures the estimated area curve is included as an additional point of reference in assessing trends in the ice area data. The formula should NOT be regarded as providing "truth."] The ice areas for Tunnel H are greater than those for all the other tunnels.

Although the estimated area is basically in the middle of the test results for the LWC = 0.5 g/m^3 cases, it is generally higher than the test results (ignoring Tunnel H) for the LWC = 1.0 g/m^3 cases.

Figure B13 shows the S5 (Total Ice Area) parameter for run ID 7 through 11 - the rime cases - with the estimated area included. Again, the ice areas for Tunnel H are greater than those for the other tunnels. The estimated area tracks well with the test results (ignoring Tunnel H results).

B.7.4 S6 - Leading Edge Minimum Thickness

The leading edge minimum thickness, as calculated by THICK, is really the minimum between the two horns that THICK has chosen. It is calculated from the unwrapped plot and is not necessarily at the leading edge. Therefore, it might not be the appropriate thickness if THICK has chosen the horns badly or if THICK has introduced anomalies into the unwrapped plot. Only one such case was encountered in the cylinder data so, the data were manually corrected.

Figure B14 shows the S6 (Leading Edge Minimum Thickness) parameter for run ID 1 through 6 - the glaze cases, with the incorrect Tunnel H value replaced by the correct leading edge minimum value.

B.7.5 S7 and S8 - Upper and Lower Icing Limits

A normal line is projected out from each point on the airfoil. The first and last such points which intersect the ice shape are considered the icing limits. Note that if there are “overhangs” in the ice shape, the icing limits chosen by THICK may be aft of the actual ice locations on the clean shape. Figure B15 shows the S7 (Upper Icing Limit) parameter for run ID 1 through 6 - the glaze cases. Figure B16 shows the S8 (Lower Icing Limit) parameter for run ID 1 through 6 - the glaze cases. Figure B17 shows the S7 (Upper Icing Limit) parameter for run ID 7 through 11 - the rime cases. Figure B18 shows the S8 (Lower Icing Limit) parameter for run ID 7 through 11 - the rime cases.

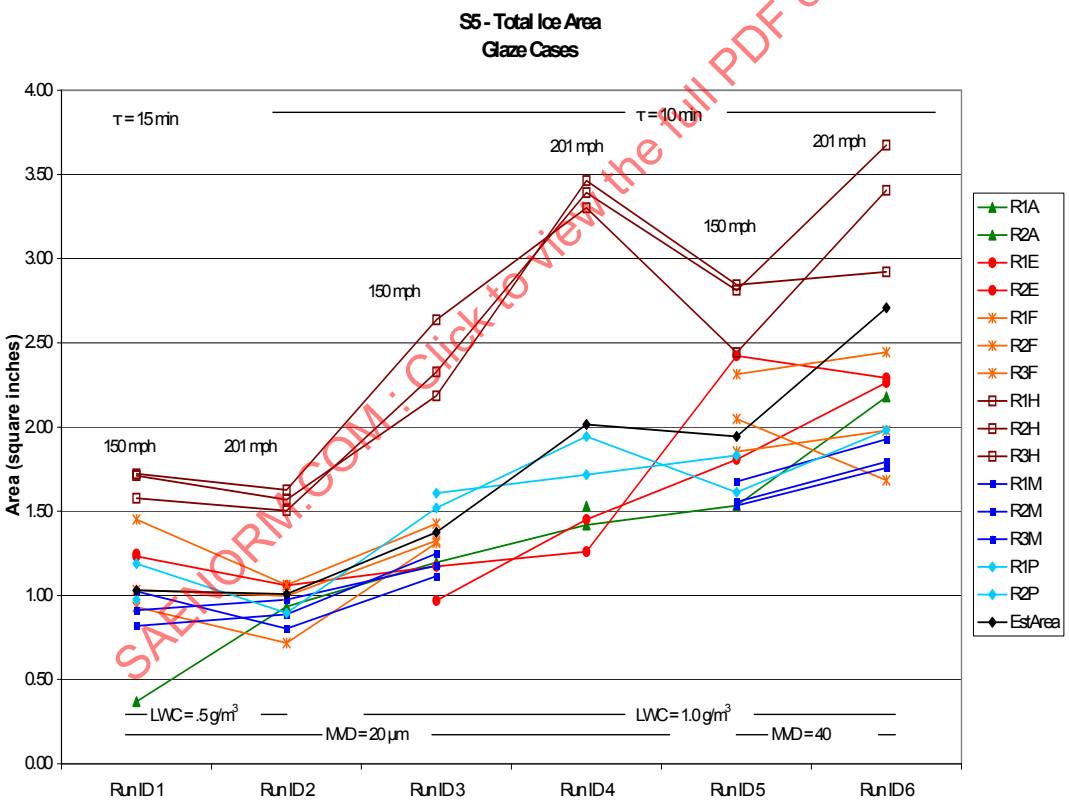

FIGURE B12 - S5 - GLAZE CASES

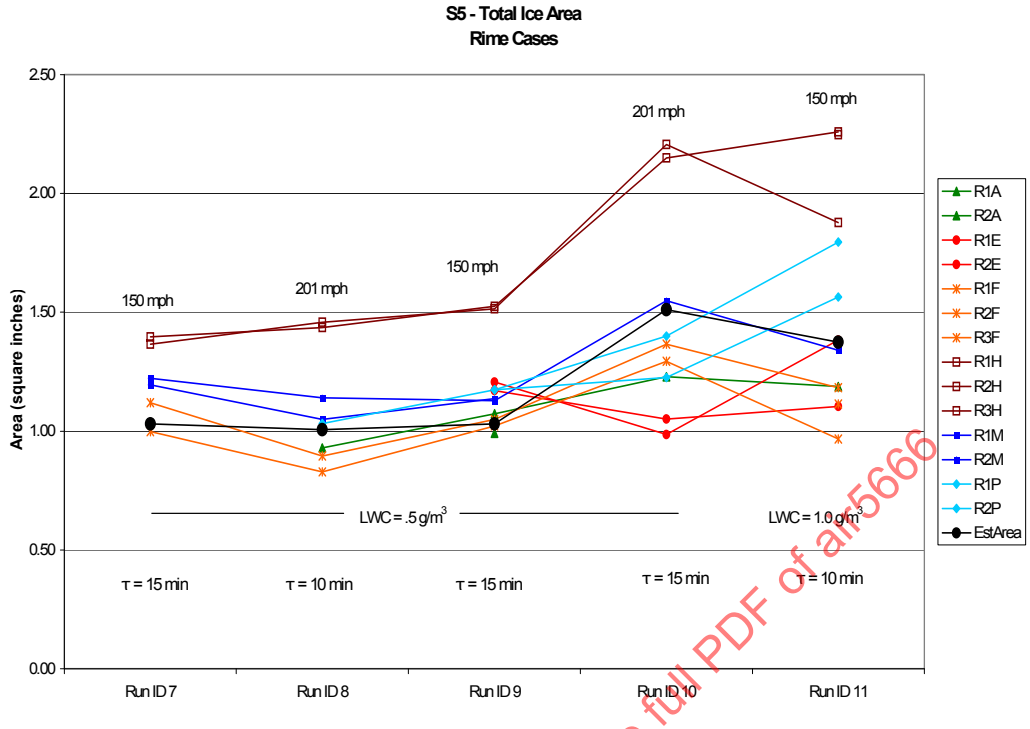

FIGURE B13 - S5 - RIME CASES

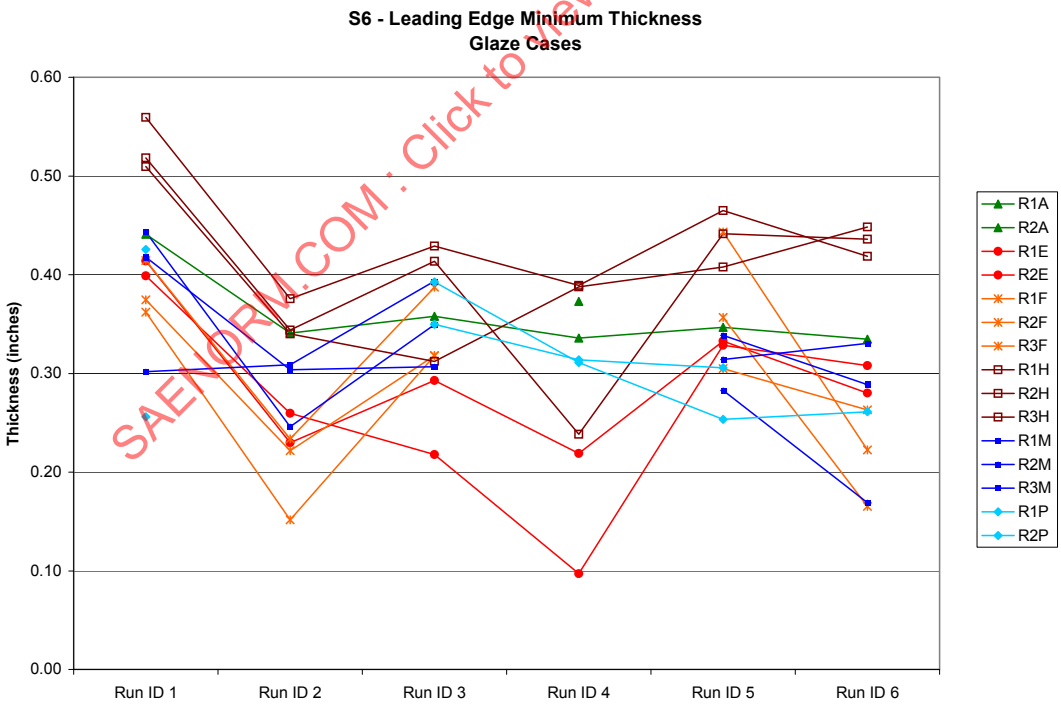

FIGURE B14 - S6 - GLAZE CASES WITH ANOMALOUS POINT REPLACED

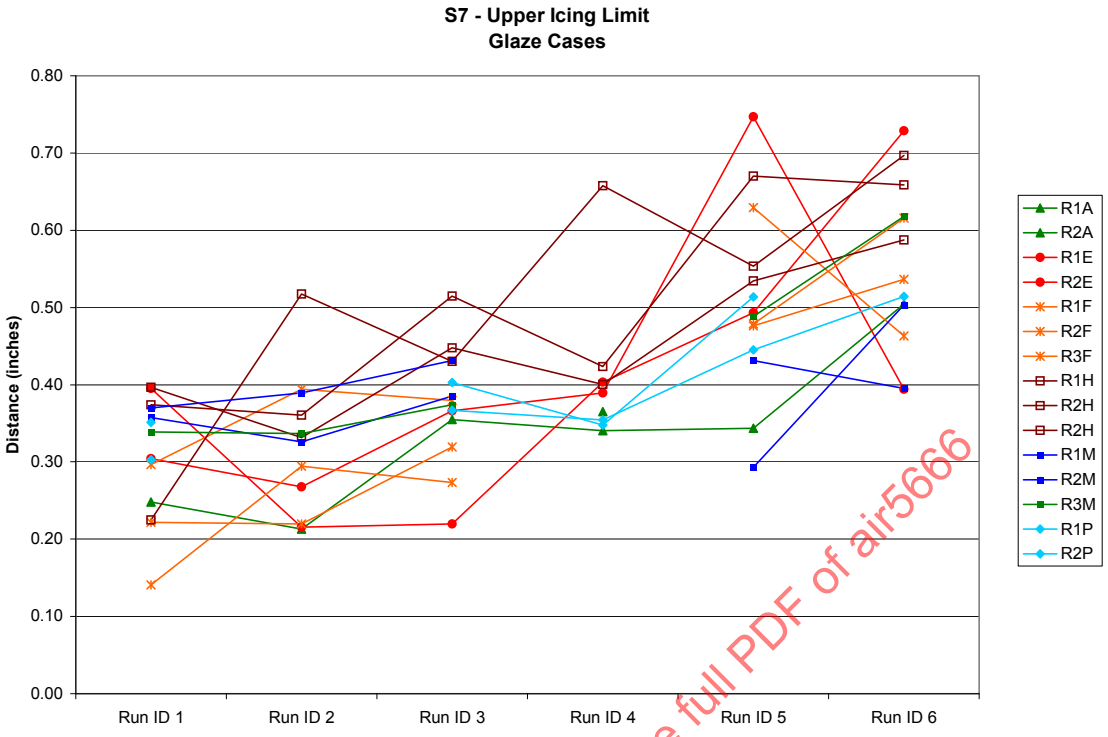

FIGURE B15 - S7 - GLAZE CASES

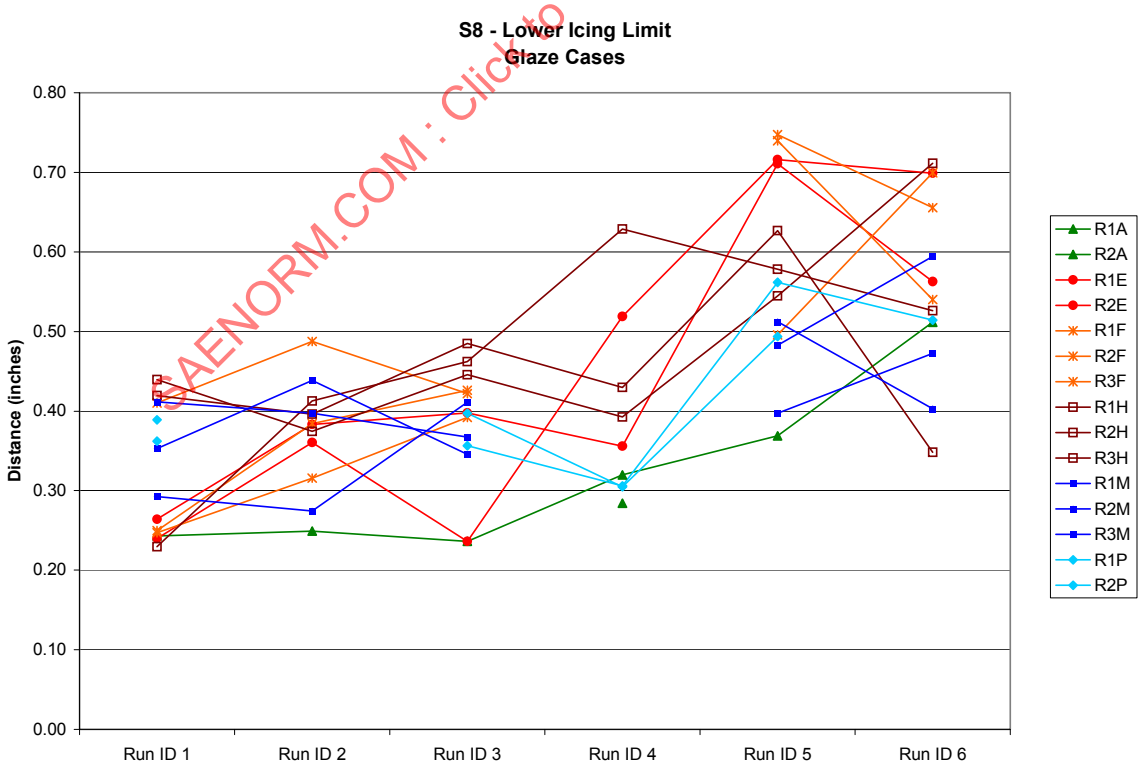

FIGURE B16 - S8 - GLAZE CASES

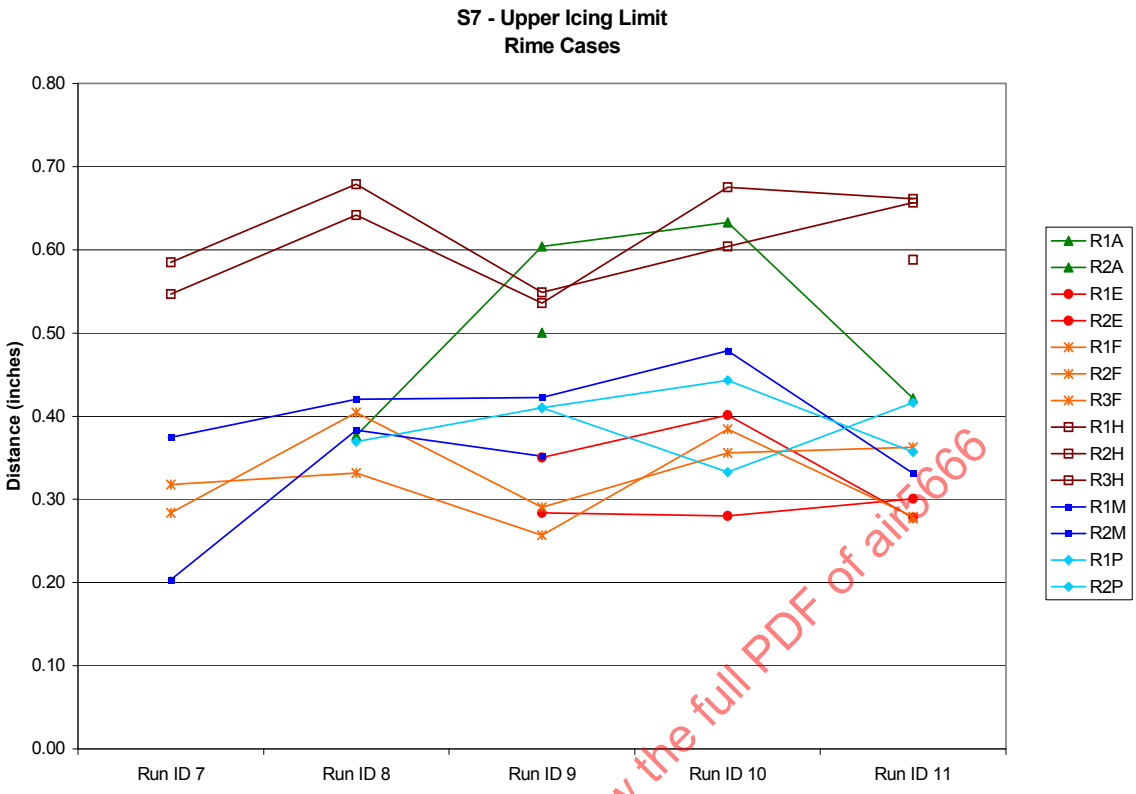

FIGURE B17 - S7 - RIME CASES

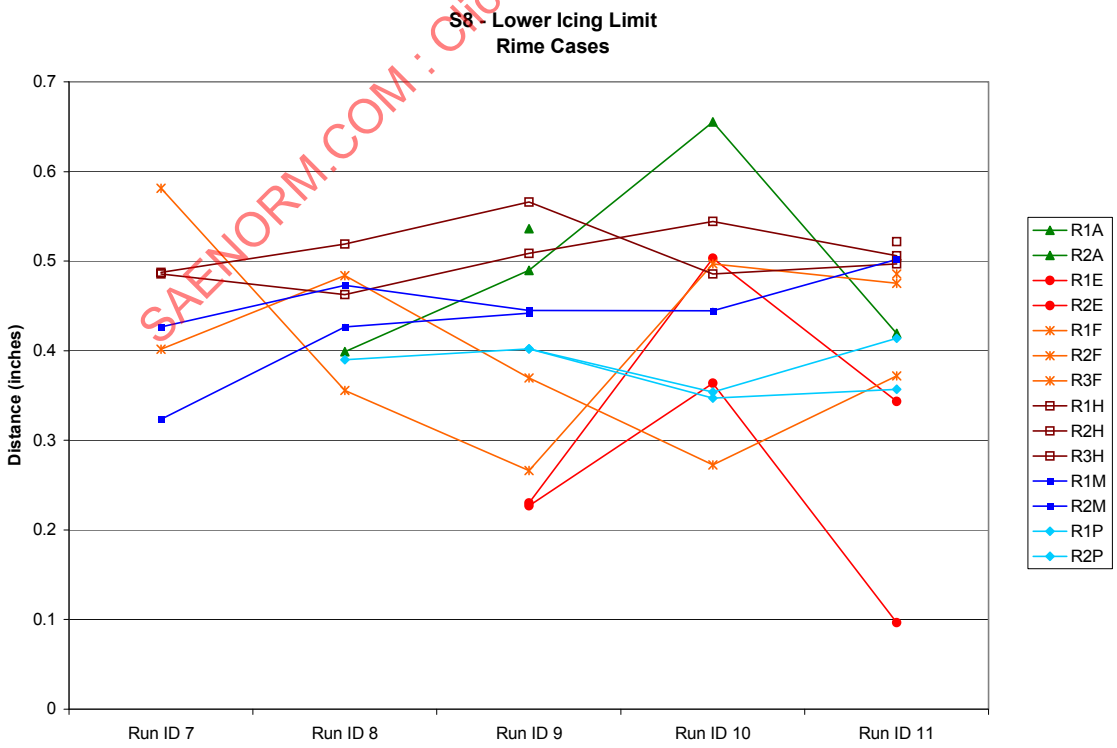

FIGURE B18 - S8 - RIME CASES

B.8 PROPOSED NEW PARAMETERS

The cylinders used for these tests do not have a reference mark to identify the absolute horizontal position. Therefore, as has been noted, testers may have rotated the template with respect to its correct position on the cylinder, thereby causing a rotation in the resulting ice shape tracing. If two tracings have about the same number of degrees between the upper and lower horns, but the horns themselves are displaced, this could indicate a rotation of the template rather than an actual difference in horn locations on the ice shapes. This comparison could only be implemented for the glaze cases.

Figure B19 shows the angular difference between the upper and lower horn for each tunnel run. It appears that this parameter is more suited to identifying repeatability of tunnel results rather than rotation.

B.9 CONCLUSIONS

THICK results support the earlier assessment that there are substantial facility to facility discrepancies in ice shapes. They also provide good quantitative measures of the discrepancies. Plots show that trends in the ice thickness and ice area parameters are generally consistent among the facilities and with the theoretical formulae.

The parameters proposed to identify tracing template rotation fail to do so.

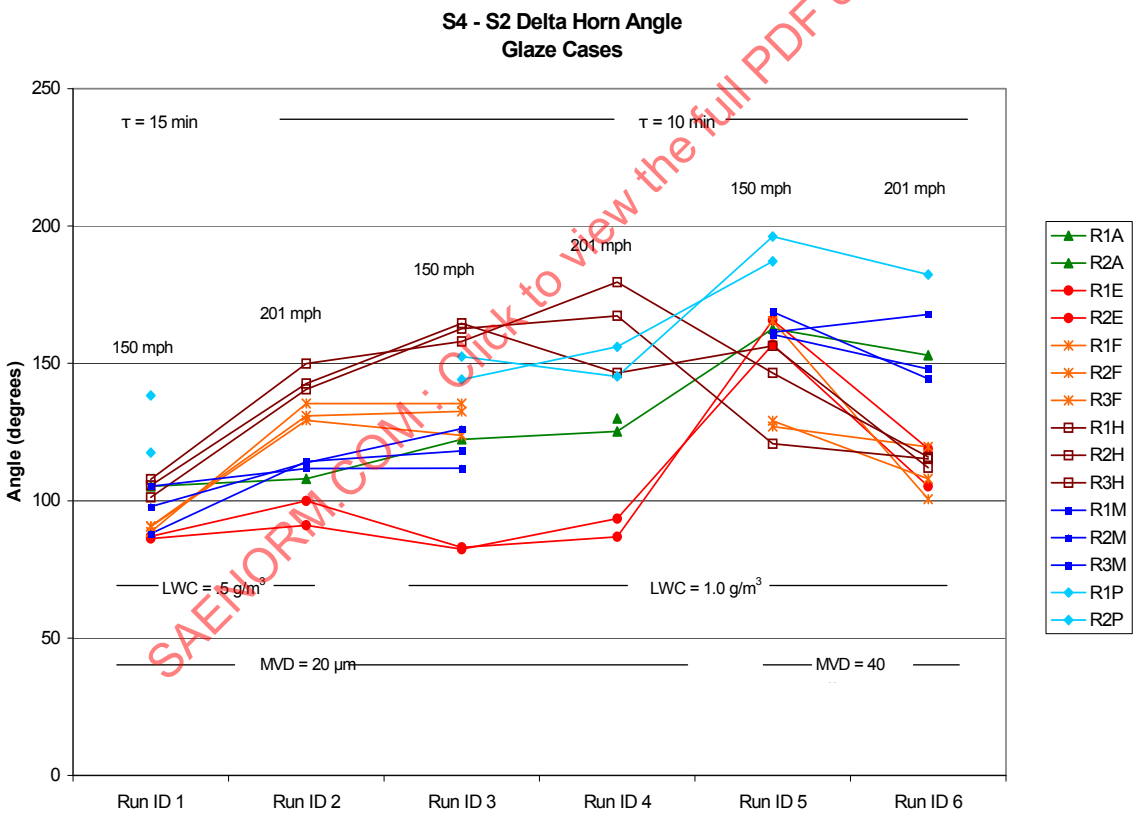

FIGURE B19 - DIFFERENCE BETWEEN UPPER AND LOWER HORN ANGLES- FREEZING FRACTION ANALYSIS

APPENDIX C

C.1 NOMENCLATURE

A_c Accumulation parameter, dimensionless

b Relative heat factor, dimensionless

c Airfoil chord, cm

c_p Specific heat of air, cal/g K

$c_{p,ws}$ Specific heat of water at the surface temperature, cal/g K

CL Tunnel centerline (mid-span) position

d Twice the leading-edge radius for airfoils, or diameter for cylinders, cm. For Equation C10, cylinder radius is substituted for d

D_v Diffusivity of water vapor, cm^2/sec

h_c Convective heat-transfer coefficient, $cal/s\,m^2\,K$

h_G Gas-phase mass-transfer coefficient, $g/s\,m^2$

k_a Thermal conductivity of air, $cal/s\,m\,K$

K Inertia parameter, dimensionless

K_0 Modified inertia parameter, dimensionless

LWC Cloud liquid-water content, g/m^3

MVD Water drop median volume diameter, μm

n_0 Stagnation freezing fraction, dimensionless

$n_{0,a}$ Freezing fraction calculated using Messinger analysis, dimensionless

$n_{0,e}$ Freezing fraction from stagnation ice thickness, dimensionless

Nu Nusselt number, dimensionless

p Static pressure, Nt/m^2

p_w Vapor pressure of water in atmosphere, Nt/m^2

p_{ww} Vapor pressure of water at the icing surface, Nt/m^2

r Recovery factor, dimensionless

Re Reynolds number of model, dimensionless

Re_δ Reynolds number of water drop, dimensionless

Sc Schmidt number, dimensionless

t_f Freezing temperature of water, °C

t_s Surface temperature, °C

t Temperature, °C

T Absolute temperature, K

V Free-stream velocity of air, m/s

β_0 Stagnation collection efficiency, dimensionless

Δ_0 Ice thickness at stagnation line, cm

ϕ Water drop energy transfer parameter, °C

λ Water drop range, m

λ_{Stokes} Water drop range if Stokes Law applies, m

Λ_f Latent heat of freezing of water, cal/g

Λ_v Latent heat of evaporation of water, cal/g

μ Viscosity of air, g/m s

θ Air energy transfer parameter, °C

ρ Air density, g/m^3

ρ_i Ice density, g/m^3

ρ_w Liquid water density, g/m^3

τ Accretion time, min

Subscripts

st Static

tot Total

C.2 BACKGROUND AND METHOD

One of the most important non-dimensional parameters used in ice-accretion modeling and scaling studies is the freezing fraction, *n*. Since Messinger introduced the term in his surface heat balance analysis more than fifty years ago (Messinger [1953]), this parameter has been shown to have a strong effect on the shape of ice accretions (Ruff [1986] and Anderson [2001]). Messinger defined the freezing fraction as the fraction of water flux entering a control volume that freezes within the control volume. Along the stagnation line of an unswept cylinder or airfoil there is no runback water from adjacent regions; thus, water reaches the surface only by impingement. The portion that freezes is represented by the accumulated ice thickness. This stagnation ice thickness, Δ_0, is defined in Figure C1. It is related to the stagnation freezing fraction, n_0, by:

$$\frac{\Delta_0}{d} = n_0 \beta_0 A_c \qquad \text{(Eq. C1)}$$

where:

A_c = the accumulation parameter

β_0 = stagnation collection efficiency

These parameters can be calculated from the test conditions and various properties using Equation C5 and Equation C6 in the next section. In Equation C1, *d* is either the cylinder diameter or twice the leading-edge radius for an airfoil. For the NACA 0012, the leading-edge radius provided by Abbott and von Doenhoff [1959] gives,

$$d = 0.0316c \qquad \text{(Eq. C2)}$$

where:

c = the chord

Equation C1 shows that the stagnation freezing fraction can be calculated from experimental ice shapes simply by measuring the stagnation ice thickness, if the test conditions are known. The stagnation freezing fraction derived from the stagnation ice thickness will be called $n_{0,e}$:

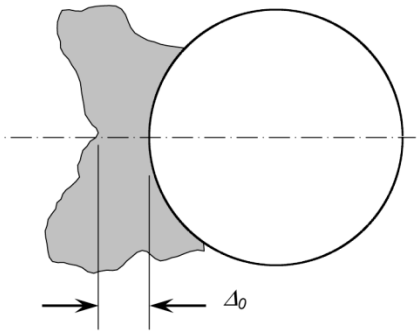

FIGURE C1A - CYLINDER WITH GLAZE ICE

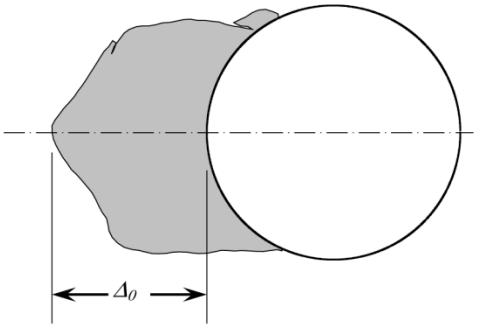

FIGURE C1B - CYLINDER WITH RIME ICE

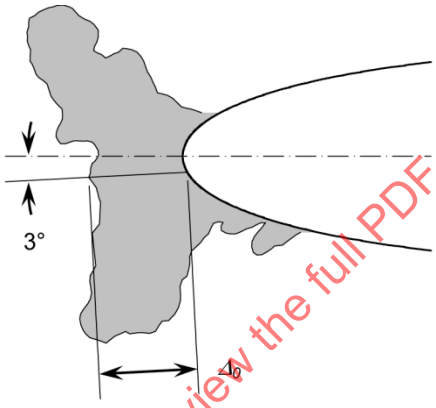

FIGURE C1C - AIRFOIL AT 3° AOA WITH GLAZE ICE

FIGURE C1 - STAGNATION ICE THICKNESS

$$n_{0,e} = \frac{\Delta_0}{d}\frac{1}{\beta_0 A_c} \qquad \text{(Eq. C3)}$$

A second way to determine n_0 is by applying Messinger's surface energy balance. That analysis gives an analytical stagnation freezing fraction,

$$n_{0,a} = \frac{c_{p,ws}}{\Lambda_f}\left(\phi + \frac{\theta}{b}\right) \qquad \text{(Eq. C4)}$$

where:

ϕ = the water energy transfer parameter

θ = the air energy transfer parameter

b = the relative heat factor

The individual terms in this expression, introduced by Tribus, et. al. [1948], can be evaluated from the equations in the next section.

The analysis used here is that described by Anderson and Tsao [2002]. It compares the experimental stagnation freezing fraction, $n_{0,e}$ (Equation C3), with the Messinger-analysis freezing fraction, $n_{0,a}$ (Equation C4), by plotting the former against the latter, as shown in Figure C2. This comparison was first suggested by Bilanin in 1988 (see Bilanin [2003]) as a way to test the validity of the analysis used for $n_{0,a}$. However, because the value of $n_{0,e}$ from Equation C3 is strongly dependent on the value of LWC, and somewhat less on MVD, assumed for the icing tests, this method of assessment can be used to test the calibration for the icing facility in which the tests are conducted.

Figure C2 is an example of the results obtained by Anderson and Tsao in the NASA Glenn Icing Research Tunnel (IRT). The data for $n_{0,e}$ were determined from mid-span (CL) ice tracings. The solid line represents perfect agreement of the two freezing fractions and the shaded band indicates the limits for ±10% agreement. A linear fit to the data is shown as a dashed line.

For the present analysis the stagnation ice thickness was determined for each centerline ice tracing provided in the Facility Standards tests for which the stagnation location could be identified. From that, an experimental stagnation freezing fraction was calculated using Equation C3 and compared with the Messinger stagnation freezing fraction from Equation C4. Note that the expression for $n_{0,a}$ applies to a clean model, but the geometry and, consequently, the stagnation freezing fraction varies as the ice accretes. Thus, $n_{0,e}$ is an average value over the accretion time. In general, then, perfect equality between these two freezing fractions should not be expected, except with rime ice conditions for which $n_{0,e} = n_{0,a} = 1$ for both the clean model and the model with accreted ice. However, two of the three terms used to calculate $n_{0,a}$ are independent of geometry. Therefore, the actual stagnation freezing fraction may not vary significantly during accretion. The good agreement between $n_{0,a}$ and $n_{0,e}$ displayed in Figure C2 over the entire range of freezing fraction would tend to validate this last supposition. Consequently, the two freezing fractions should compare well if the *LWC* and *MVD* calibrations are accurate.

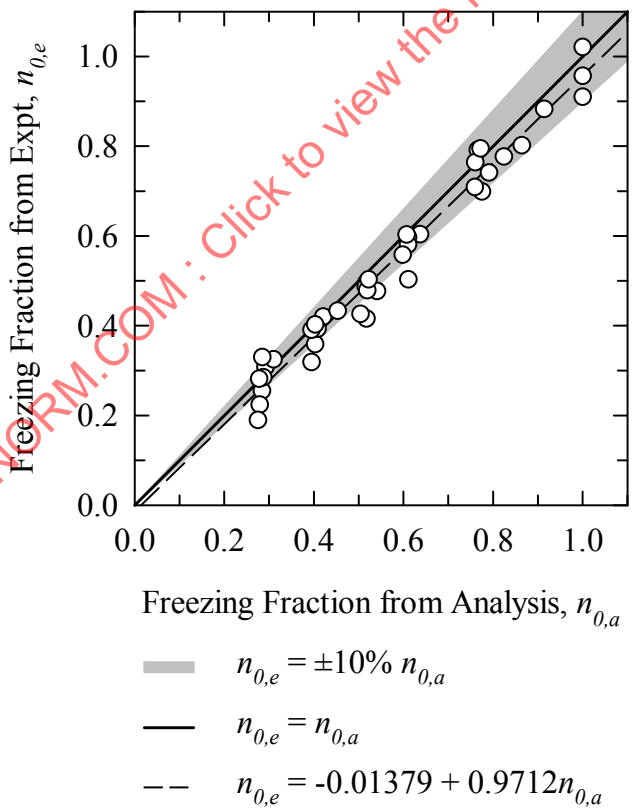

FIGURE C2 - EXPERIMENTAL AND ANALYTICAL FREEZING FRACTIONS COMPARED 2001 AND 2002 TESTS IN THE IRT WITH NACA 0012 MODELS AT 0 DEGREES AOA

C.3 PARAMETER DEFINITIONS

A_c is the accumulation parameter

$$A_c = \frac{LWC\ V\ \tau}{d\ \rho_i} \quad \text{(Eq. C5)}$$

and β_0 is the collection efficiency of water drops at the stagnation line. The stagnation collection efficiency, β_0, in Equation C1 was calculated from the expression given by Langmuir and Blodgett:

$$\beta_0 = \frac{1.40\left(K_0 - 0.125\right)^{0.84}}{1 + 1.40\left(K_0 - 0.125\right)^{0.84}} \quad \text{(Eq. C6)}$$

where the modified inertia parameter, K_0, is:

$$K_0 = \frac{1}{8} + \frac{\lambda}{\lambda_{Stokes}}\left(K - \frac{1}{8}\right) \quad \text{(Eq. C7)}$$

Here λ/λ_{Stokes} is the drop range parameter, defined as the ratio of actual drop range to that if Stokes drag law for solid-spheres applied. It is a function only of the drop Reynolds number, Re_δ and was tabulated by Langmuir and Blodgett. The following fit to the Langmuir and Blodgett tabulation was used:

$$\frac{\lambda}{\lambda_{Stokes}} = \frac{1}{0.8388 + 0.001483 Re_\delta + 0.1847\sqrt{Re_\delta}} \quad \text{(Eq. C8)}$$

where the drop Reynolds number is

$$Re_\delta = \frac{V\ MVD\ \rho_w}{\mu} \quad \text{(Eq. C9)}$$

The inertia parameter, K, in Equation C7 is

$$K = \frac{\rho_w\ MVD^2\ V}{18 d\ \mu} \quad \text{(Eq. C10)}$$

In Equation C10, d is the cylinder radius, or, for airfoils, twice the leading-edge radius. Note that this nomenclature differs for cylinders from that used in other expressions in this appendix. For them, d is the cylinder diameter or twice the leading-edge radius for an airfoil.

The parameters ϕ, θ and b in (Equation C4) are defined as

$$\phi = t_f - t_{st} - \frac{V^2}{2c_{p.ws}} \quad \text{(Eq. C11)}$$

$$\theta = \left(t_s - t_{st} - \frac{rV^2}{2c_p} \right) + \frac{h_G}{h_c} \left(\frac{\frac{p_{ww}}{T_{st}} - \frac{p_{tot}}{T_{tot}} \frac{p_w}{p_{st}}}{\frac{1}{0.622} \frac{p_{tot}}{T_{tot}} - \frac{p_{ww}}{T_{st}}} \right) \quad \text{(Eq. C12)}$$

$$b = \frac{LWC\, V\, \beta_0\, c_{p,ws}}{h_c} \quad \text{(Eq. C13)}$$

Equation C12 includes compressibility effects. The second term in Equation C12 accounts for evaporation. The gas-phase mass-transfer coefficient, h_G, can be found from

$$h_G = \frac{h_c}{c_p} \left(\frac{Pr}{Sc} \right)^{0.67} \quad \text{(Eq. C14)}$$

where the Prandtl number is

$$Pr = \frac{c_p \mu}{k_a} \quad \text{(Eq. C15)}$$

and the Schmidt number is given by

$$Sc = \frac{\mu}{\rho D_v} \quad \text{(Eq. C16)}$$

Diffusivity of water vapor in air, D_v, can be computed with the following expression from Pruppacher and Klett [1980]:

$$D_v = 0.211 \frac{\text{cm}^2}{\text{s}} \left(\frac{T_{film}}{273.15\text{K}} \right)^{1.94} \left(\frac{1.0132 \times 10^5\, \text{Pa}}{p_{st}} \right) \quad \text{(Eq. C17)}$$

The convective heat-transfer coefficient, h_c, was determined from the Nusselt number:

$$h_c = \frac{k_a}{d} Nu \quad \text{(Eq. C18)}$$

The evaluation for *Nu* at the stagnation line of a cylinder with laminar flow was reported by Kreith [1958]:

$$Nu = 1.14 Pr^{0.4} Re^{0.5} \quad \text{(Eq. C19)}$$

with

$$Re = \frac{Vd\rho}{\mu} \quad \text{(Eq. C20)}$$

The air properties used in Equation C19 should be based on the film temperature. Poinsatte's 10 measurements of heat-transfer coefficients at the stagnation line of an NACA 0012 airfoil in the IRT gave correlations consistent with the expression for cylinders in Equation C19 if twice the airfoil leading-edge radius was substituted for cylinder diameter.

C.4 RESULTS

Not all facilities reported ice shapes for each condition specified in the original plan. In some cases, the stagnation location could not easily be defined for the shapes reported, so these cases were not included in the analysis. Thus, the same tests were not analyzed for each facility. Table C1 indicates those ice shapes analyzed for each facility with an 'x' in the test condition ID column.

Figure C3 shows the $n_{0,e}$ plotted against $n_{0,a}$ for each facility for the cylinder model. The solid line in each graph represents equality between the two stagnation freezing fractions, and a shaded band indicates ±10% variation of the $n_{0,e}$ about the line of equality. Equal scales are used for both axes to facilitate comparison. Of course, $n_{0,a}$ cannot be greater than unity (rime), while $n_{0,e}$ is not constrained. The largest scatter typically would be expected at the lowest freezing fractions, where ice thickness is least and small errors in tracing could have a relatively large impact on $n_{0,e}$. For rime conditions, the most accurate values of $n_{0,e}$ are expected because the leading edge thickness is greater for rime than glaze, so small errors in tracing or measurement are relatively less important.

Furthermore, the stagnation line is more easily located for rime shapes. Even for rime, however, errors in recording ice thickness are still possible: For example, if the tracing template is not inserted all the way to the model surface, an ice thickness will be registered that is too small. The resulting $n_{0,e}$ will be less than $n_{0,a}$ in this case. The way the ice is cut and the pencil is held relative to the ice surface also affect the recorded ice thickness, indicating either a thicker or thinner leading edge than the actual accretion. Consequently, scatter in the value of $n_{0,e}$ relative to $n_{0,a}$ is typical.

The values of both $n_{0,e}$ and $n_{0,a}$ are subject to uncertainties in test conditions, as well. In particular, MVD and LWC are the conditions known with the least certainty. In the IRT, for example, LWC is estimated to be known to ±10% and MVD to within ±12%. These values translate to an uncertainty of ±15% in $n_{0,a}$. The value of $n_{0,e}$ found from Equation C3 is inversely proportional to the value of LWC through the accumulation parameter (Equation C5) and is also influenced by MVD through β_0.

TABLE C1 - ICE SHAPES USED IN ANALYSIS

TABLE C1A - CYLINDERS

Facility		ID 1	2	3	4	5	6	7	8	9	10	11
A	R1	x	x	x	x	x	x		x	x	x	x
	R2				x							
E	R1	x	x	x	x	x	x			x	x	x
	R2	x	x	x	x	x	x			x	x	x
F	R1	x	x	x		x	x	x	x	x	x	x
	R2	x	x	x		x	x	x	x	x	x	x
	R3	x	x	x		x	x					x
H	R1	x	x	x	x	x	x	x	x	x	x	x
	R2	x	x	x	x	x	x	x		x	x	x
M	R1	x	x	x		x	x	x	x	x	x	x
	R2	x	x	x		x	x	x	x	x		
	R3	x	x	x		x	x					
P	R1	x	x	x	x	x	x		x	x	x	x
	R2			x	x	x				x	x	x

TABLE C1B - 12-IN NACA 0012

Facility		ID 1	2	3	4	5	6	7	8	9	10	11
A	R1	x	x	x						x	x	x
	R2		x	x						x	x	
E	R1	x								x	x	
	R2	x								x	x	
F	R1	x	x			x	x	x	x	x	x	x
	R2		x			x	x	x	x	x	x	x
	R3		x			x	x					x
H	R1	x	x	x	x	x	x	x	x	x	x	x
	R2	x	x	x	x	x	x			x	x	x
M	R1	x	x	x		x	x	x	x	x	x	x
	R2	x		x		x		x	x	x	x	x
P	R1		x				x	x		x	x	x
	R2		x									

TABLE C1C - 36-IN NACA 0012

Facility											ID 1	2	3	4	5	6	7	8	9	10	11
A										R1	x	x	x						x	x	x
										R2	x	x	x								
E										R1	x								x	x	
										R2	x								x	x	
F										R1	x					x	x		x	x	x
										R2	x					x	x		x	x	x
										R3	x					x					x
H										R1		x		x	x	x			x	x	
	R2		x		x	x	x			x	x										
M	R1	x	x	x		x	x	x		x	x		x								
	R2	x	x	x		x	x	x		x	x		x								
	R3	x	x	x		x	x														
P	R1	x				x		x		x			x								
	R2	x								x			x								

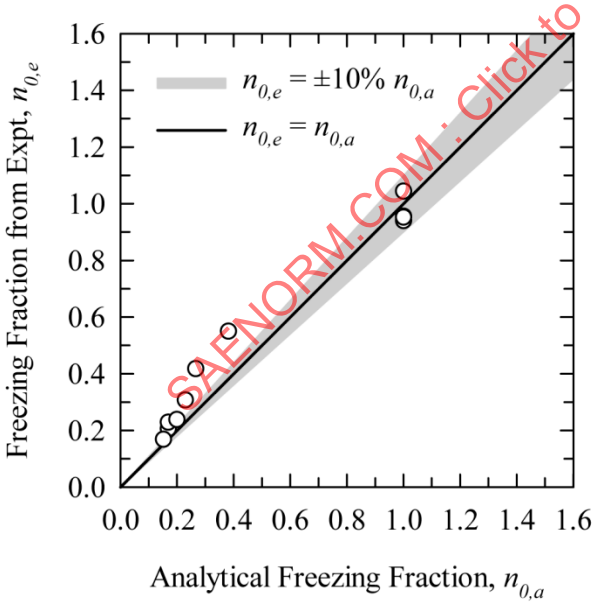

FIGURE C3A - FACILITY A

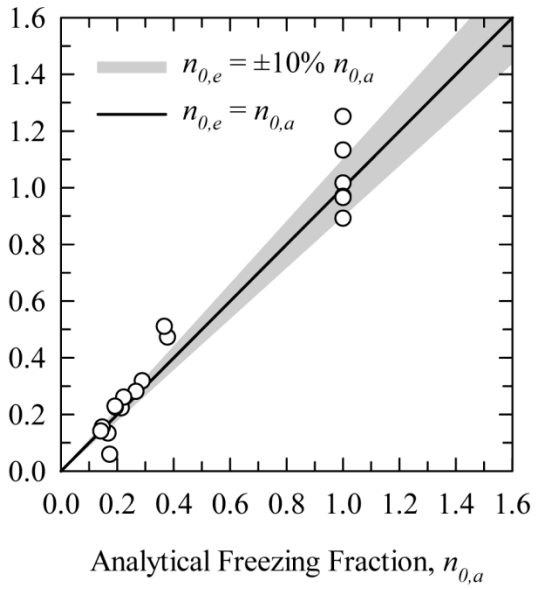

FIGURE C3B - FACILITY E

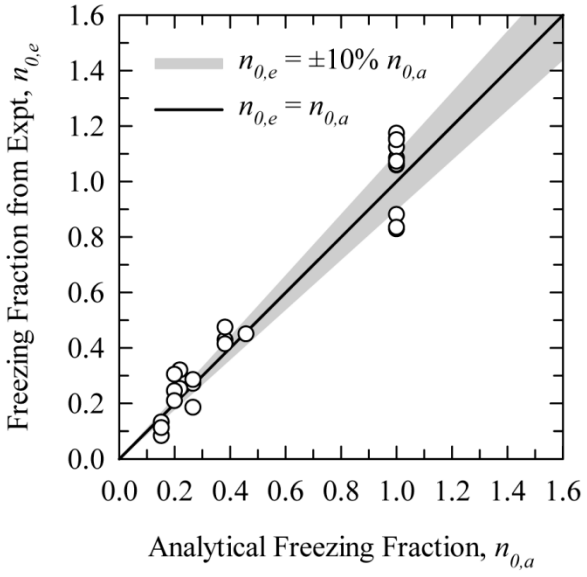

FIGURE C3C - FACILITY F

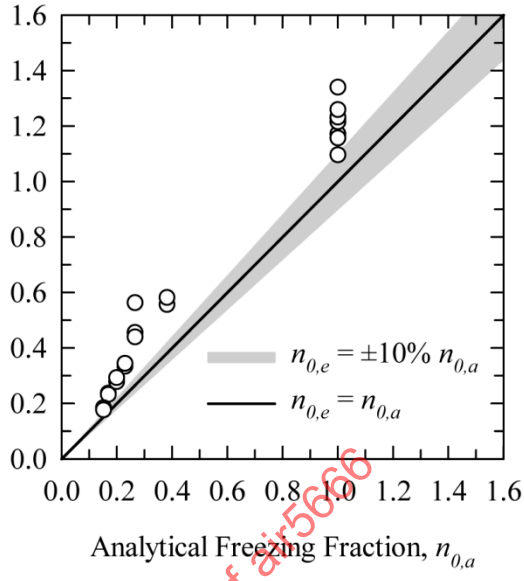

FIGURE C3D - FACILITY H

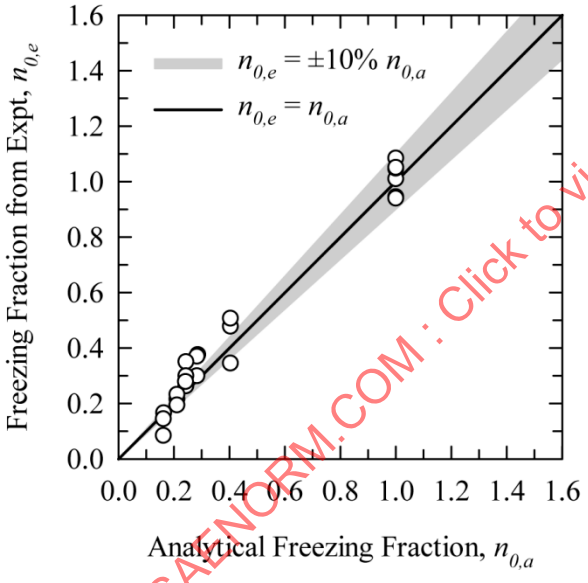

FIGURE C3E - FACILITY M

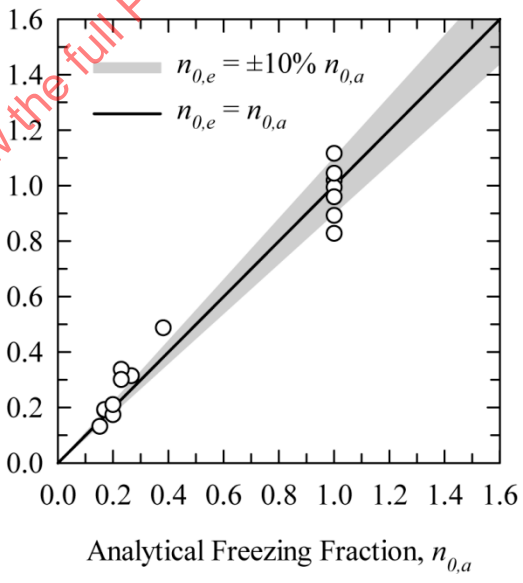

FIGURE C3F – FACILITY P

FIGURE C3 - FREEZING-FRACTION ANALYSIS RESULTS FOR CYLINDERS CENTERLINE ICE SHAPES

The freezing-fraction analysis is most sensitive to errors in LWC calibration at rime conditions. For the rime conditions included in these tests even a significant increase in LWC would not change the rime character of the ice. Therefore, if the test LWC were higher than the calibrated value by, say, 30%, the stagnation ice thickness would be greater than the expected value by 30%. In this example, then, the value determined for $n_{0,e}$ would be higher than $n_{0,a}$ by 30%, assuming the ice thickness and all test conditions were recorded accurately. For glaze conditions, the situation is more complicated. If the true LWC were higher than the calibrated value, not only would the quantity of ice be greater than expected, but the actual stagnation freezing fraction for the test would be lower than expected. The stagnation ice thickness would tend to increase due to the larger total quantity of ice, but would tend to decrease with the lower stagnation freezing fraction. Depending on the test conditions, an increase in LWC of 30% would increase the stagnation thickness by only 5 to 10%, with a consequent increase in $n_{0,e}$ of the same amount.

Similarly, if the *MVD* calibration is not correct, the stagnation thickness will not be consistent with the stagnation freezing fraction ($n_{0,a}$) calculated from the indicated test conditions. The effect of *MVD* on the total amount of ice is determined by β_0, which is not very sensitive to *MVD* when β_0 is already high. A doubling of *MVD* from 20 to 40 μm, for example, for the conditions of these tests will increase β_0 by no more than about 33%. This drop-size increase will also reduce the stagnation freezing fraction for glaze ice by about 10% or less. The net effect on the stagnation thickness is an increase of less than 10% for glaze. For rime conditions, the change in stagnation thickness will be directly proportional to the change in β_0. Nevertheless, it is apparent that the stagnation thickness, and the resulting value of $n_{0,e}$ calculated from it, will be much more sensitive to errors in the *LWC* calibration than in the *MVD* calibration. Therefore, when $n_{0,e}$ is found to be consistently higher than $n_{0,a}$ the most likely explanation is that the true tunnel *LWC* is higher than that indicated by the calibration.

Cylinder results for facilities A, E, F, M and P displayed approximately equal scatter above and below the $n_{0,e} = n_{0,a}$ line fairly consistently over the range of freezing fractions tested. This result suggests that actual cloud *LWC* and *MVD* agreed fairly well with calibrated values for these facilities. Facility H, however, showed higher $n_{0,e}$ than $n_{0,a}$, suggesting that the true *LWC*, and perhaps *MVD*, for that facility were higher than indicated by the calibration.

The freezing-fraction analysis was also performed using the data provided for the 12-in and 36-in NACA 0012 models. This kind of analysis for airfoils is best performed when tests are made without AOA, because the position of the stagnation line of the ice is generally easier to locate. Identification of stagnation for a symmetrical model and with no angle of attack is facilitated because the ice shape should be nearly symmetrical. For glaze ice, stagnation will occur at the minimum ice thickness near y = 0; for rime, at the maximum. Note that even with 0 degree AOA, however, some displacement of stagnation from y = 0 is possible due to flow angularity in the facility.

Because the airfoil models in the Facility Standard Tests were tested at an angle of attack, there are two concerns about the results. First, the stagnation region of the ice is not always as well defined for glaze conditions, as it would be at 0 degree AOA. The wrong estimate of stagnation ice thickness can result if the leading edge is not properly located. For this analysis, if a particular ice accretion did not have features that allowed a clear definition of the stagnation region, that accretion was not included in the analysis. Second, with an airfoil at angle of attack, some cloud movement compared with an empty tunnel will take place; consequently, the model leading edge may be exposed to a different part of the cloud than was calibrated at the tunnel center. For this analysis, however, no information was available to permit correction for LWC or MVD values due to cloud movement, and only reported test conditions were used.

Figure C4 shows the results of the freezing-fraction analysis for the 12-in-chord NACA 0012 model. Values of the two stagnation freezing fractions were in reasonable agreement for glaze conditions for the six facilities. However, for rime ice, which was shown above to be most sensitive to errors in cloud calibration, the rime $n_{0,e}$ values for facilities E and H were significantly higher than $n_{0,a}$. This result suggests that the model was exposed to an *LWC* or *MVD* or some combination of the two that was significantly higher than the calibration indicated for these facilities. Lift generated by the model at AOA would result in the stagnation line encountering a different portion of the cloud than was calibrated at the tunnel center, and this factor may account for some of the discrepancy between the two stagnation freezing fractions.

Figure C5 gives the results for the 36-in-chord NACA 0012 model. The freezing-fraction analysis for facilities A, F, and M showed reasonable agreement between the two stagnation freezing fractions, much like the 12-in-chord-model comparisons. For glaze ice, facility E provided only two ice shapes to analyze for the 36-in-chord model, and agreement between $n_{0,e}$ and $n_{0,a}$ was reasonable for these. For rime conditions, that facility provided ice shapes for two conditions, with each repeated once. The repeat test for ID 9 produced a significantly larger stagnation thickness than the original run; the $n_{0,e}$ calculated from this thickness was 40% higher than $n_{0,a}$.

As already seen for the cylinder tests (see Figure C3D), the facility H analysis for the 36-in-chord 0012 model gave consistently higher $n_{0,e}$ than $n_{0,a}$ for both rime and glaze conditions. Repeat test results showed no significant differences from the original ice shapes and stagnation thicknesses for that facility. Facility P showed $n_{0,e}$ 29 and 36% higher than $n_{0,a}$ for the two tests of ID 11, but other rime results showed good agreement of the two stagnation freezing fractions.

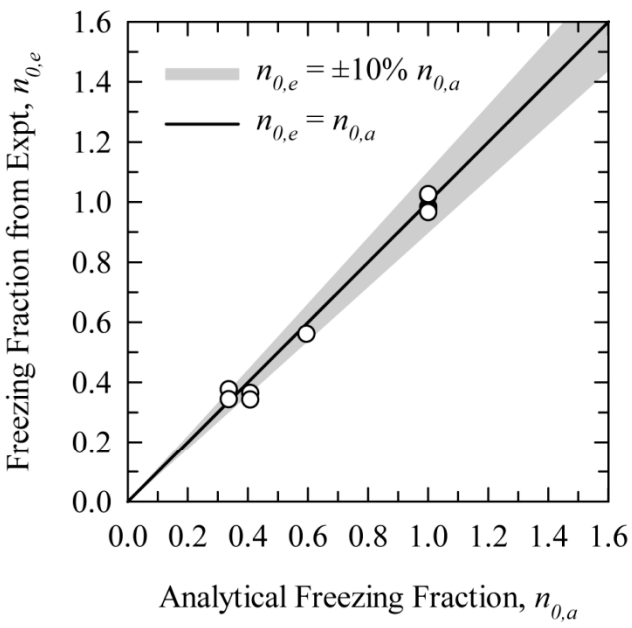

FIGURE C4A – FACILITY A

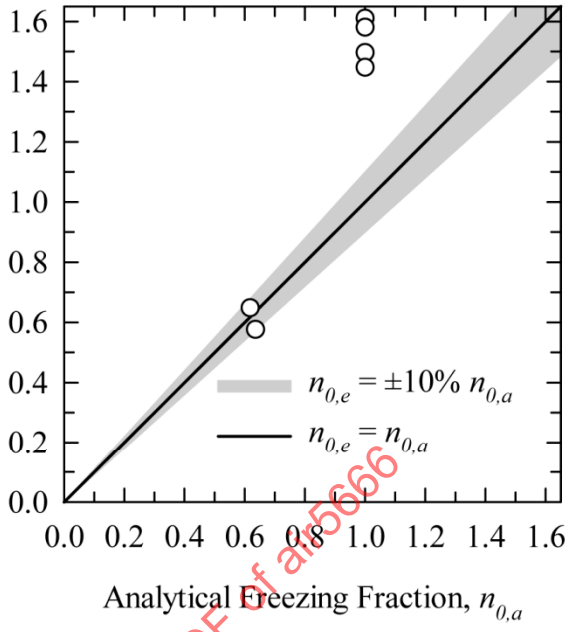

FIGURE C4B – FACILITY E

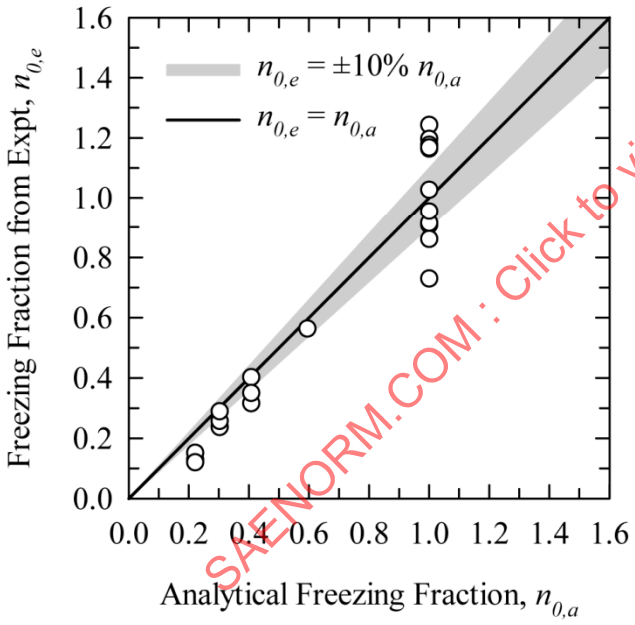

FIGURE C4C – FACILITY F

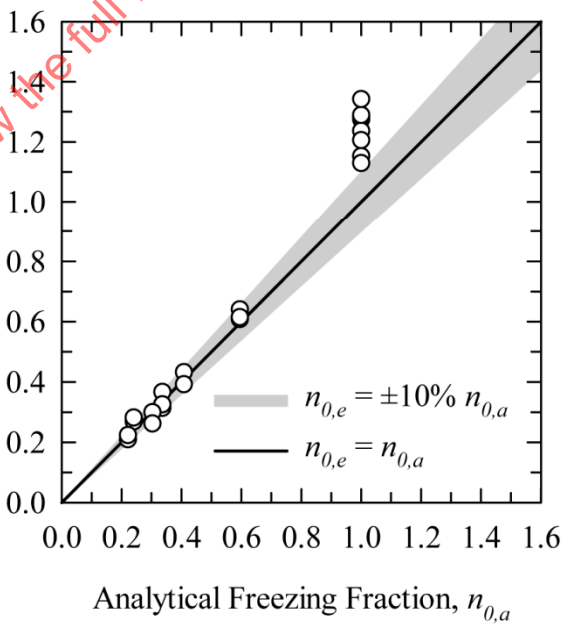

FIGURE C4D – FACILITY H

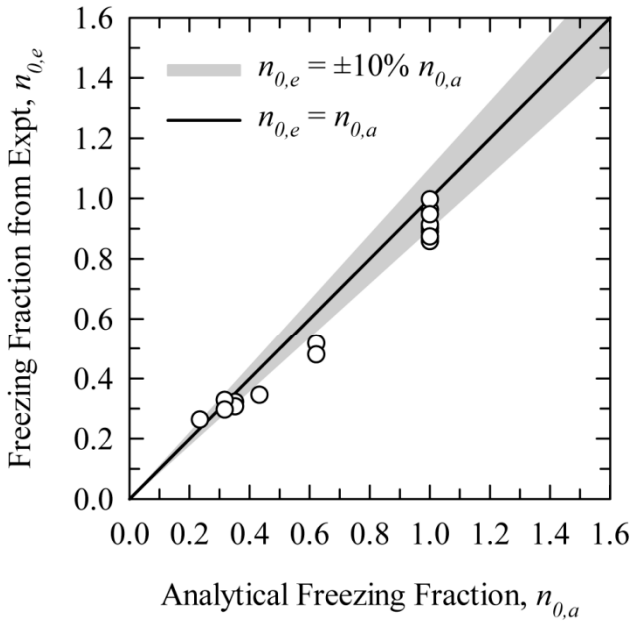

FIGURE C4E – FACILITY M

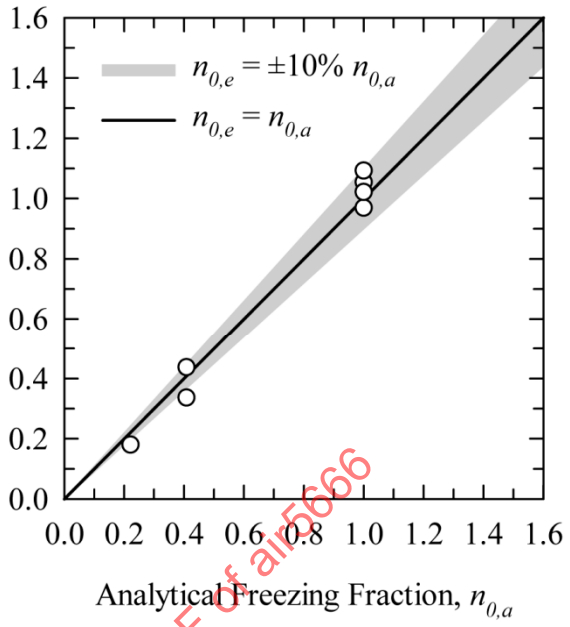

FIGURE C4F – FACILITY P

FIGURE C4 - FREEZING-FRACTION ANALYSIS FOR 12-IN-CHORD NACA 0012 AIRFOILS AT 3 DEGREES AOA CENTERLINE ICE SHAPES

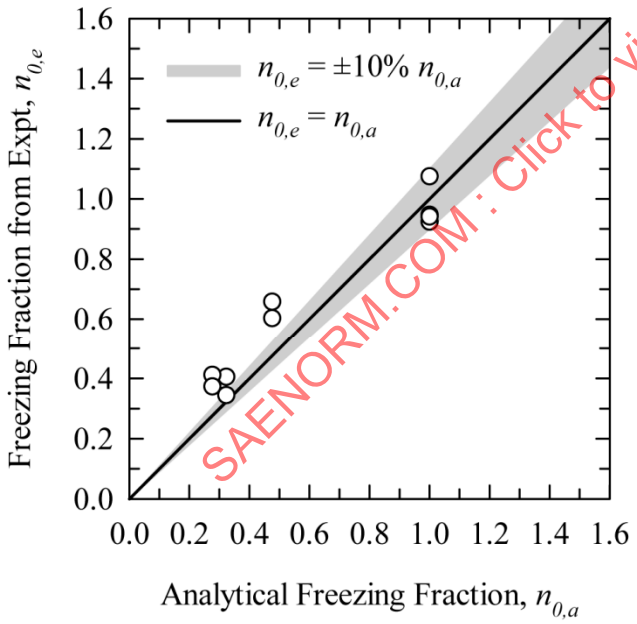

FIGURE C5A – FACILITY A

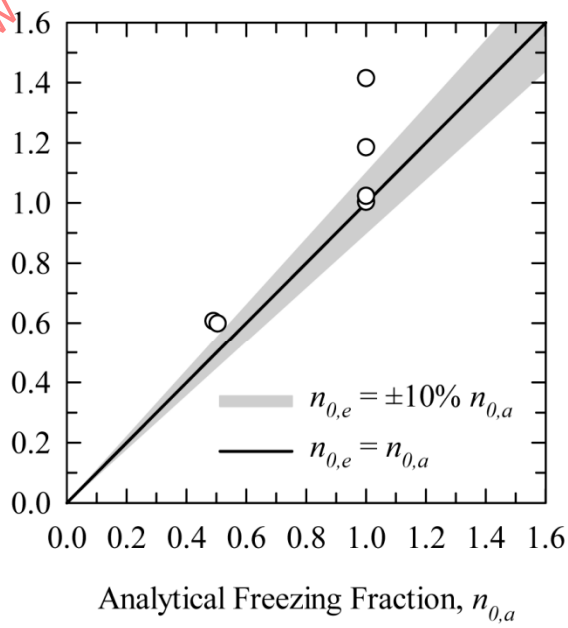

FIGURE C5B – FACILITY E

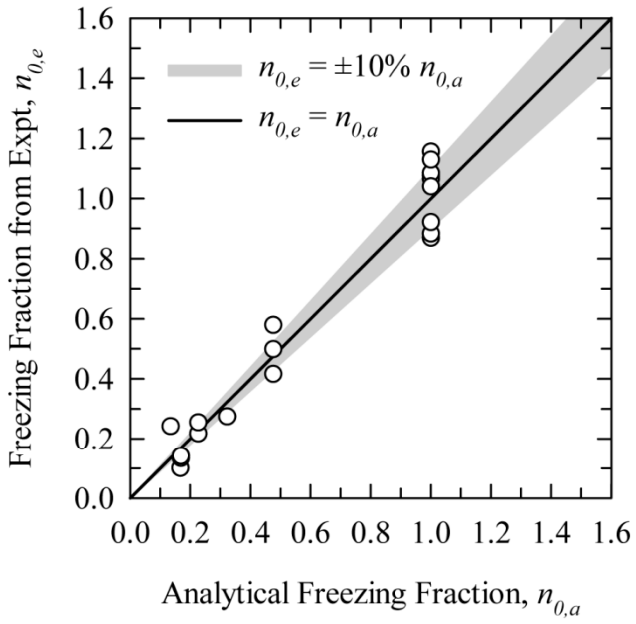

FIGURE C5C – FACILITY F

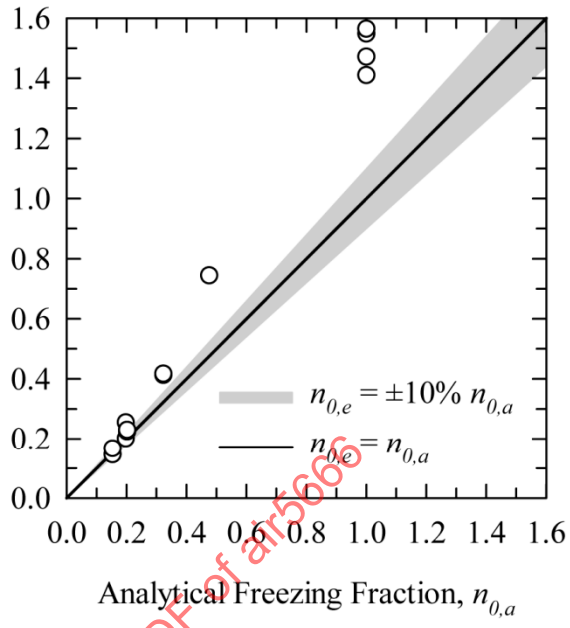

FIGURE C5D – FACILITY H

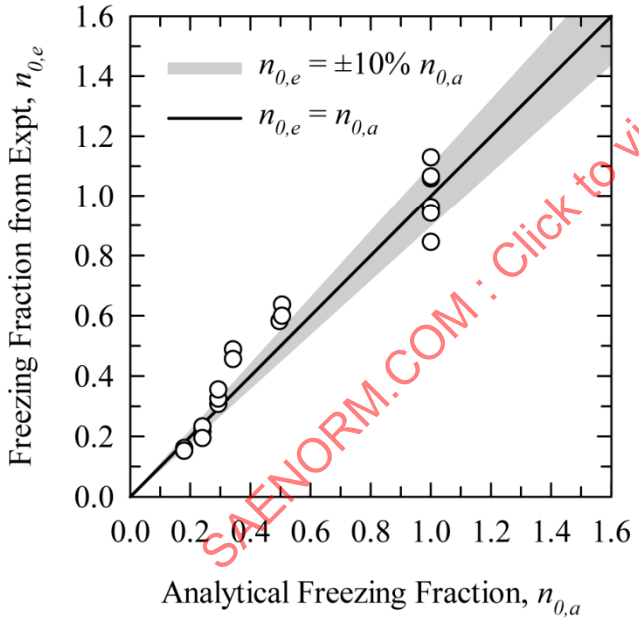

FIGURE C5E – FACILITY M

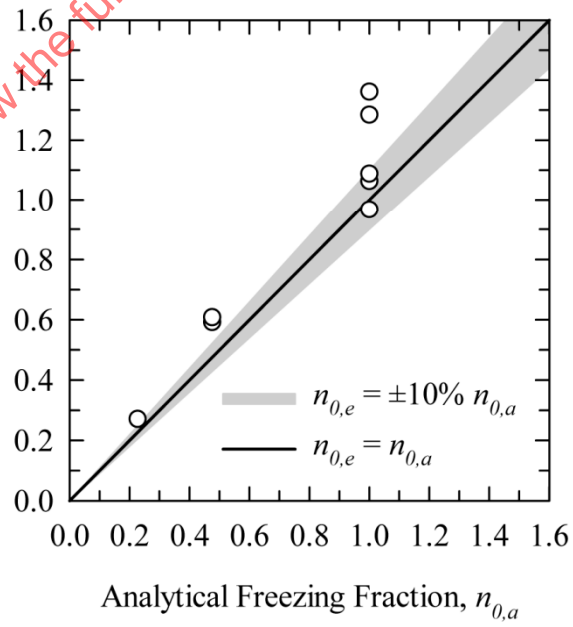

FIGURE C5F – FACILITY P

FIGURE C5 - FREEZING-FRACTION ANALYSIS FOR 36-IN-CHORD NACA 0012 AIRFOIL AT 3 DEGREES AOA CENTERLINE ICE SHAPES

C.5 CONCLUSIONS

The observations for the $n_{0,e}$ - $n_{0,a}$ comparisons for each of the facilities and models are summarized as follows. Due to the inherent errors in tracing glaze ice shapes and the much greater sensitivity of the rime stagnation thickness on the cloud calibration, comparisons of the two stagnation freezing fractions at rime are considered more significant than results for glaze.

- Facility A: The two n_0 values for rime conditions were within ±10% for the three models. Glaze test conditions for both the cylinder and 36-in-chord model produced values of $n_{0,e}$ typically higher than $n_{0,a}$, while good agreement of the two resulted for the 12-in-chord model.

- Facility E: The cylinder tests gave agreement betweew the two n_0 values for both rime and glaze conditions within about ±25%, while the 12-in-chord airfoil tests resulted in $n_{0,e}$ as much as 60% higher at rime conditions than $n_{0,a}$. For the 36-in-chord 0012 repeatability for the conditions of ID 9 was poor, while the agreement between $n_{0,e}$ and $n_{0,a}$ was typically better than for the 12-in model.

- Facility F: Typical agreement betweew the two n_0 values was within approximately ±20 - 25% for all models and conditions.

- Facility H: Both glaze and rime tests gave $n_{0,e}$ higher than $n_{0,a}$ for the cylinder. For the 12-in 0012, glaze tests showed good agreement between the two stagnation freezing fractions, but rime $n_{0,e}$ were consistently higher than $n_{0,a}$. For the 36-in-chord model both rime and glaze conditions gave $n_{0,e}$ significantly higher than $n_{0,a}$ except at the lowest freezing fractions tested.

- Facility M: For all the models agreement of ±15 - 20% between the two freezing fractions was seen for both glaze and rime test conditions.

- Facility P: Typically, the agreement between n_0 values was ±20% for the cylinder and 12-in-chord airfoil. For the 36-in-chord model, few glaze ice shapes were available to analyze; these tended to produce $n_{0,e}$ somewhat higher than $n_{0,a}$, but there are insufficient data to attach any significance to this comparison. For that model at rime conditions, several conditions gave $n_{0,e}$ within ±10% of $n_{0,a}$, while two produced $n_{0,e}$ of 29 and 36% higher than $n_{0,a}$. The amount of data is not sufficient to draw conclusions regarding the significance of this disagreement.

For most icing tests it is very important that facility *LWC* calibrations be correct. This analysis showed how stagnation ice thickness measurements and the $n_{0,e}$ derived from them can be used to infer the accuracy of the tunnel *LWC* calibration.

C.6 REFERENCES

Messinger, B.L., “Equilibrium Temperature of an Unheated Icing Surface as a Function of Airspeed,” *J. Aeron. Sci*. vol. 20 no. 1, January 1953, pp 29-42.

Ruff, G.A., “Analysis and Verification of the Icing Scaling Equations,” AEDC-TR-85-30, vol 1 (Rev), March 1986.

Anderson, David N., “Acceptable Tolerances for Matching Icing Similarity Parameters in Scaling Applications,” AIAA-2001-0832, January 2001.

Abbott, Ira H. and von Doenhoff, Albert E., Theory of Wing Sections, Dover, New York, 1959, p321.

Tribus, Myron, Young, G.B.W. and Boelter, L.M.K., “Analysis of Heat Transfer Over a Small Cylinder in Icing Conditions on Mount Washington,” Trans. ASME vol. 70, November 1948, pp 971-976.

Anderson, David N., and Tsao, Jen-Ching, “Evaluation and Validation of the Messinger Freezing Fraction,” AIAA-2002-0522, January 2002.

Bilanin, A.J., “Proposed Modifications to the Ice Accretion/Icing Scaling Theory,” AIAA Paper AIAA-2003-1218, January 2003.

Pruppacher, Hans R. and Klett, James D., Microphysics of Clouds and Precipitation, Reidel, Boston, 1980.

Kreith, Frank, Principles of Heat Transfer, International Textbook Co., Scranton, 1958.

Poinsatte, Philip E., “Heat Transfer Measurements from a NACA 0012 Airfoil in Flight and in the NASA Lewis Icing Research Tunnel,” NASA CR 4278, March 1990.

APPENDIX D - ANALYSIS REPORT

D.1 INTRODUCTION

This appendix contains comparisons of ice shapes generated in the different facilities. The approach taken is to show a qualitative comparison of ice shapes, and to form groups of ice shapes from different facilities that show reasonable agreement. Each test condition for each model is treated separately. This appendix shows all ice shapes from all facilities for the 12-in chord 0012 airfoil. Comparisons are also shown for representative examples from each of the other two models tested for both the glaze and rime ice conditions. Tables are included that summarize the comparative results for each model. Table 2 provides the tunnel settings for each test condition.

NOTE: The original analysis of data was done with color plots. Since SAE does not print in color the figures were converted to black and white. Some figures had too many curves to be able to discern which curve belongs to which facility when converted to black and white. These curves are generally figures with tracings from all facilities, and although individual facility data cannot be identified, the range of ice accretion for each case can be seen.

D.2 NACA 0012 12-IN CHORD AIRFOIL

Figure D1 shows the results from test point 1, a glaze ice accretion. For this case all facilities show reasonable agreement. There were two groups of facilities that showed very good agreement.

Figure D2 shows the results from test point 2, a glaze ice accretion at higher airspeed. For this case the overall agreement between facilities is poor. Figure D2A reveals that important features of the ice shapes such as horn angle and impingement limits vary widely among facilities. Figure D2B shows a grouping of facilities with similar horn characteristics, but different horn angles. Figure D2C shows the extremes of horn angles among facilities. These differences in horn angle are probably due to differences in drop size calibrations from facility to facility.

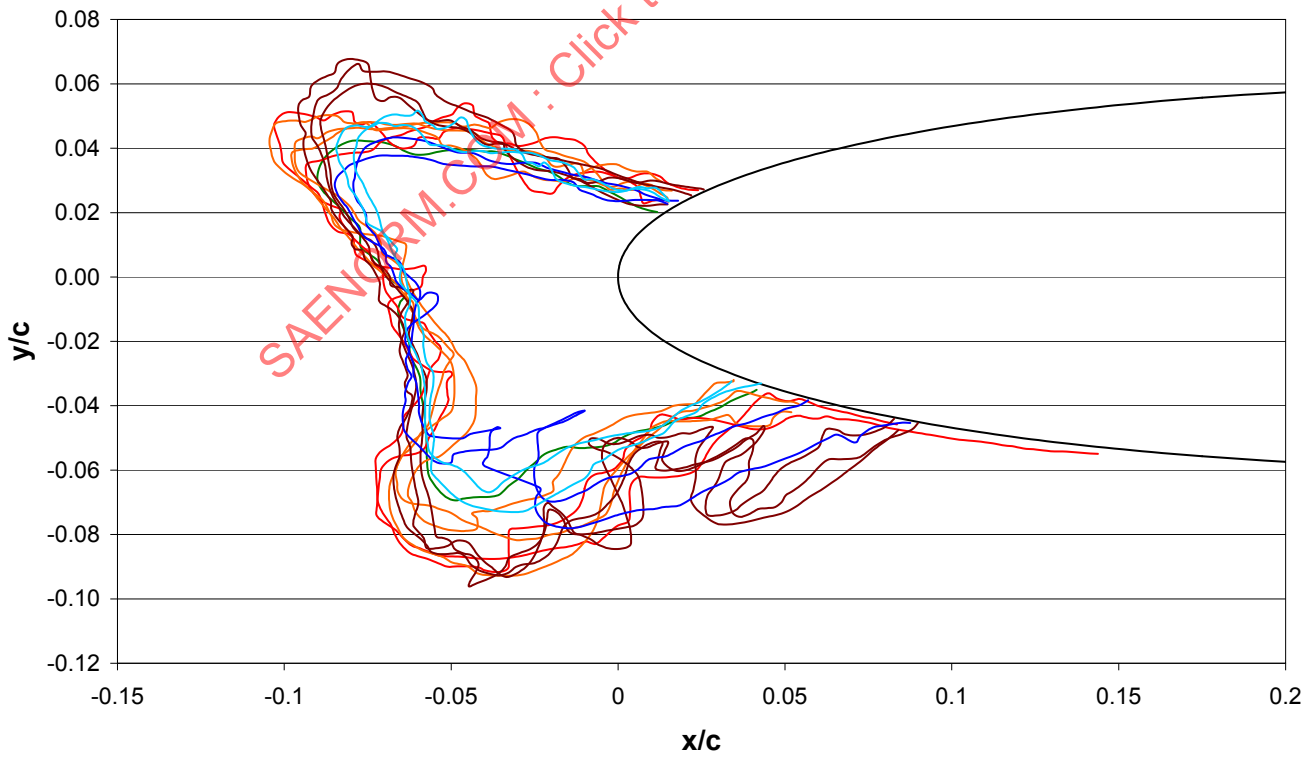

FIGURE D1A - TRACINGS FROM ALL FACILITIES

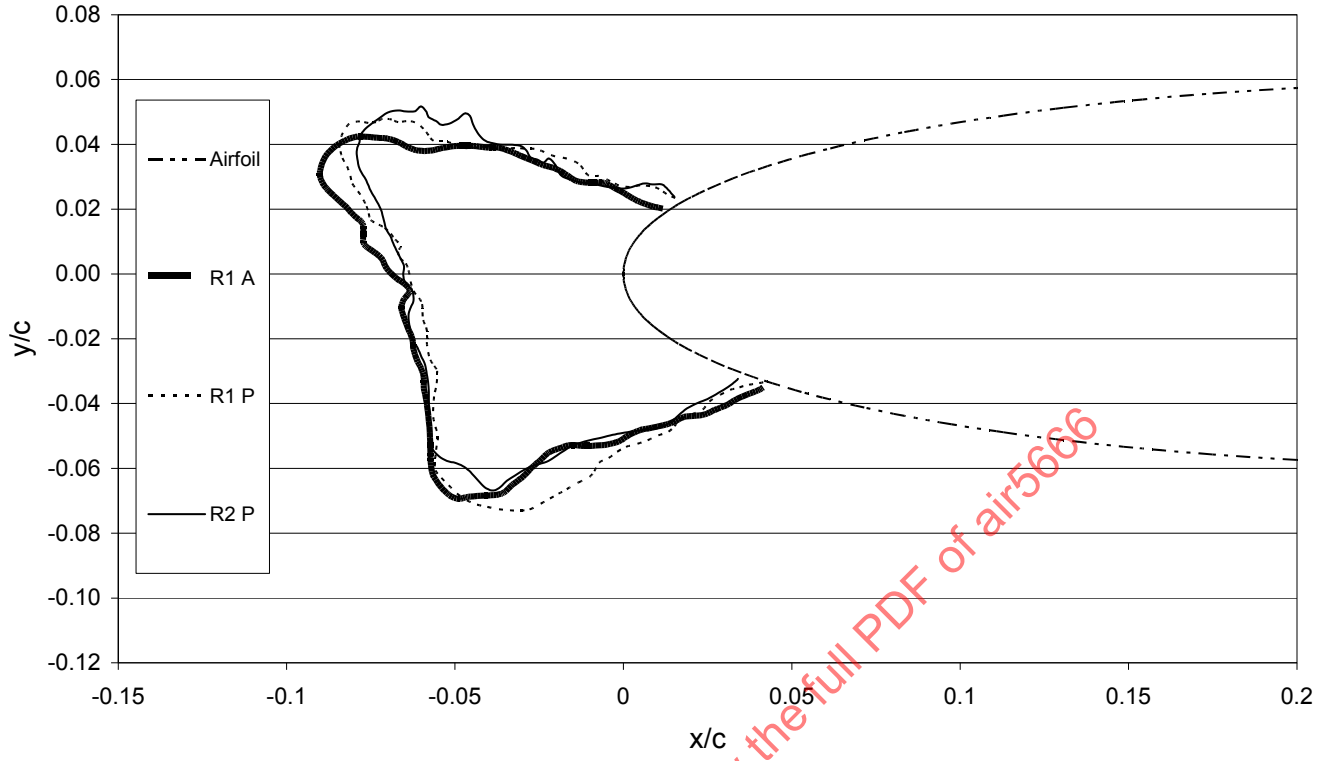

FIGURE D1B - TRACINGS FROM FACILITIES A AND P

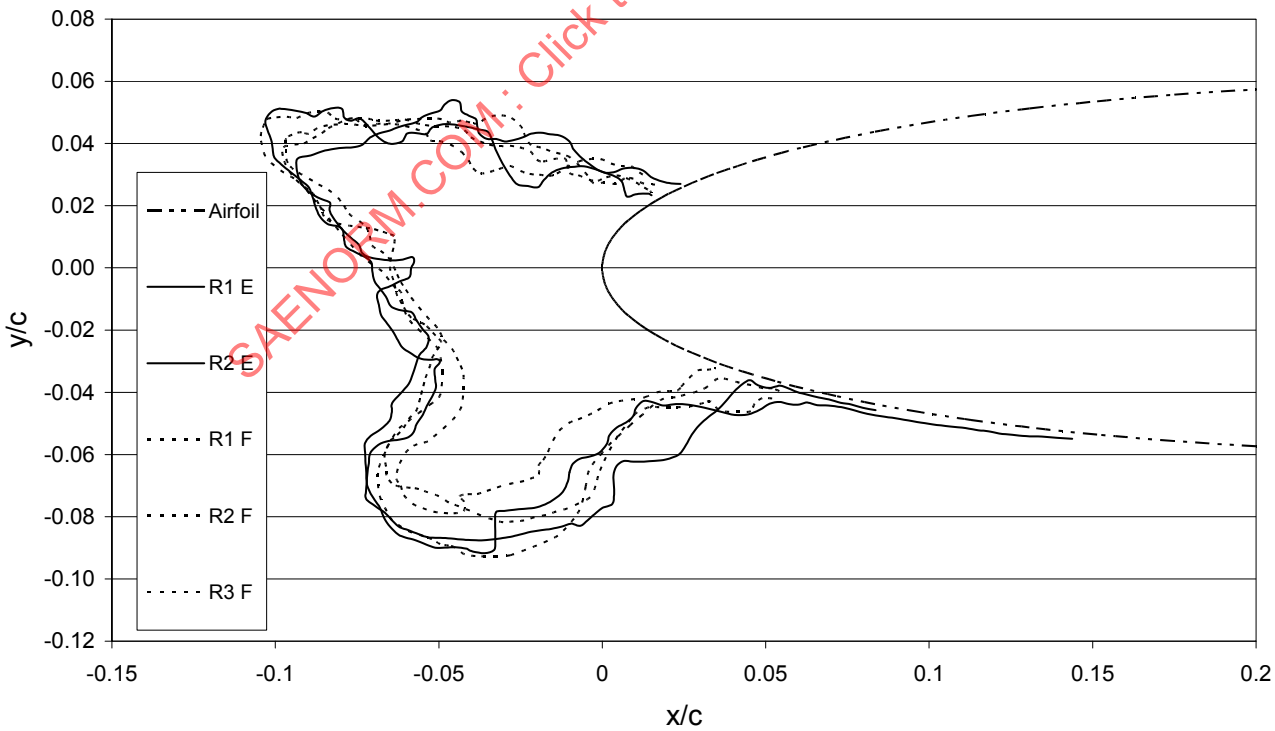

FIGURE D1C - TRACINGS FROM FACILITIES E AND F

FIGURE D1 - RESULTS FOR 12 IN CHORD AIRFOIL TEST POINT 1 GLAZE ICE ACCRETION

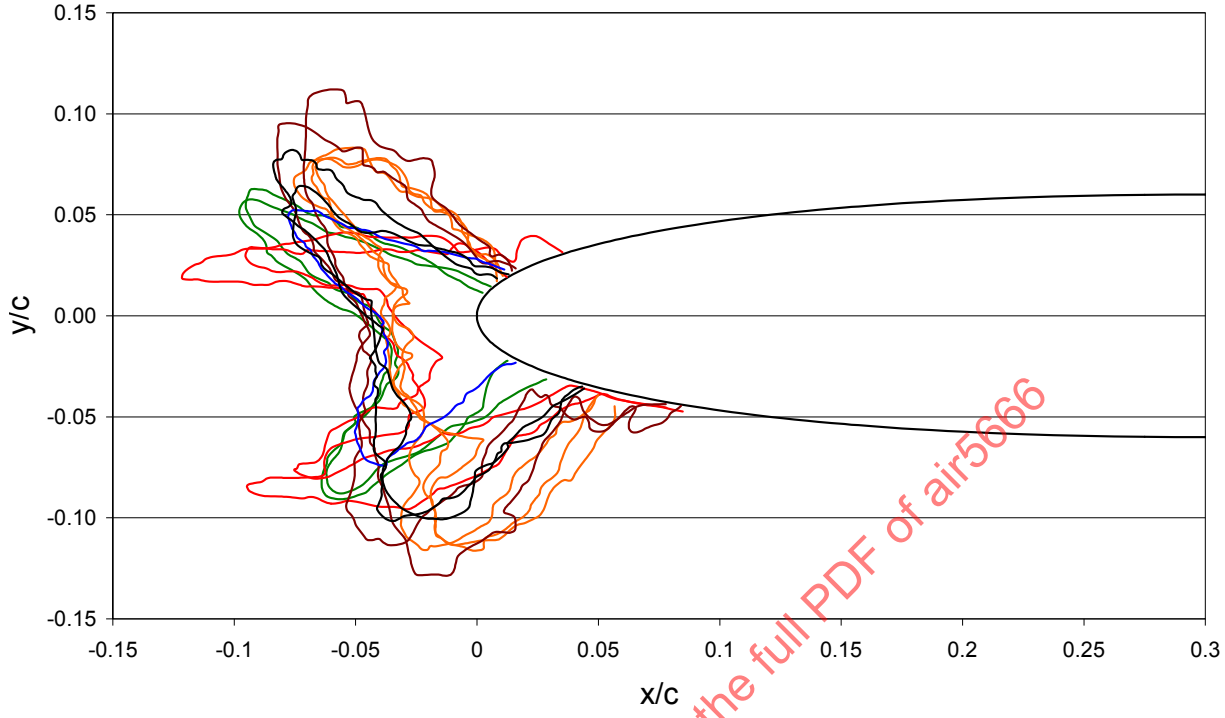

FIGURE D2A - TRACINGS FROM ALL FACILITIES

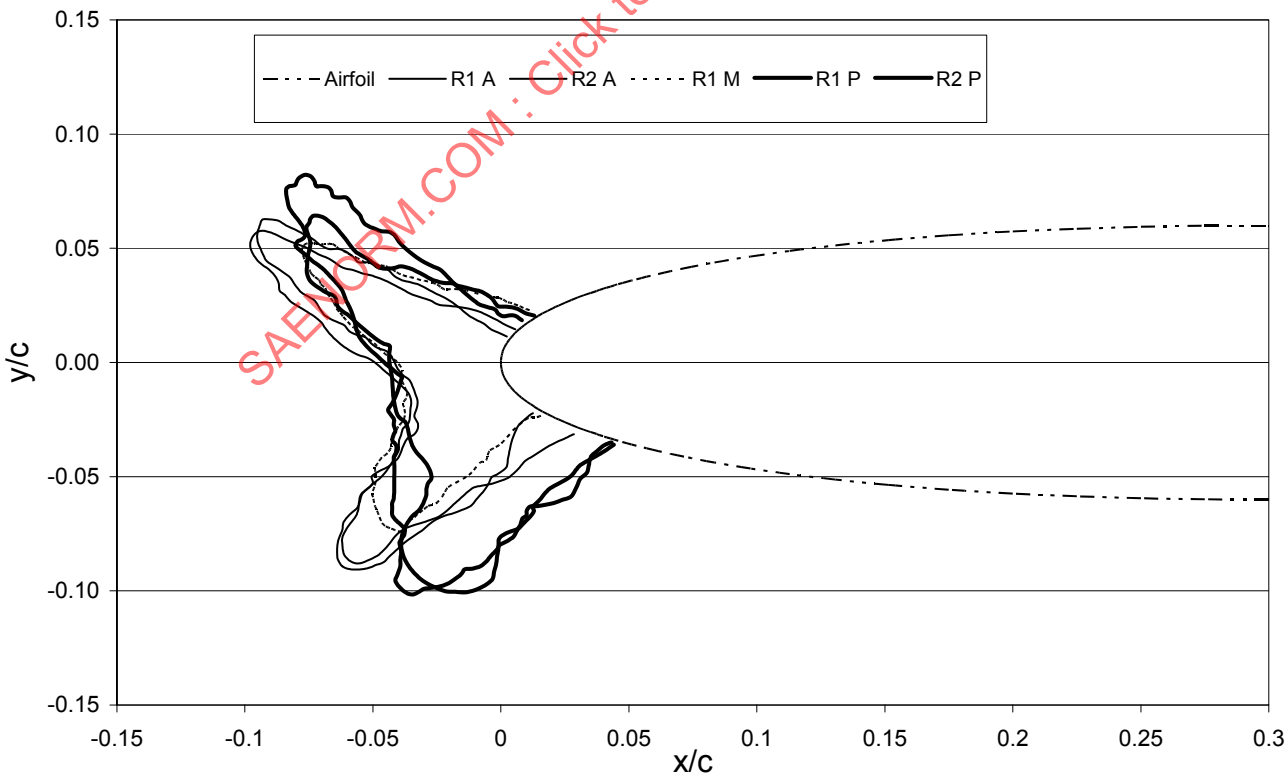

FIGURE D2B - TRACINGS FROM FACILITIES A, M AND P

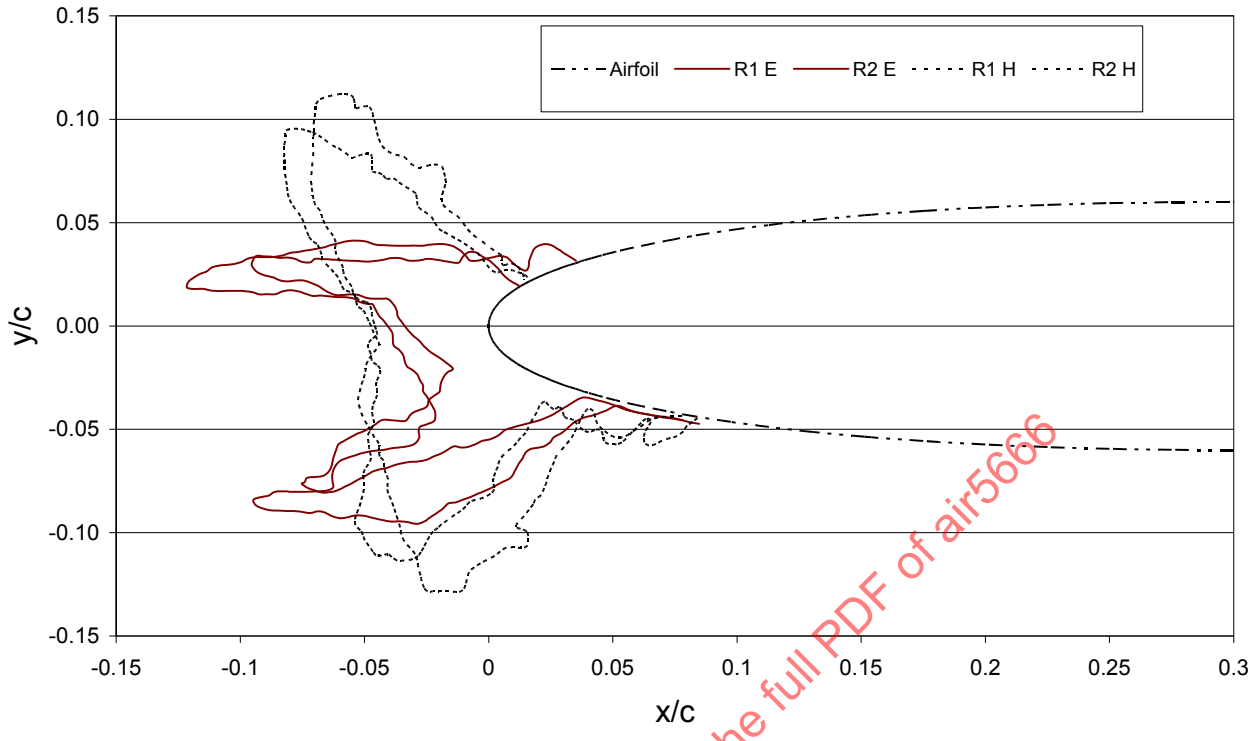

FIGURE D2C - TRACINGS FROM FACILITIES E AND H

FIGURE D2 - RESULTS FOR 12 IN CHORD AIRFOIL TEST POINT 2 GLAZE ICE ACCRETION AT HIGHER SPEED

Figure D3 shows the results for test point 3, a glaze ice accretion at higher liquid water content. For this condition the facilities fell into two groups as shown in Figures D3B and D3C.

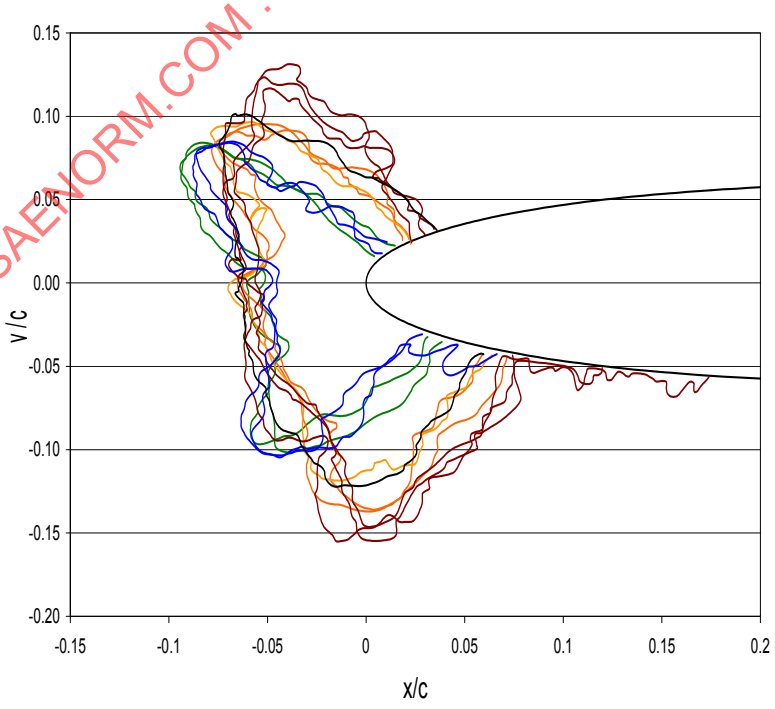

FIGURE D3A - TRACINGS FOR ALL FACILITIES

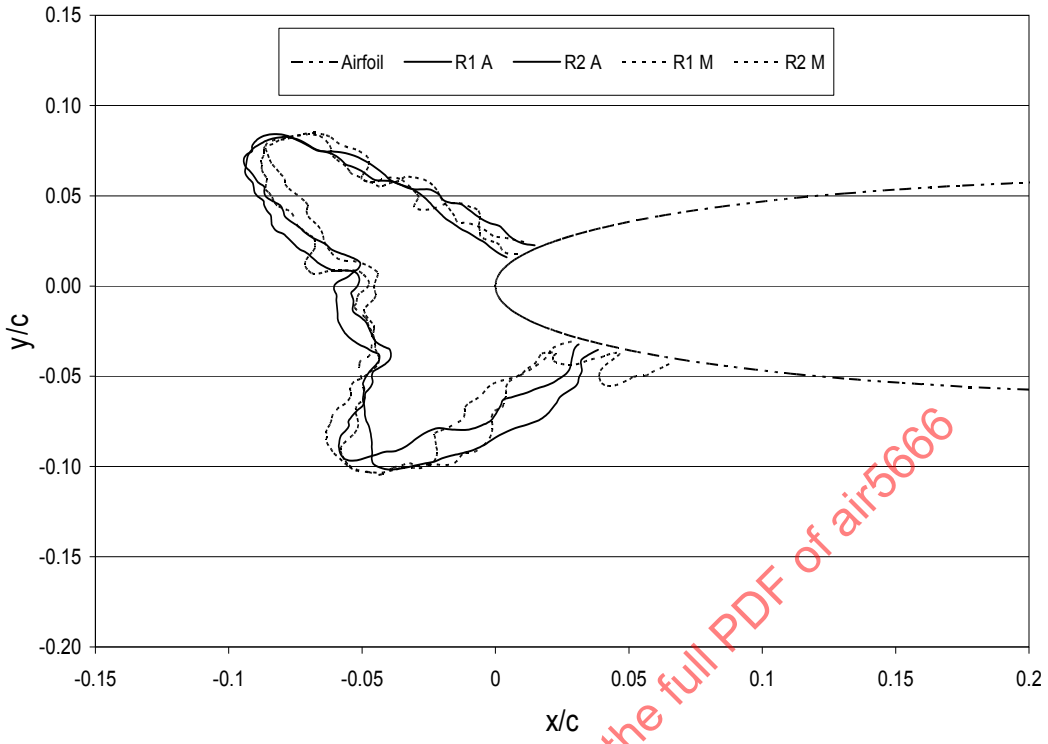

FIGURE D3B - TRACINGS FOR FACILITIES A AND M

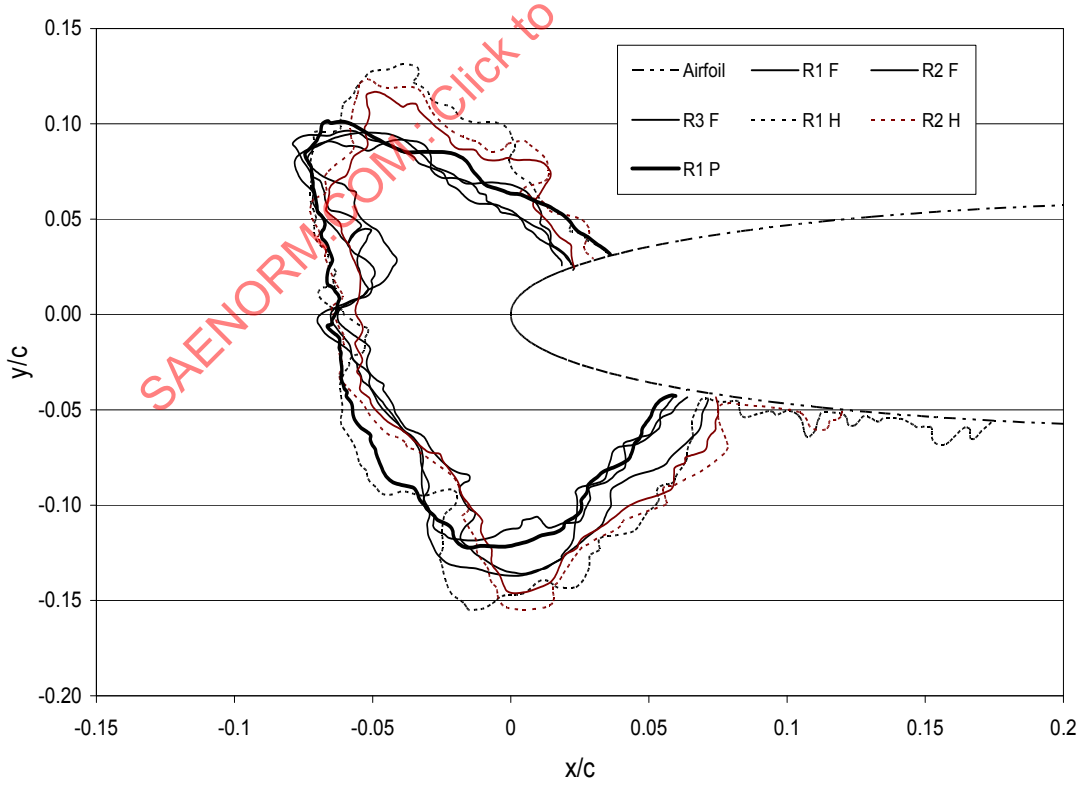

FIGURE D3C - TRACINGS FOR FACILITIES F, H AND P

FIGURE D3 - RESULTS FOR 12 IN CHORD AIRFOIL TEST POINT 3 GLAZE ICE ACCRETION AT HIGHER LIQUID WATER CONTENT (MVD FOR FACILITY F = 24 MM)

Figure D4 contains the results for test point 4, a glaze ice accretion at the higher LWC and airspeed. Similar to the last test point, two groupings of results are found as shown in Figures D4B and D4C. Note the much wider extent of ice on the lower surface shown in D4C as compared to D4B. This is a possible indication of larger drop size.

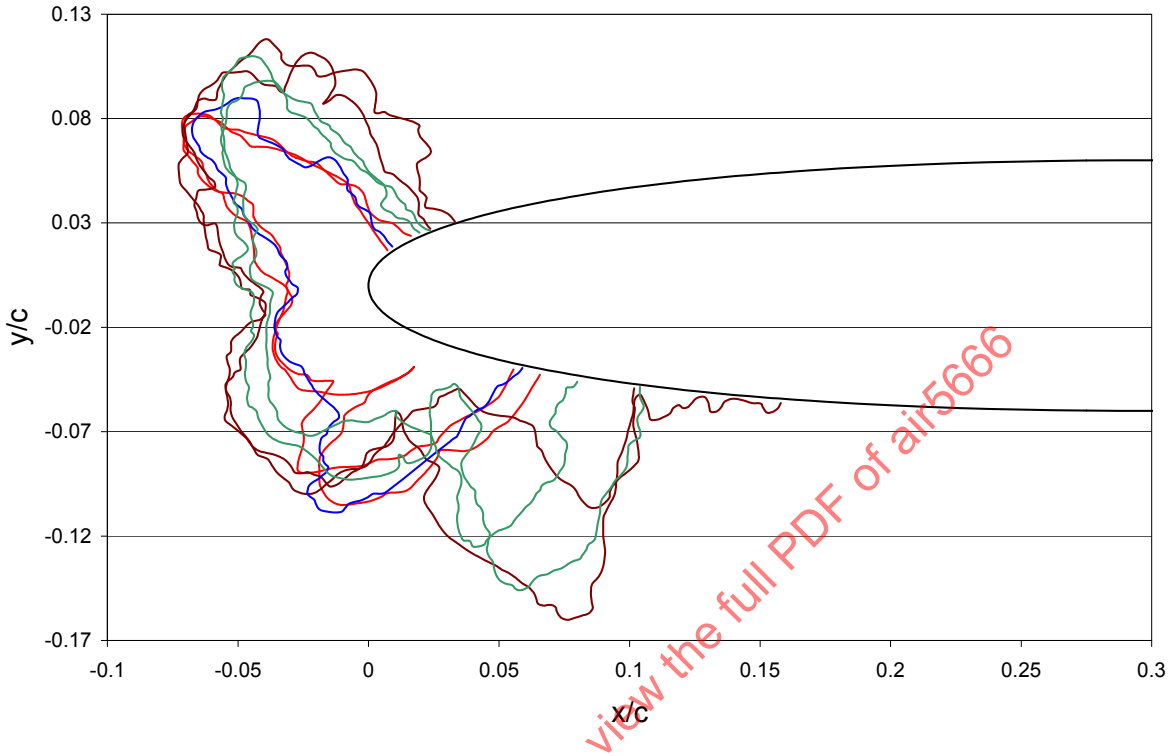

FIGURE D4A - TRACINGS FOR ALL FACILITIES

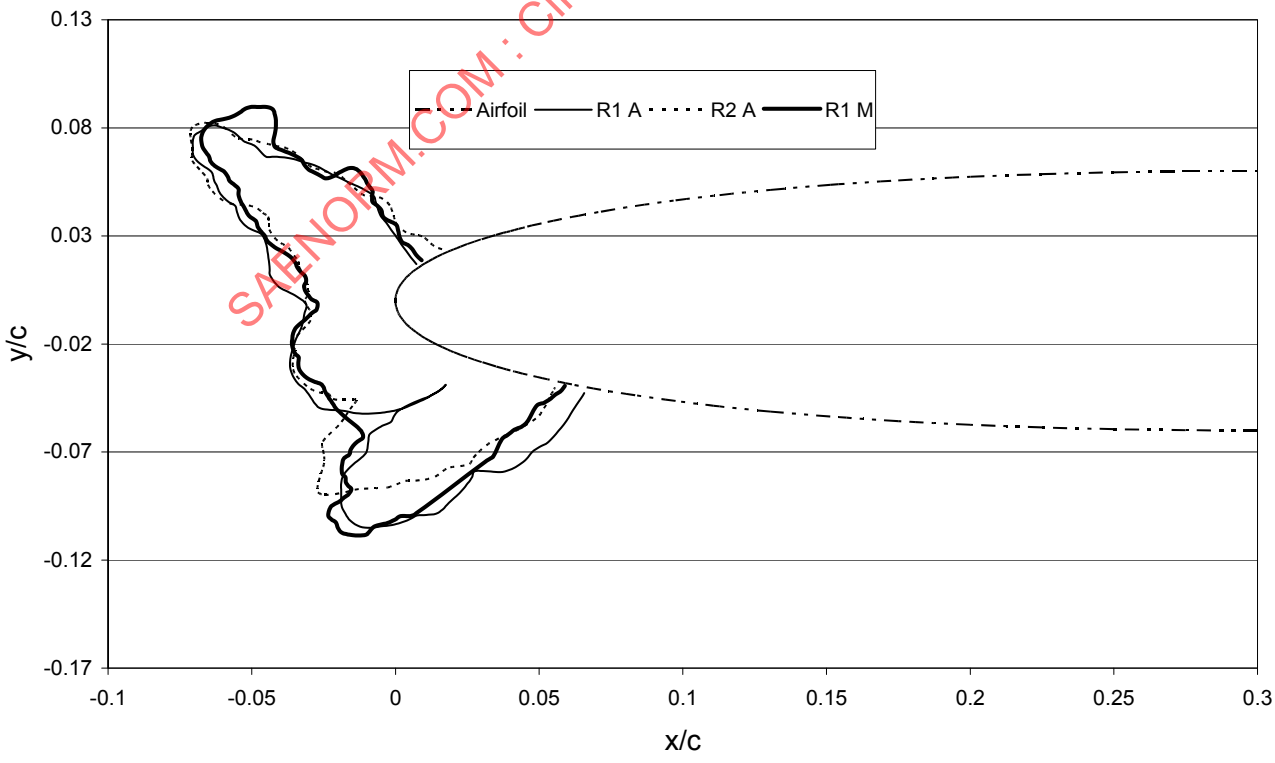

FIGURE D4B - TRACINGS FOR FACILITIES A AND M

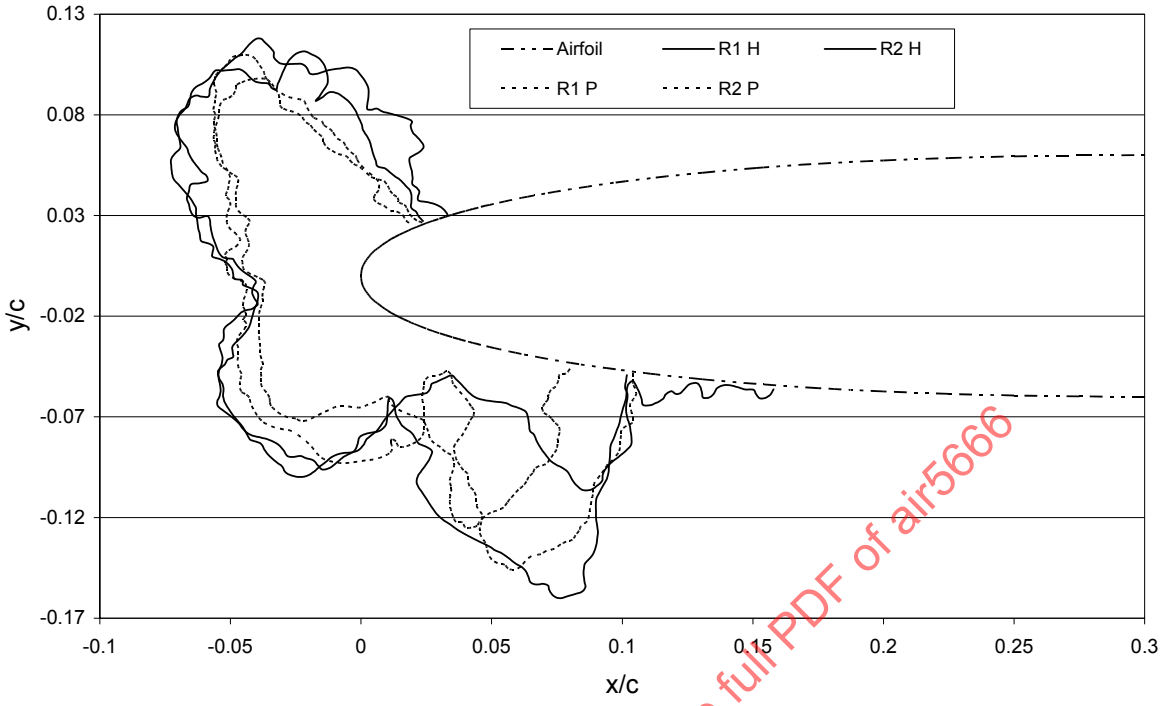

FIGURE D4C - TRACINGS FOR FACILITIES H AND P

FIGURE D4 - RESULTS FOR 12 IN CHORD AIRFOIL TEST POINT 4 GLAZE ICE ACCRETION AT HIGHER LWC AND AIRSPEED (MVD FOR FACILITY F = 24 MM)

Figure D5 shows the ice tracings for test point 5, a glaze ice accretion using a larger drop size. Again there are two groupings of facilities as shown in Figures D5B and D5C.

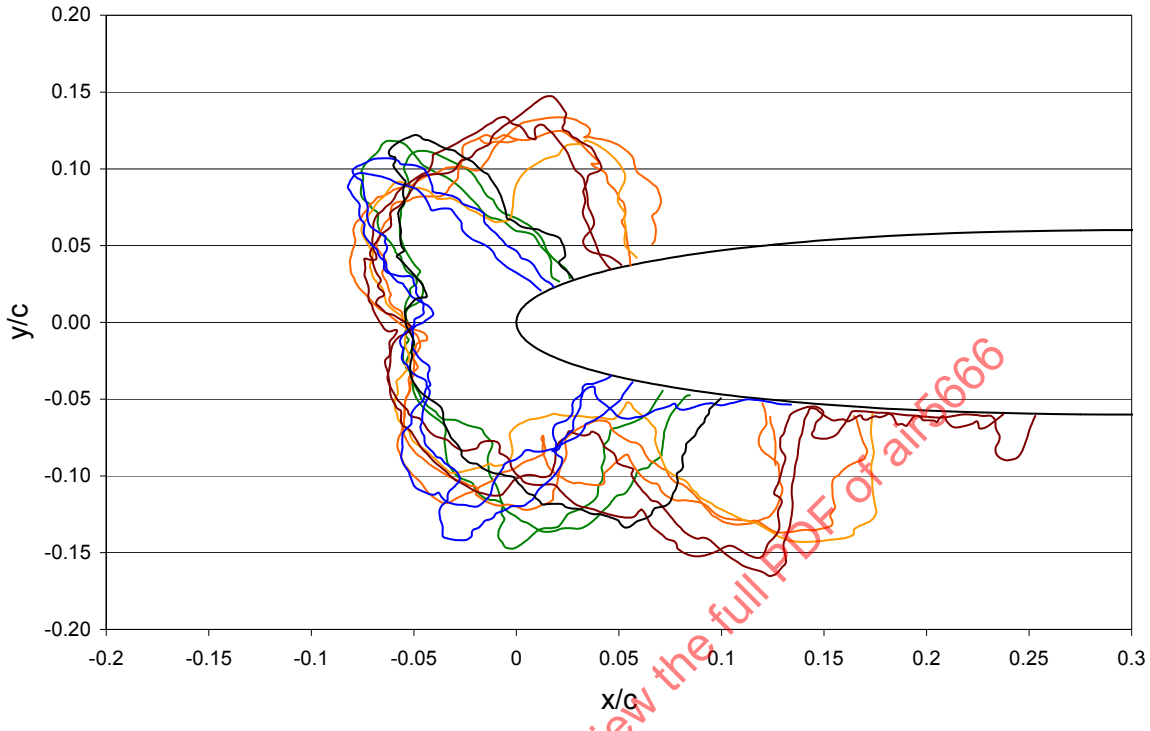

FIGURE D5A - TRACINGS FOR ALL FACILITIES

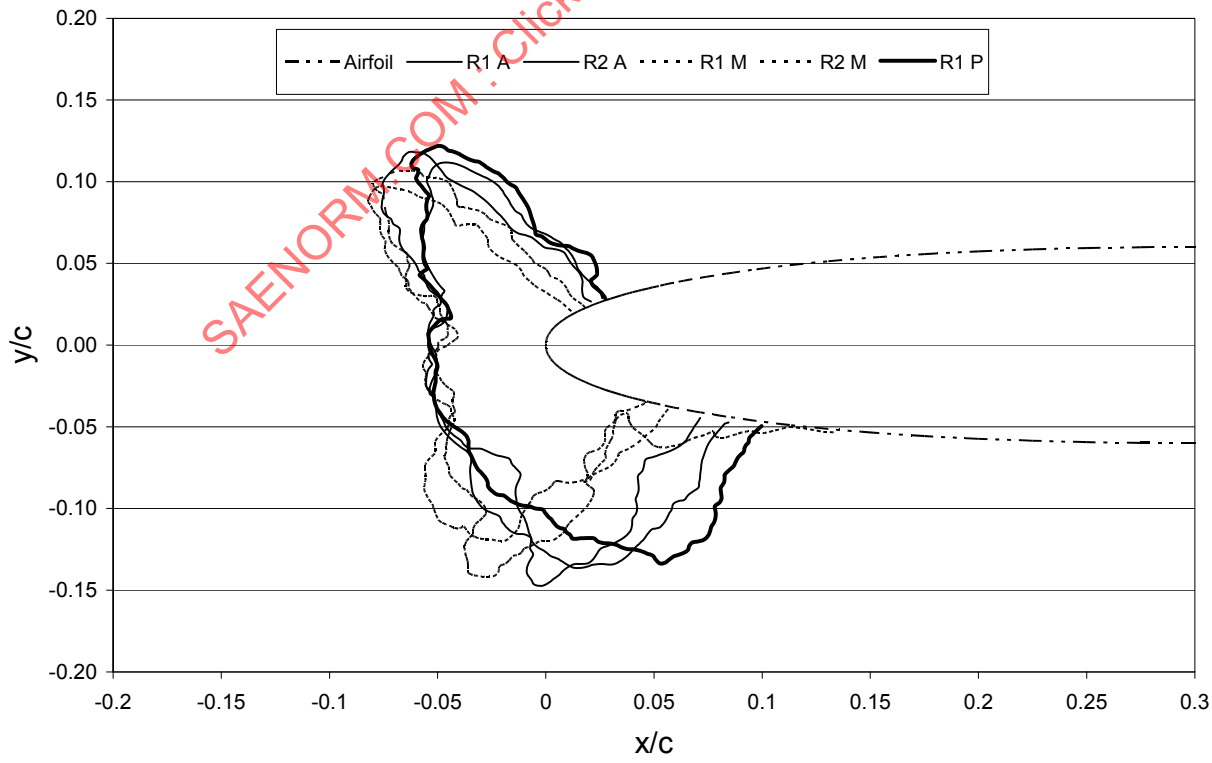

FIGURE D5B - TRACINGS FOR FACILITIES A, M AND P